THESIS

INVESTIGATION OF ON ROAD PARTICULATE MATTER CHARACTERISTICS FROM BRAKE WEAR MECHANISMS

WORAWAT SONGKITTI

GRADUATE SCHOOL, KASETSART UNIVERSITY
Academic Year 2021

THESIS APPROVAL
GRADUATE SCHOOL, KASETSART UNIVERSITY

DEGREE: Doctor of Engineering (Mechanical Engineering)

MAJOR FIELD: Mechanical Engineering

DEPARTMENT: Mechanical Engineering

TITLE: Investigation of On Road Particulate Matter Characteristics from Brake Wear Mechanisms

NAME: Mr. Worawat Songkitti

THIS THESIS HAS BEEN ACCEPTED BY

THESIS ADVISOR

(Associate Professor Ekathai Wirojsakunchai, Ph.D.)

THESIS CO-ADVISOR

(Assistant Professor Tanet Aroonsrisopon, Ph.D.)

DEPARTMENT HEAD
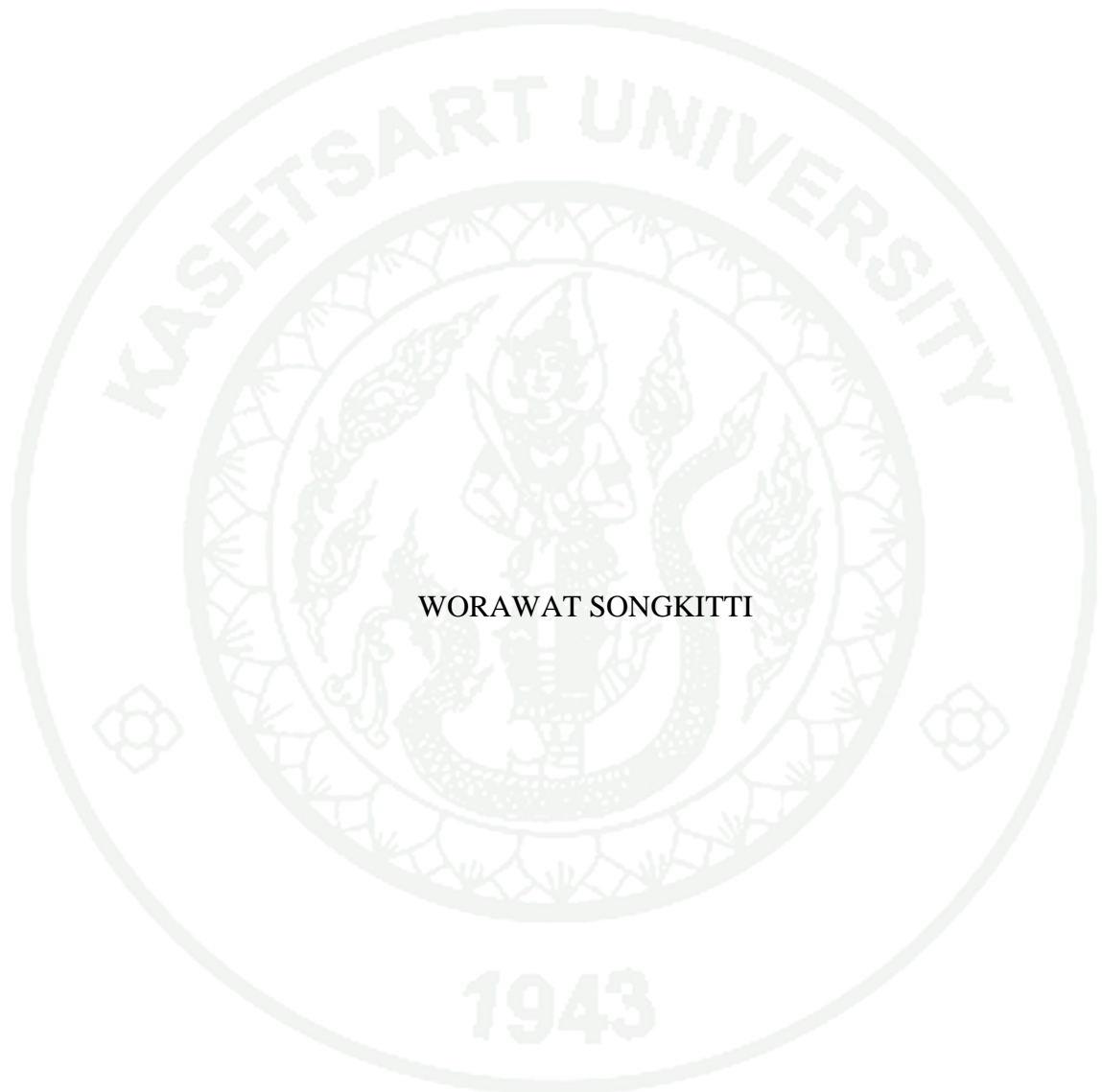
(Assistant Professor Prapot Kunthong, Ph.D.)

DEAN

(Associate Professor Srijidtra Charoenlarpnopparut, Ph.D.)

THESIS

INVESTIGATION OF ON ROAD PARTICULATE MATTER
CHARACTERISTICS FROM BRAKE WEAR MECHANISMS

WORAWAT SONGKITTI

A Thesis Submitted in Partial Fulfillment of
the Requirements for the Degree of
Doctor of Engineering (Mechanical Engineering)
Graduate School, Kasetsart University
Academic Year 2021

Particulate Matter (PM) is one of the world's most problematic pollutants. It has been found out that PM emission levels are very high during traffic congestion. Many literatures suggested that PM emitted during braking sequence from vehicles are considered high and could be the major cause of this issue. Many studies regarding to PM from brake wear were done in the brake dynamometer that might not represent real-world driving scenarios. Various studies of on road non-exhaust PM measurement were mostly focused on driving cycles. Parametric studies to identifying factors that affect brake wear during real-world driving scenarios are still needed for more investigations. The current study focuses on fundamental understanding of particulate matter characteristics from brake mechanisms. A PM sampling device is attached on the left front wheel of the tested vehicle. This device is specifically designed to mimic PM sampling setup in the laboratory environment. PM measurements including mass and number of size distributions are monitored during the braking sequence. Parametric studies on brake wear PM characteristics and morphology, including driving behavior, temperature of brake pad, payloads (weight of additional mass on vehicle), and type of vehicles (passenger car and SUV) are observed. Based on experiments, it is found out that the pattern of PM emissions observed by number of size distributions from brake wear is consistent with driving behavior as suggested in many literatures. Increasing payloads results in higher amounts of PM emissions (with increasing around 97%). PM emissions are also observed to be significantly increased at the brake temperature of 130°C the amounts rise 120% in hot test as compared with the cold test. Based on PM size distribution from brake wear, 64% of total PM emissions are considered as PM_1. In terms of chemical composition in both cold and hot tests, Oxygen, Carbon (mostly organic) and Nitrogen come from binder and reinforcement. While in the hot test, the additional metal components come from fillers and abrasive are found. Furthermore, when the temperature rises above 230°C (only in passenger car), Pt and Zn from disc brake are the additional fall-out. In terms of morphology, spherical shape particles are found in the cold test while rough-surface particles are found in the hot test.

_____   _____   ____ / ____ / ____

  Student's signature   Thesis Advisor's signature

ACKNOWLEDGEMENTS

TABLE OF CONTENTS

Page

D

LIST OF TABLES

LIST OF FIGURES

LIST OF ABBREVIATIONS

ABS	=	Anti-lock Braking System
ASP	=	Air Sampling Pump
A_T	=	Throat Area
BD	=	Brake Dynamometer
CVS	=	Constant Volume Sampling
C_D	=	Discharge Coefficient
d	=	diameter
DPF	=	Diesel Particulate Filter
DT	=	DustTrak
EC	=	Elemental carbon
EDS	=	Energy Dispersive x-ray Spectrometer
EEPS	=	Engine Exhaust Particle Sizer
ELPI	=	Electrical Low-Pressure Impactor
HEV	=	Hybrid Electric Vehicle
IC	=	Inorganic Carbon
ISO	=	International Organization for Standardization
kPa	=	kilopascal
LM	=	Low Metallic
MCE	=	Mixed Cellulose Ester
nm	=	nanometer
NAO	=	Non-Asbestos Organic
OC	=	Organic Carbon
OPC	=	Optical Particle Counter
PM	=	Particulate Matter
PN	=	Particle Number
PoD	=	Pin-on-Disc
P_T	=	Pressure Downstream

LIST OF ABBREVIATIONS (Continued)

P_0	=	Upstream Pressure
RDC	=	Real world Driving Cycle
R	=	gas constant
SEM	=	Scanning Electron Microscope
SM	=	Semi Metallic
SUV	=	Sports Utility Vehicle
TC	=	Total Carbon
TSP	=	Total Suspended Particles
T_0	=	Upstream Temperature
µm	=	micrometer
γ	=	specific heat ratio

INTRODUCTION

Air quality is a large concern in the world. Particulate Matter (PM) is one of the world's most problematic pollutants in terms of harm to human health. PM is often divided into PM_{10} and $PM_{2.5}$, which represent particles with a diameter of less than 10 µm and 2.5 µm, respectively. Traffic is one of the main reasons why PM levels are too high, and it is the primary source of PM in urban areas. One of the strategies being adopted in many countries to improve air quality is incentivizing the electrification of passenger cars. The switch to EVs has been proposed as a solution to air pollution, offering zero emissions and promising cleaner air for everyone. However, when modelling the impact of EVs on air quality, (Soret, Guevara, & Baldasano, 2014), (Kuenen, Visschedijk, Jozwicka, & Denier van der Gon, 2014) found that fleet electrification would not significantly reduce PM emissions due to the importance of non-exhaust emissions. Vehicles emit PM not only through their exhaust but also through non-exhaust sources, such as brake wear is caused by the friction between the brake pad and disc brake, tyre wear and road surface wear are caused by the friction between the tyre thread and road surface, and resuspension of road dust is caused by the diffusion of air current underneath and behind vehicles. Report contribution of brake wear is 42% to the non-exhaust PM emission of all part of vehicle (Jens Wahlström, 2009).

Non-exhaust emissions tend to contain mostly PM_{10}, but a significant proportion of the emissions contains fine $PM_{2.5}$ as well. The chemical characteristics of non-exhaust PM emissions vary per source, but are mainly made up of heavy metals such as zinc (Zn), copper (Cu), iron (Fe) and lead (Pb), among others (A. Thorpe & Harrison, 2008). One of the most important non-exhaust traffic-related source is considered to be brake wear, Several studies can be found in the scientific literature concerning the relationship existing between wear mechanisms in disc brakes and relevant emissions of airborne PM (Kukutschová et al., 2009), (Kukutschová et al., 2010), (W. Österle, Prietzel, Kloß, & Dmitriev, 2010), (Jens Wahlström, 2011), (Jens Wahlström, Olander, & Olofsson, 2010), (Lawrence et al., 2013), but all these studies doesn't measure the brake wear particles while driving. During forced deceleration, vehicle brake linings are subject to large frictional heat generation and associated wear. This mechanically induced wear generates brake lining particles which are subsequently released to the environment. It was already hypothesized that PM emissions from brake wear were highly influenced by vehicle weight, as stated in past studies (Garg et al., 2000), (Barlow, 2014). They focused on measuring non-exhaust PM emissions between passenger cars and Light Duty Vehicles (LDV). Their result showed that LDV emitted more brake wear PM than passenger cars (Luekewille et al., 2001). Driving behaviors, the frequency and severity of braking events, should be an important determinant of brake temperature and wear. Because brake wear only occurs during forced decelerations, the highest concentrations of brake wear particles should be observed near busy junctions, traffic

lights, pedestrian crossings, and corners. (Grigoratos & Martini, 2015) found that the mass of friction material lost per stop increased with an increase in brake temperature, though in all cases the percent of total wear detected as airborne PM was higher for a brake temperature of 100°C than for a brake temperature of 400°C.

Based on previous literature it can be concluded that, the main factors contribute to PM emissions are: 1.) weight of vehicle (payloads), 2.) driving behaviors, 3.) brake temperature, and 4.) types of vehicles to which effect brake wear. This study was focused on investigating brake wear particles emitted from vehicle(s) during braking sequences. The tests were performed using a PM sampling device that mimic the PM sampling system (commonly used in an engine laboratory). This PM sampling device was directly attached on to a moving vehicle nearby the left front wheel. PM mass and size distributions were measured. Driving behavior, temperatures of brake pad to find the effect of braking temperature in cold tests (less than 130°C) and hot tests (above 130°C) on brake wear characteristics and morphology, as well as payloads were varied to investigate PM emission fluctuations from brake wear during on-road driving conditions. The outcomes of this research are, first, identifying factors that affect PM formation from brake wear PM emission, second, understanding the physical and chemical properties of PM from brake wear, and finally, gaining fundamental understandings of PM formation mechanism from brake wear PM emission.

OBJECTIVE

1. Determine the effective method for real-time measurement of PM from brake wear during real word driving cycle.
2. Investigate relationships of PM characteristics among braking behaviors, payloads, and brake temperature.
3. Gain fundamental understandings of PM formation from brake wear mechanism.

SCOPE OF WORK

1. Testing brake wear PM emissions from semi-metallic brake in internal combustion engine vehicles whose weights are under 2,000 kilograms.
2. Testing on close road.
3. Testing in Real world Driving Cycle (RDC) and ISO 21994:2007 standard.

LITERATURE REVIEW

Non-Exhaust PM Emissions

Particulate Matter (PM) refers to very small particles of solid or semi-solid material. Particles with a diameter larger than 50 microns (µm) tend to fall and settle on the ground. Those smaller than 50 microns are suspended in the air. The particles can be divided into the following groups:

- TSP: Total Suspended Particulate. Particles between 0.1 and 50 microns in diameter.
- PM_{10}: Particulate matter with diameters of 10 microns or less.
- $PM_{2.5}$: Particulate matter with diameters of 2.5 microns or less.
- PM_1: Particulate matter with diameters of 1 micron or less.
- $PM_{0.1}$: Particulate matter with diameters of 0.1 micron or less.

Both PM_{10} and $PM_{2.5}$ can be breathed into the lungs causing health effects. $PM_{2.5}$ will penetrate deeper into the alveoli of the lungs than PM_{10}. Particulate matter can reduce lung function and cause lung disease such as emphysema, bronchiectasis, pulmonary fibrosis, and cystic lungs. Long term effects can also lead to lung cancer (Barlow, 2014).

It has been known that vehicle emit PM by exhaust and non-exhaust sources. Exhaust PM emissions are mainly made up of $PM_{2.5}$ and contain a variety of hydrocarbons, which can contribute to respiratory disease or lead to increased incidence of cancer (Kagawa, 2002). Non-exhaust emissions initiate from brake wear, tyre wear, road surface wear and resuspension of road dust. There are several toxicological studies that have found links between non-exhaust emissions and adverse health effects, such as lung-inflammation and DNA damage (Cassee, Héroux, Gerlofs-Nijland, & Kelly, 2013).

Up until the early 1990s, road transport emissions were dominated (80% - 90%) by exhaust emissions (Kuenen et al., 2014); but over time, PM_{10} tends to decrease as depicted in **Figure 1A** (in Netherlands 1990 – 2015). The trend as shown for the Netherlands, with the brake-even point between exhaust and wear emissions around the year 2012 as depicted in **Figure 1B** (in Norway and Switzerland 2000 - 2014). As can be seen in **Figure 1A**, since 1990 the exhaust emission reduction strategies have been extremely successful and currently wear emissions dominate over combustion emissions.
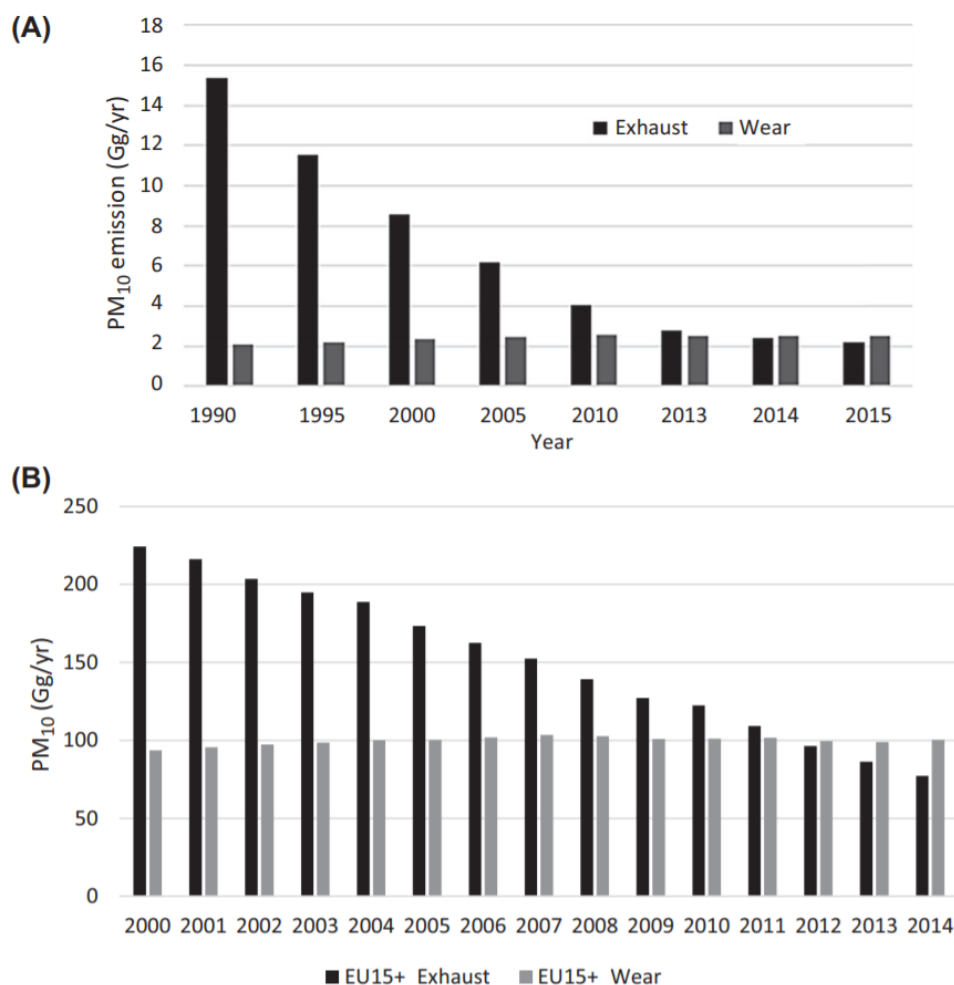
Figure 1 PM$_{10}$ emission from road transport exhaust and wear: (A) in Netherlands; (B) in Norway and Switzerland
Source: (Denier van der Gon et al., 2018)

In order to put this decrease in emissions into perspective, the average PM$_{10}$ and PM$_{2.5}$ emissions of passenger cars must be determined. As we know, passenger cars emit PM through exhaust and non-exhaust pathways.

1.) Exhaust emissions

Since PM emission standards for vehicle exhausts have become increasingly strict and now all new diesel passenger cars are fitted with a diesel particulate filter (DPF), (Bergmann, Kirchner, Vogt, & Benter, 2009) found that DPFs are very effective at reducing PM emissions, lowering the emitted mass of PM by 99.3%. This has resulted in greatly reduced particle emissions from diesels in the last ten years (Europe-ICCT, 2018). From the announcement by the European Commission (EU, 2007), it was stated that new diesel and other petrol vehicles must comply with the EURO 6 standards within the next decade. The EURO 6 standards allow almost zero PM emissions from vehicles (as depicted in **Table 1**). However, PM emissions is beyond the current scope of this research study.

Table 1 EURO 6 standards

Emissions	Petrol	Diesel
CO	1.0 g/km	0.5 g/km
THC	0.1 g/km	-
NMHC	0.068 g/km	-
NOx	0.06 g/km	0.08 g/km
HC + NOx	-	0.17 g/km
PM	0.005 g/km	0.005 g/km
PN	6.0×10^{11} /km	6.0×10^{11} /km

Source: (RAC, 2019)

2.)   Non-exhaust emissions

Non-exhaust particulate emissions come from several sources. The most significant are:

- Brake wear, from the use of the vehicle's brakes.
- Tyre wear, from the interaction of the tyres and road surface.
- Road surface wear, from the wearing of the road surface
- Resuspension, due to the particulates lying on the road being disturbed by the wake of the vehicle

Further studies consider brake wear separately and report contributions of brake wear is 42% to the non-exhaust PM emission of all of part vehicle as depicted in **Table 2**. Therefore, this research focuses on brake wear emission.

Table 2 Emission inventories on average brake wear, tyre wear and exhaust for passenger cars.

Emission Source	PM_{10} (mg/vkm)		$PM_{2.5}$ (mg/vkm)	
	Gasoline EURO 6	Diesel EURO 6	Gasoline EURO 6	Diesel EURO 6
Brakes	9.3	9.3	2.2	2.2
Tyres	6.1	6.1	2.9	2.9
Exhaust	3.1	2.4	3.0	2.4

Source: (Simons, 2013)

Numerous studies have investigated the brake wear emission phenomena. There are various methodologies to perform this task. The next chapter will explain methods for measuring brake wear emissions.

Methods for determining brake wear emissions

The most common methods are:

- Estimation: emission factors can be estimated based on national statistics of brake use, average weight lost per brake, and average distance before a brake needs to be replaced. Some manufacturers also provide information on the rate of wear on brakes, which can be used to estimate emission factors. Examples of studies that use this method are those by (Legret & Pagotto, 1999), (Barlow, 2014).

- Laboratory measurements: laboratory measurements usually use a circular road simulator and weighted wheels, with or without brakes to test tyre, brake, and road wear. Alternatively, tests can be done on a track in a wind tunnel to more closely simulate reality. Examples of studies which use a road simulator are (Cadle & Williams, 1978), (K. Kupiainen, Tervahattu, & Räisänen, 2003), (K. J. Kupiainen et al., 2005), (Bukowiecki et al., 2010), (Dahl et al., 2006), (Gustafsson et al., 2009), (Sakai, 1995) and (Sanders, Xu, Dalka, & Maricq, 2003) used a wind tunnel and track, while (Chow et al., 1994) used a resuspension chamber to investigate the composition of road dust.

- Roadside and tunnel measurements: it is possible to calculate exhaust and non-exhaust emission factors by measuring PM levels near a road or at the inlet and outlet of a tunnel, comparing this to the background levels of PM and apportioning the difference to exhaust and non-exhaust sources by analyzing the chemical composition of PM. Examples of tunnel studies are those by (Lawrence et al., 2013). Roadside measurement studies were done by (A. J. Thorpe, Harrison, Boulter, & McCrae, 2007), (Sjöberg & Ferm, 2005).

- Mobile on-board measurement: mobile on-board measurement is done by attaching sampling devices directly onto a moving vehicle or in a trailer behind a moving vehicle. This type of study was performed by (Fitz & Bufalino, 2002), (Bukowiecki et al., 2009), (Nicolas et al., 2009), (Mathissen, Scheer, Kirchner, Vogt, & Benter, 2012) and to determine resuspension emission factors. This method can be measuring the PM while real driving, therefore this method by direct sampling brake wear will be adopted in this research study.

(Farwick zum Hagen et al., 2019) tests of brake wear by using On-road vehicle measurements (direct sampling) were investigated during on-road driving with a midsize passenger car on a closed test track. The setup was customized for testing at the left front brake of a midsize passenger car. For stable flow conditions, the air flow of the system was driven constantly by blower at the end of the transport line. The high negative pressure of the blower (stand-alone specification: 1,100 Pa at 250 m³/h) was roughly estimated in order to properly compensate the pressure drop

along the capturing cone and the transport line, as sketched in **Figure 2**, ambient air from the vehicle underbody was sucked in at the front wheel. The air passed the dust shields before flushing the brake. The aerosol was then routed through a swivel joint connecting the rotating cone on one side to a stationary hose (d = 38 mm, l = 1.4 m) on the other side. The hose was routed in a horizontal U-bend and later expanded to a larger diameter hose (d = 100 mm, l = 5 m) that minimized particle losses. It was further routed over the hood along the right A-pillar onto the vehicle roof entered the passenger cabin at the right rear window and was connected to the sampling tube (d = 100 mm, l = 0.6 m) in the trunk of the car. This tube was positioned in front of the blower and was used for aerosol sampling and continuous monitoring of the air velocity inside (air velocity transducer, TSI 8455). The aerosol was sampled in the center of the tube with an isokinetic adjusted probe considering an estimated setup flow of 89 m^3/h (Paul Baron, Pramod, & Klaus, 2011). The probe was connected via a flow splitter to an Aerodynamic Particle Sizer (APS, TSI 3321; sampling rate: 1 Hz; particle size range (aerodynamic): 0.5-20 µm; number of channels: 52), DustTrak (DT, TSI 8533; sampling rate: 1 Hz) with PM_{10} impactor upstream, and an Engine Exhaust Particle Sizer (EEPS, TSI 3090; sampling rate: 10 Hz; particle size range (electrical mobility): 5.6 – 560 nm; number of channels: 32). Downstream of the blower, the aerosol was routed out of the passenger cabin. For PM background monitoring a second DT device was used sampling at the left rear window.
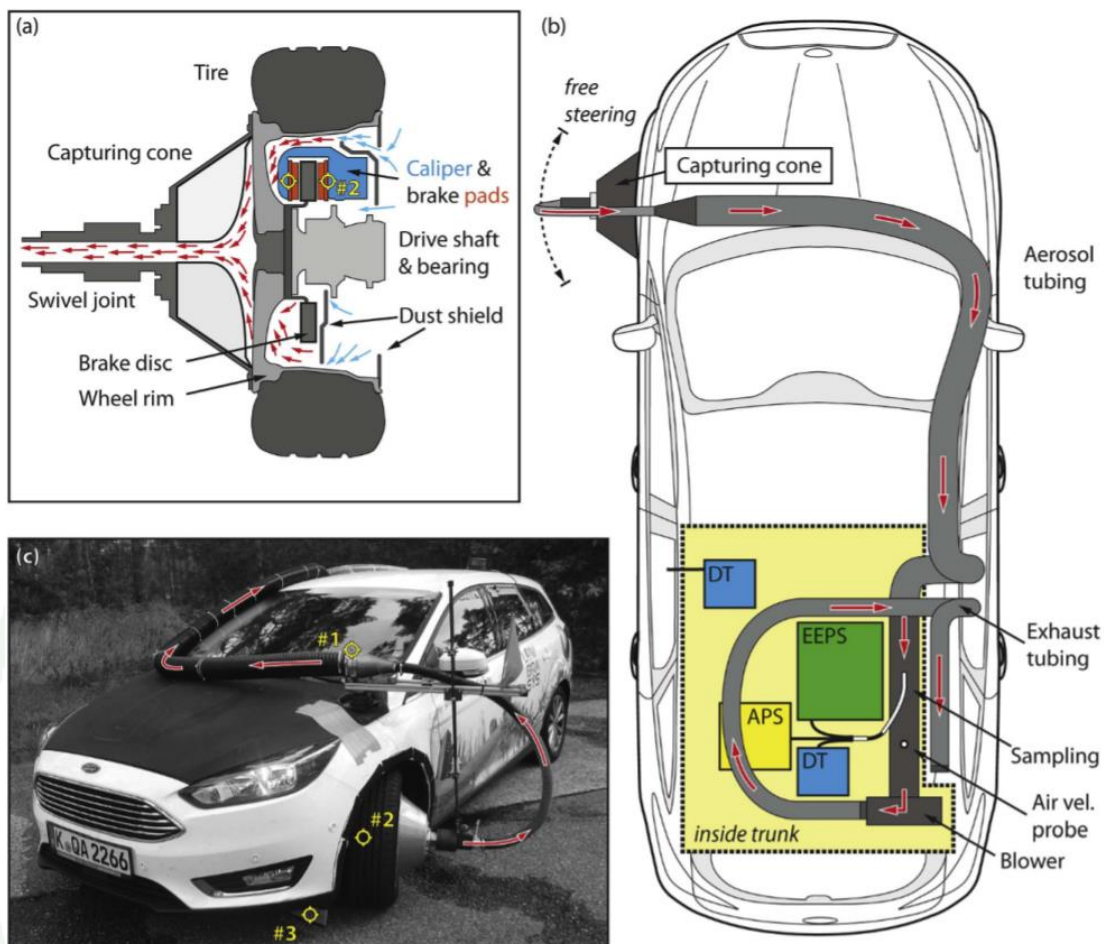
Figure 2 (a) Dust capturing cone at left front wheel. (b) Test car with measuring setup. (c) Schematic Chart of measurement setup
Source: (Farwick zum Hagen et al., 2019)

It can be summarized from above literature reviews that there are numerous details on measurements of PM from brake wear system due to complexity of the PM formation/generation. The following chapter will discuss on the PM formation/generation mechanism.

PM formation from brake wear mechanism

The materials used in the production of brake pads can be classified in terms of different criteria. The most important one is the role the substance plays in the process of braking. Based on this criterion there are binders, additives, fillers, and abrasives (**Figure 3**) (Xiao, Yin, Bao, Lu, & Feng, 2016), (Gujrathi & Damale, 2015), and (Aza, 2014).
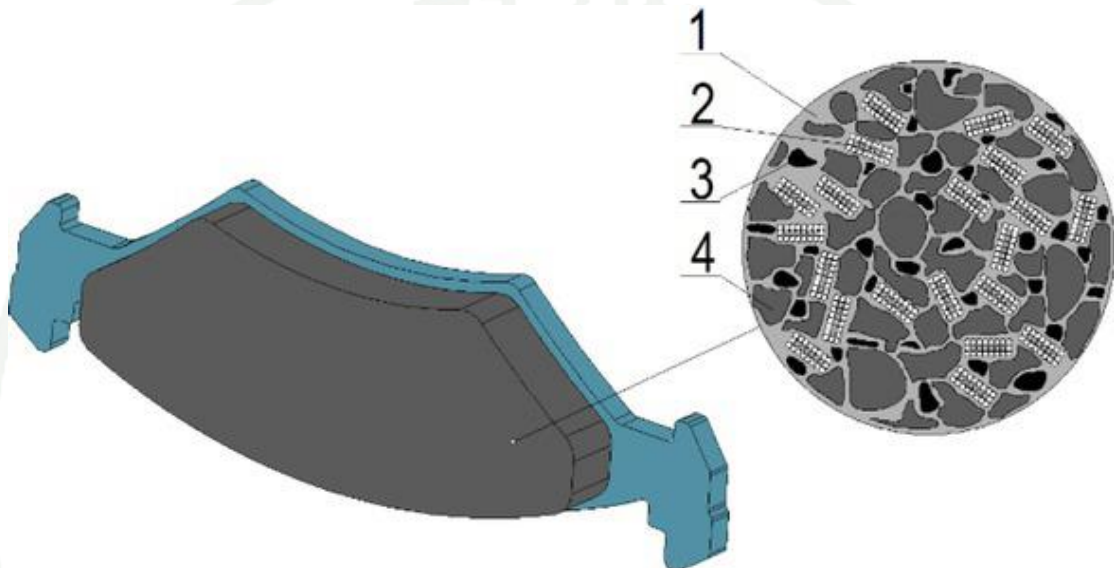
Figure 3 Brake pad friction material structure: 1 - binder, 2 - reinforcement, 3 - filler, 4 - abrasive
Source: (Borawski, 2020)

The binder is the flue that hold all the components of the pad. This substance must be characterized by high and stable coefficient of friction, resistance to high and rapidly changing temperatures and low mass (the binder usually makes up approximately 20% of the pad volume) (Bijwe, 1997). Also, the material must not react with any other component of the pad, as this might lead to changes in overall material characteristic or cause delamination of the composite and greatly limit the efficiency of the braking system. The binder is usually made from epoxy or silicone resin (Chan & Stachowiak, 2004).

The reinforcement is a fibrous material (one or more) which improves the binder's mechanical properties (increasing its strength). Different types of reinforcement materials have a significant impact on the durability and resistance of the brake pad. Therefore, the selection cannot be random. In the past, asbestos was an excellent reinforcement fiber. However, due to its harmful properties (Lemen, 2004), it was necessary to find a replacement which today is no problem at all, since there is a whole range of materials which can be used successfully to this end (Ikpambese, Gundu, & Tuleun, 2016) and (Ganguly & George, 2008)).

Fillers are used to filling up the empty spaces between the other components of the brake pad. They can make up for up to 10% of the brake pad volume, which is why using the right substance is so important. Most common fillers include vermiculite, perlite, mica, barium sulphate, and calcium carbonate, due to the substances resistance to high temperature, lack of reaction with other components of brake pads, and low price (Y. C. Kim, Cho, Kim, & Jang, 2008).

Abrasives are used for modifying (increasing or decreasing) the coefficient of friction. Additives such as steel, cast-iron, flame-resistant oxides and silicates or quartz, due to their hardness, are used for increasing the coefficient of friction between the brake pad and disc and therefore increasing the operating life of the pad. Additionally, the effect is reinforced by the adhesion with the disc material, especially in terms of metals. The substances also create contact zones, which are the main friction areas in the pair of elements (Eriksson, Lord, & Jacobson, 2001), (Mitsumoto, 2017). Unfortunately, due to friction in the contact areas, excessive temperatures are generated. This may lead to destruction of the pad's structure and lead to separation of its components. That is why lubricants are used, which usually improve the thermal conductivity of the pad. Lubricants improve the removal of energy from the contact area and prevent the friction elements from overheating (S. J. Kim, Cho, Cho, & Jang, 2007), (Gudmand-Høyer, Bach, Nielsen, & Morgen, 1999) and (Szpica, 2019). The most common lubricants are metallic sulphates (such as copper or tin) and graphite. Their lubricity depends on the content in the pad (approximately 10% of volume yields the best results) and the size of lubricant particles (Dmitriev, Öesterle, & Kloss, 2011).

There are two main brake system configurations in current use: disc brakes, in which flat brake pads are forced against a rotating metal disc, and drum brakes, in which curved pads are forced against the inner surface of a rotating cylinder. Disc brakes tend to be used in smaller vehicles (passenger cars and motorcycles) and on the front wheels of light-duty trucks. Traditionally, drum brakes tend to be used in heavier vehicles, although disc brakes are increasingly used in newer heavy-duty vehicles. Disc brakes, in which flat brake pads are forced against a rotating metal disc (**Figure 4**), during forced deceleration, vehicle brake linings are subject to large frictional heat generation and associated wear. This mechanically induced wear generates brake lining particles which are subsequently released to the environment. In other words, the frictional contact between the disc and the pad generates particles of various sizes. During a braking event, the caliper acts mechanically on the pad, which slides against the disc and transforms vehicle kinetic energy into thermal energy. Apart from the mechanical abrasion, vehicle brakes become subject to large frictional heat generation with subsequent wear of linings and rotors. It is estimated that front brakes have to provide approximately 70% of total braking power and therefore have to be replaced more frequently than rear ones. The majority of car braking systems consist of frictional pairs made of a disc, a pad and a caliper. **Figure 4** depicts a disc brake assembly with a single-piston floating calipers and a ventilated rotor (Jens Wahlström, 2009). It is therefore no surprise that front brake linings have

to be replaced more frequently than rear brake linings. It has been estimated that front disc brakes last for around 35,000 miles (56,000km) under normal usage, while rear brakes can be expected to last around 70,000 miles (112,000 km) (Garg et al., 2000). During a brake's lifetime, 80% of the friction material will have worn away. Finally, some disc-brake systems require the pads to be in low-pressure contact with the rotor in order to ensure robust brake performance. This leads in higher particle release in the environment (Söderberg, Sellgren, & Andersson, 2008).
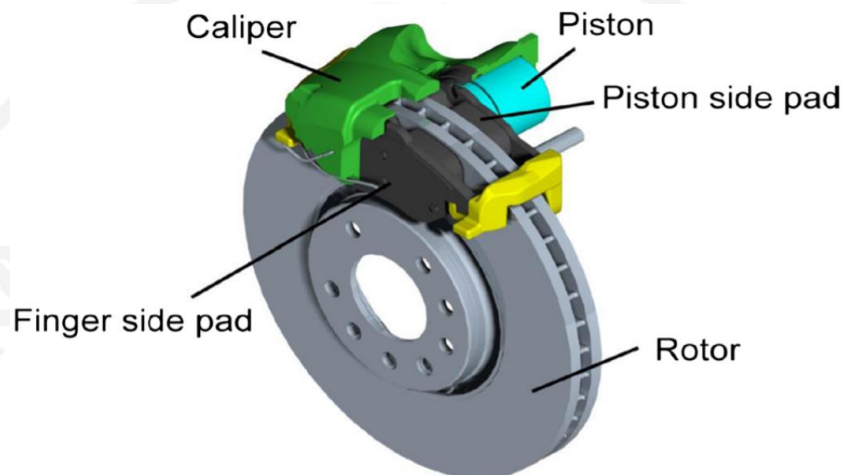
Figure 4 Graphic representation of a disc brake system.
Source: (Jens Wahlström, 2009)

While most of the brake wear deposits either on road or vehicle sites (Kumar, Pirjola, Ketzel, & Harrison, 2013), about 35 – 55% becomes airborne (Garg et al., 2000), (Harrison, Jones, Gietl, Yin, & Green, 2012). (Sanders, Dalka, Xu, Maricq, & Basch, 2002) even report airborne fractions of 50 – 70% escaping the wheel, while about 15 – 25% remains on wheel.

Typically, the regular vehicles have four common brake pad types: (AZUMA, 2020), (Auto, 2019).

- Semi-Metallic; with long-term durability and excellent heat transfer capability: - semi-metallic is the most common brake pad type widely used in different vehicles. It is made of steel wire or wool, graphite or copper, and friction modifiers. This type of brake pad contains 30 – 65% metallic compositions. It creates more noises, wears down rotors faster, and underperforms at low temperatures.
- Non-Asbestos Organic (NAO); fibers, high-temperature resins, and filler materials are used in the making of this brake pad type. If compared to the semi-metallic type, they are softer and create less noise; but deteriorate faster and create more dust. These types of brake pads are sometimes listed as organic or NAO.
- Low-Metallic NAO; these brake pads are made of organic materials with 10%-30% metal such as steel or copper in the mix. Though they

create more noise and brake dust, their braking and heat transfer capabilities are excellent.

- Ceramic; these brake pads are generally the most expensive, but are cleaner and produce less noise than other materials. Ceramic brake pads last longer than semi-metallics as well. (Auto, 2019) says ceramics outperform organic pads.

Overview of the published brake wear studies trying to quantify direct brake emissions generated mainly by a brake dynamometer (**Table 3**) clearly shows impossibility to make a comparison of quantity of brake wear emissions, as there are several variables (testing device, testing procedure, sampling conditions, brake materials, etc.) and no recommended approach for generation, measurement and expression of brake wear emissions is clearly defined.

Table 3 Overview of Studies Quantifying the Airborne Fraction of Direct Brake Wear Particulate Emissions

Reference	Pads	Type of Testing	Testing Procedure	Particle Quantification	Output
(Garg et al., 2000)	SM, NAO	BD	Wear Test-General Motors BSL-035 (Deceleration 2.94 m/s^2, max. speed 50 km/h, temperatures 100, 200, 300, and 400˚C)	Mass of filters (TSP sampling, size resolved by MOUDI)	Overall average: 4.6-12.1 mg of PM_{10}/mile/vehicle 3.4-8.9 mg of $PM_{2.5}$/mile/vehicle 1.9-5.0 mg of $PM_{0.1}$/mile/vehicle
(Sanders et al., 2003)	LM, SM, NAO	BD	Urban driving program (deceleration < 1.6 m/s^2, max. speed 90 km/h)	Mass of filters (TSP sampling, size resolved by MOUDI and ELPI)	~8 mg of TSP/stop/brake (LM) ~2 mg of TSP/stop/brake (SM) ~2 mg of TSP/stop/brake (NAO)
(Hagino, Oyama, & Sasaki, 2015)	NAO	BD	Own urban driving program (deceleration < 3.0 m/s^2, max. speed 60 km/h)	Mass of filters (DustTrak + impactor)	0.006-0.016 mg of PM_{10}/braking/ wheel
(Hagino, Oyama, & Sasaki, 2016)	NAO	BD	• Wear test-JASO C427 (deceleration 2.94 m/s^2, max. speed 50 km/h) • Japanese exhaust emission/fuel economy tests (JC08/JE05) (max. speed 90 km/h)	Mass of filters (DustTrak + impactor)	0.04-1.4 mg of PM_{10}/km/vehicle 0.04-1.2 mg of $PM_{2.5}$/km/vehicle
(Perricone et al., 2017)	LM, NAO	BD	Modified wear test (SAE J 2707) (max. deceleration 3.92 m/s, max. speed 100 km/h, initial rotor temperature 100 -200˚C)	Mass of filters Number concentration (ELPI + cascade impactor)	14.5-46.4 mg of PM_{10}/stop/brake (LM) 8.5-9.2 mg of PM_{10}/stop/brake (NAO) 8-91 x 10^{10}# of PM_{10}/stop/brake (LM) 153 x 10^{10}# of PM_{10}/stop/brake (NAO)
(Nosko & Olofsson, 2017)	LM	PoD	Own testing program (contact pressure 0.5-1.5 MPa, deceleration 0.8-1.6 m/s)	Calculation of volume concentration based on size distribution (FMPS, OPS)	~200 mg of PM_{10}/m^3

Source: (Kukutschová & Filip, 2018)

(BD, brake dynamometer; LM, low-metallic; NAO, non-asbestos organic; PoD, pin-on-disc; SM, semi metallic; TSP, total suspended particles.)

(Sanders et al., 2003) and (Garg et al., 2000) also conducted dynamometer measurements with SM (Semi-Metallic), LM, and also NAO brake materials typically used for midsize and full-size cars as well as the full-size trucks. (Sanders et al., 2003) used an open disc system, while the measurements by (Garg et al., 2000) were carried out in a closed chamber. Dynamometer testing simulated regular on-road braking events "typical for urban driving," i.e., speed from 90 to 0 km/h (Sanders et al., 2003) and from 50 to 0 km/h (Garg et al., 2000), deceleration below 1.6 m/s^2 (Sanders et al., 2003) and 2.94 m/s^2 (Garg et al., 2000) and, importantly, the data generated for the particle mass and the particle number distributions, as well as the chemical composition of direct wear debris, were compared with the on-vehicle brake particle measurements (Sanders et al., 2003). The number distribution was dominated by particles larger than 200 nm in diameter, which is not in agreement with the discussed pin-on-disc studies (Nosko, Olofsson, Metinoz, & Alemani, 2015), (Nosko & Olofsson, 2017) and later dynamometer study (Kukutschová et al., 2011), which detected particles down to 10 nm in diameter. (Sanders et al., 2003) estimated the major difference between LM and NAO pad formulations in number concentration of wear particles with LM formulation generating two to three times larger number of wear particles than SM and NAO (**Figure 5**). By comparison of final pad and rotor mass, (Sanders et al., 2003) observed that when LM brake pads are used, 60% of the wear debris comes from the rotor and 40% from the pads. Because rotors are contributing to direct brake wear, observations regarding the presence of iron in wear debris, as the most dominant metallic element, are consistent in numerous studies (Garg et al., 2000), (Kukutschová et al., 2011), (Werner Österle et al., 2014), (Sanders et al., 2003) and (J Wahlström, Söderberg, Olander, Olofsson, & Jansson, 2010). The elements detected by (Sanders et al., 2003) with the highest frequency and in the highest amounts were Fe, Cu, Si, Ba, K, and Ti. However, they did not observe any difference in distribution of elements among studied size fractions, i.e., coarser and finer fractions were of similar elemental composition.
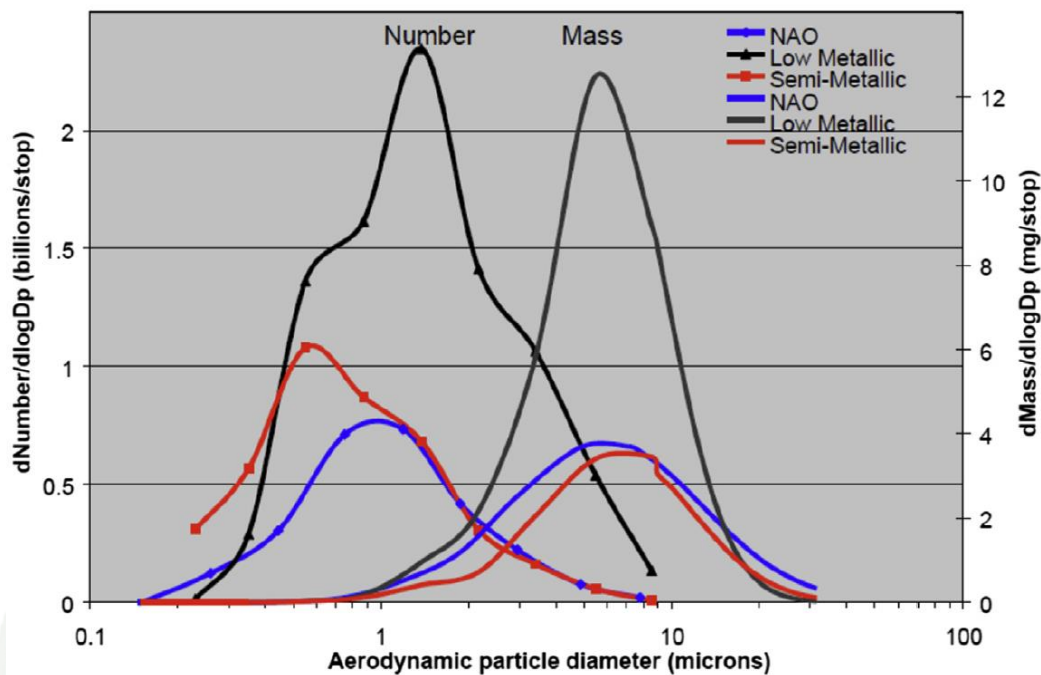
Figure 5 Number versus mass distributions of brake wear particles generated from low-metallic, semi-metallic, and non-asbestos organic (NAO) brake pad materials.
Source: (Kukutschová & Filip, 2018)

They account for 20 – 40% of the lining material and are made of modified phenol-formaldehyde resins. Reinforcing fibers provide mechanical strength and structure to the lining. They usually account for 6 – 35% (by mass) of the lining material and can be classified as metallic, mineral, ceramic or organic. They mainly consist of copper, steel, brass, potassium titanate, glass, organic material and Kevlar. Fillers are used in order to improve thermal and noise pad properties and also reduce the manufacturing cost. They usually consist of inorganic compounds (barium and antimony sulphate, magnesium, and chromium oxides), silicates, ground slag, stone and metal powders and account between 15 and 70% (by mass) of the lining material. Lubricants influence the wear characteristics of the lining. They can be inorganic, metallic or organic. Graphite is usually employed, but other common materials include ground rubber, metallic particles, carbon black, cashew nut dust and antimony trisulphide. They usually make up 5 – 29% by mass of the brake lining. Abrasives are used in order to increase friction, maintain cleanliness between contact surfaces and limit the buildup of transfer films. They typically account for up to 10% by mass of the lining. Aluminum oxide, iron oxides, quartz and zircon are the most common abrasive constituents (Grigoratos & Martini, 2014), (Eriksson et al., 2001). The proportions of the abovementioned components vary according to the type of lining and the manufacturer.

The microstructure of brake wear is shown in **Figure 6**, particles of different sizes generated as a result of brake wear tests performed in the laboratory (Kukutschová et al., 2011). (Jens Wahlström, 2011) provided a simplified visual explanation of the model which is given in **Figure 7**. It has been shown that a

transparent disc is moving from left to right. Some of the wear particles pile up against the contact plateaus and create secondary plateaus. A flow of wear particles in the gap between the pad and disc wear the lowlands of the pad through three-body abrasion, the plateau surface is covered by a nanocrystalline third body formed by the wear particles and that this third body is mainly made of iron oxides (Werner Österle & Urban, 2006). The third body differs in structure composition and properties from the two first bodies, pad and disc in our case (Werner Österle & Dmitriev, 2014). Much detailed work has been published on this field by several researchers (G. Ostermeyer, 2014), (G. P. Ostermeyer & Müller, 2008) and (G. P. Ostermeyer, 2007).
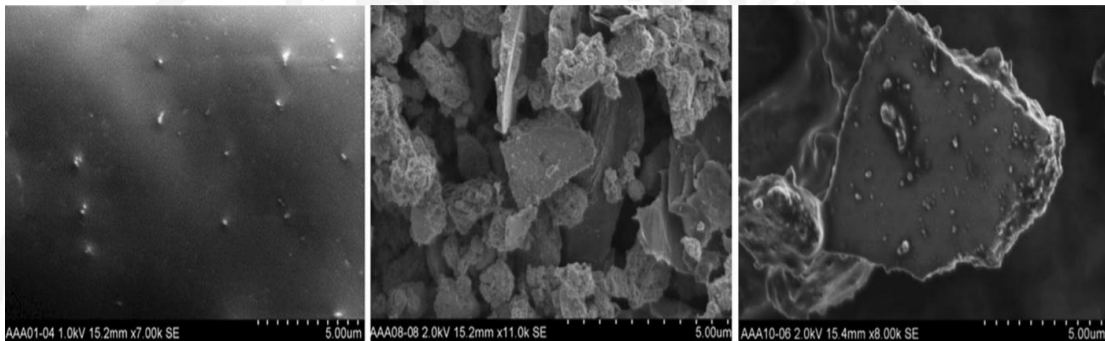
Figure 6 SEM images of brake wear particles (left<56nm, middle $PM_{2.5}$, right PM_{10})
Source: (Kukutschová et al., 2011)
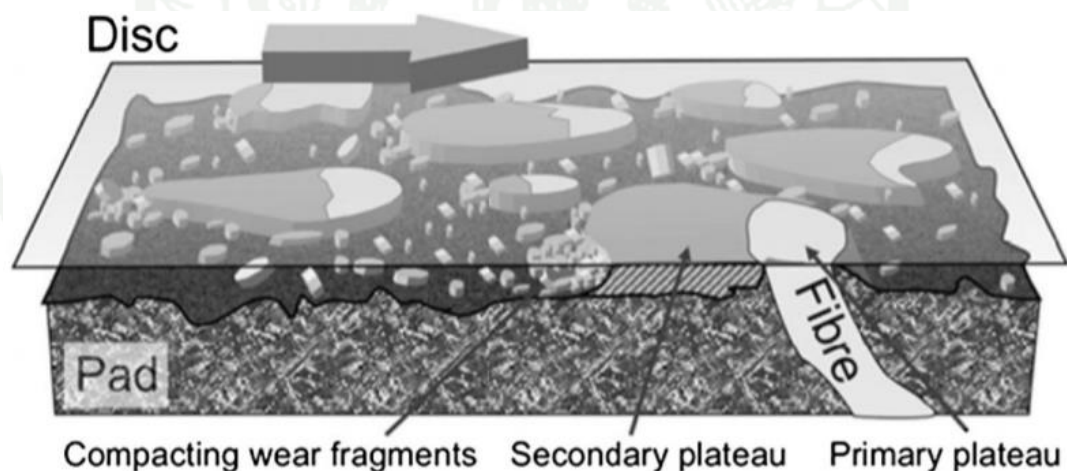
Figure 7 Illustration of the contact situation between the pad and disc
Source: (Jens Wahlström, 2011)

The metal contents of brakes determined in three studies (Brewer, 1997), (VROM, 1997), (Legret & Pagotto, 1999) are presented in **Table 4**. The results show that significant amounts of copper (up to 1.4% by mass) and iron (up to 4% by mass) can be present. Other metals, notably calcium, sodium, and zinc, are also prominent and **Table 5** reported metal concentrations in the brake linings of new passenger cars (less than four years old), older passenger cars (using replaced brake disc, drums and brake linings not originally fitted to the vehicles), heavy goods vehicles and buses, The results show that significant amounts of copper (up to 14% by mass) and iron (up to 40% by mass).

Table 4 Metal content of brake linings

Metal	Concentration range (mg/kg)	Metal	Concentration range (mg/kg)
As	10	Mn	3,220
Al	3,770	Mo	10,000
Ba	2,640	Na	15,400
Ca	14,300	Ni	210-850
Cd	2.7-29.9	Pb	1,960-3,900
Co	6.43	Sb	10,000
Cr	162-1,200	Se	20
Cu	15,100-142,000	Sn	7,000
Fe	115,000-399,000	Sr	81.4-740
K	857	Ti	3,600
Mg	6,140	V	660
Li	55.6	Zn	270-21,800

Source: (Brewer, 1997)

Table 5 Mean metal concentrations in brake linings

Vehicle type		Front linings (mg/kg)						Rear linings (mg/kg)					
		Cd	Cr	Cu	Ni	Pb	Zn	Cd	Cr	Cu	Ni	Pb	Zn
New passenger cars		11.6	137	117,941	141	9,052	23,830	8.02	73.4	92,198	69.6	18,655	16,498
Old passenger cars		8.6	92	71,990	182	13,651	17,696	3.5	151	51,240	122	9,110	7,197
Heavy goods vehicles	Volvo	<10.3	171	15,000	118	656	14,900			As front linings			
	Scania	<1.99	157	76.9	110	158	127			As front linings			
Buses	Volvo	<10.1	<20.1	27,300	140	1,020	18,500			As front linings			
	Scania	<1.98	118	88.3	178	441	172			As front linings			

Source: (Westerlund, 2001)

Chemical composition of brake wear particles should be considered when trying to fully characterize them and assess their possible adverse effects on human health. Several epidemiology studies have correlated adverse health responses with the presence of specific chemical species like carbonaceous material and trace elements (heavy metals) in the ambient PM (Kelly & Fussell, 2012), (Ostro, Broadwin, Green, Feng, & Lipsett, 2006). **Table 6** provides an overview of the concentrations of the most common elements found in brake wear dust and PM.

Table 6 Trace element concentrations found in emitted brake wear dust.

Metal	Brake dust (mg/kg)	Metal	Brake dust (mg/kg)
Al	330–20,000	Mg	(1700)–83,000
As	<2.0–(110)	Mn	620–5640
Ba	(5800)–140,000	Mo	5.0–740
Ca	500–8600	Na	80–(5100)
Cd	<0.06–11	Ni	80–730
Co	12–42.4	Pb	4.0–1290
Cr	135–12,000	Sb	4.0–19,000
Cu	70–210,000	Sn	230–2600
Fe	1300–637,000	Ti	100–110,000
K	190–39,000	Zn	120–27,300

Source: (Grigoratos & Martini, 2014)

List of key tracers used by various researchers over the last decade for identifying brake wear is given in **Table 7**. Almost researcher suggests that to consider Cu and Fe.

Table 7 Overview of most common key tracers used for brake wear emission calculation

Reference	Tracer
(Sternbeck, Sjödin, & Andréasson, 2002)	Ba, Cu, Sb
(Adachi & Tainosho, 2004)	Ba, Ce, Cu, Fe, La, Sb, Ti, Y, Zr
(Sanders et al., 2003)	Ba, Cu, Fe, Sb, Si, Zn
(Uexküll, Skerfving, Doyle, & Braungart, 2005)	Cd, Cu, Pb, Sb, Zn
(Iijima et al., 2007)	Ba, Cu
(Iijima et al., 2008)	Sb
(Kukutschová et al., 2011)	Cu, Cd
(Harrison et al., 2012)	Cu, Fe, Mo, Sb, Sn, Zn, Zr
(Kwak, Kim, Lee, & Lee, 2013)	Cu, Mo, Sb
(Gietl, Lawrence, Thorpe, & Harrison, 2010)	Ba, Cu, Fe, Sb
(Keuken, Denier van der Gon, & van der Valk, 2010)	Cu
(Amato et al., 2011)	Cu, Cr, Fe, Sb, Sn, Zn
(Apeagyei, Bank, & Spengler, 2011)	Cu, Ba, Fe, Mo, Ti, Zr
(Duong & Lee, 2011)	Cu, Ni
(Song & Gao, 2011)	Sb, Cu, Fe, Pb
(Harrison et al., 2012)	Sb, Cu, Fe, Pb
(Lawrence et al., 2013)	Ba, Cu, Fe, Mn, Ni, Pb, Sb
(Varrica, Bardelli, Dongarrà, & Tamburo, 2013)	Sb

Source: (Grigoratos & Martini, 2014)

It is obvious that results from the studies on brake wear vary as each study was performed on the various factor(s) contributing to brake wear PM emissions.

Effects of braking behavior on brake wear PM emissions and braking temperature

Braking behaviors are effect to brake wear as depicted in **Figure 8**. The half face parabola relationship between $PM_{2.5}$ and deceleration, higher deceleration affects to higher $PM_{2.5}$ emission rate.
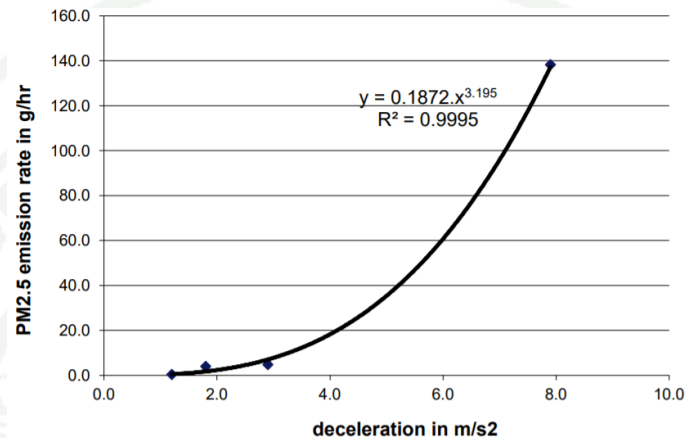
Figure 8 Brake wear $PM_{2.5}$ emission rates for light duty vehicles as a function of deceleration rate
Source: (U.S. Environmental Protection Agency, 2014)

Several demographic characterizations of brake wear particles, given in **Figure 9**, the size distribution of wear particles in the continuous, low-speed tests is shown in **Figure 9(a)**. There are two peaks in the frequency plots. The first peak occurs around 350 nm for all nominal contact pressures. The particle size at which the second peak in frequency occurs becomes bigger as the pressure increases. The particle size for the second peak is 2, 7, and 15 µm for 0.125, 0.375, and 0.625 MPa pressure, respectively. The use of discontinuous contact conditions did not affect the size of sub-micron wear particles, as shown in **Figure 9(b)**. However, it tended to reduce the particle size at which the second frequency peak occurs. **Figure 9(c)** shows the size distribution of wear debris for high-speed tests. As in previous tests, the first peak occurs around 350 nm. The location of the second peak is 3, 5, 6 µm for 0.75, 1.0, and 1.25 MPa pressure, respectively.
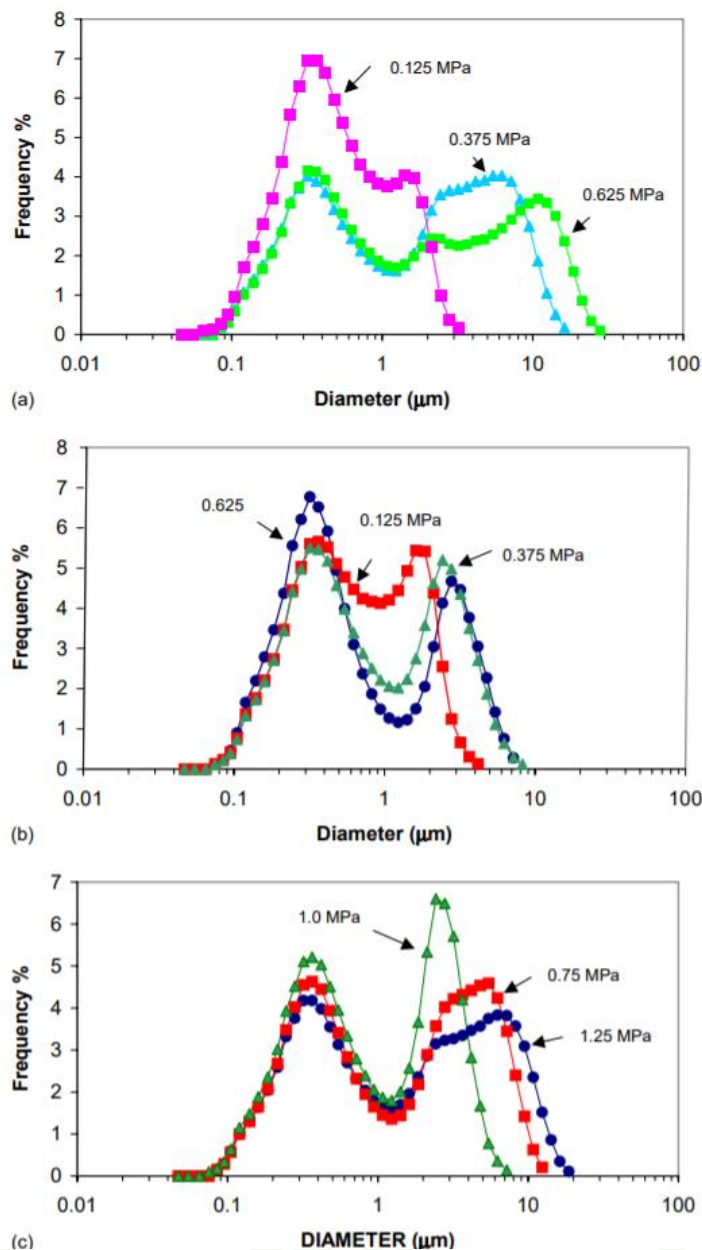
Figure 9 Size distribution of wear particles generated during the (a) low-speed, continuous tests (sliding speed = 0.275 m/s); (b) low-speed, discontinuous tests (sliding speed = 0.275 m/s) and (c) high-speed tests (sliding speed = 5 m/s).
Source: (Mosleh, Blau, & Dumitrescu, 2004)

It is reasonable to assume that the accumulation modes (50 – 1,000 nm) and coarse modes (>1,000 nm) of comparable prominence. Two aspects of these data are intriguing. First, coarse mode particle sizes are strong functions of brake styles; indeed, continuous braking and high contact pressures seems to facilitate growth or, rather, to favour agglomeration over fragmentation. The accumulation modes, by contract, were relatively indifferent to braking style. Secondly, accumulation modes are according to classical notions of aerosols that is stem from material disintegration. Conjecturally, frictional heating brought about decomposition, and the resulting

emission of some unknown vapour, the nucleation of which formed nanoparticles and the agglomeration of which formed the accumulation modes. Measurements of particle composition pointed to the brake pad as the parent material for these accumulation modes.

Scanning electron microscopy (SEM) of wear particles collected from continuous tests showed large particle agglomerates. These agglomerates consist of sub-micron and micron-sized particles in a variety of shapes. **Figure 10** are SEM micrographs of wear particles agglomerates generated during low and high-speed tests.
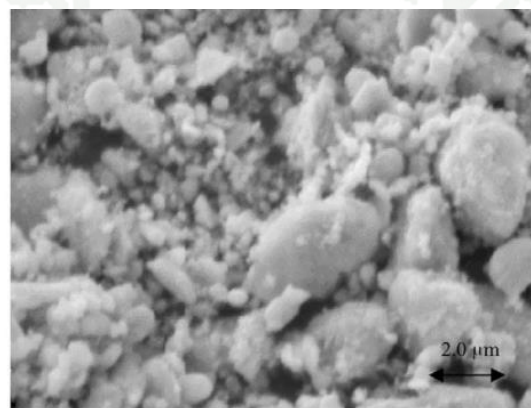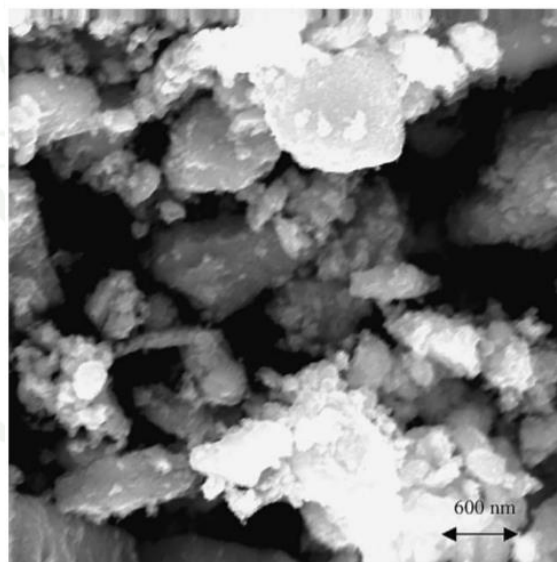
Figure 10 Wear particles of (a) low-speed continuous tests (contact pressure = 0.125 MPa, sliding speed = 0.275 m/s) and (b) high-speed tests (contact pressure = 0.75 MPa, sliding speed = 5 m/s)
Source: (Mosleh et al., 2004)

The relationship between driving cycle (braking behaviors) and PM from brake pad as shown in **Figure 11**, shows an example time series for vehicle speed and mass concentrations (mg/s/wheel) of PM10 and PM2.5 during typical JC08 and JE05 test cycle experiments (runs #1 and #10). Run #1 for each vehicle corresponded to a

cold start for the exhaust test, which resulted in lower PM emissions compared with run #10, which corresponded to a hot start. There were no significant differences in the peak emission patterns and large peaks of brake wear particles appeared during the highway-driving mode between 1040 and 1230 s for JC08 and between 1410 and 1840 s for JE05. However, the details of the emission patterns varied between different brake assemblies. The time-resolved emission profiles for PM_{10} and $PM_{2.5}$ were similar, particularly for vehicle III, which had almost similar levels of PM_{10} and $PM_{2.5}$ emissions. This suggests that both fine particles (> 2.5 µm) and coarse particles (2.5 – 10 µm) significant components of break wear particles.
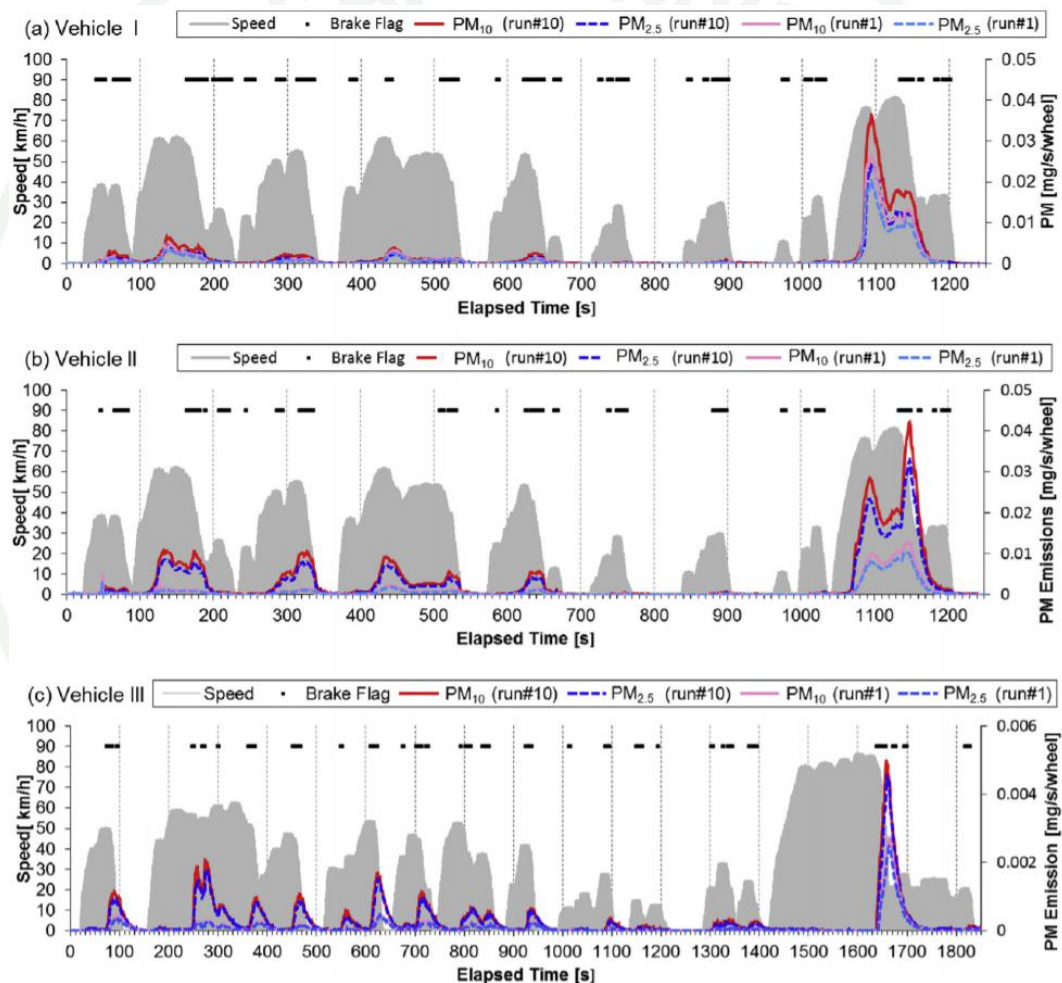
Figure 11 Time series profiles of brake wear particle mass emissions: (a) vehicle I; (b) vehicle II; and (c) vehicle III.
Source: (Hagino et al., 2016)

The time series pattern of vehicle I was roughly similar to vehicle II. Two peak types were found, one during the application of a braking force and one during wheel rotation. The first was obtained during a braking event (**Figure 11**) and indicated that brake wear particles were derived from the collision and friction between the disc and the pads. The second type was obtained during a rotor rotation and acceleration event (**Figure 11**) and these data suggest that brake wear particles

can also be derived from the detachment of wear particles from the surface of the brake and grooves. This was probably caused using a disc brake assembly with an open (not sealed) configuration (Iijima et al., 2008).

It is well known that the driving cycle (braking behavior) are consistent with the brake temperature. The recorded disc temperatures on the front left brake disc during the novel cycle are shown in **Figure 12**. The time-weighted, averaged brake temperature of the front discs was 50°C and the maximum temperature was 129°C. The timeweighted, averaged rear discs brake temperature was 43°C and the maximum temperature was 131°C. The mean ambient temperatures during testing were between 9 °C and 15 °C at a relative humidity between 50% and 90%.
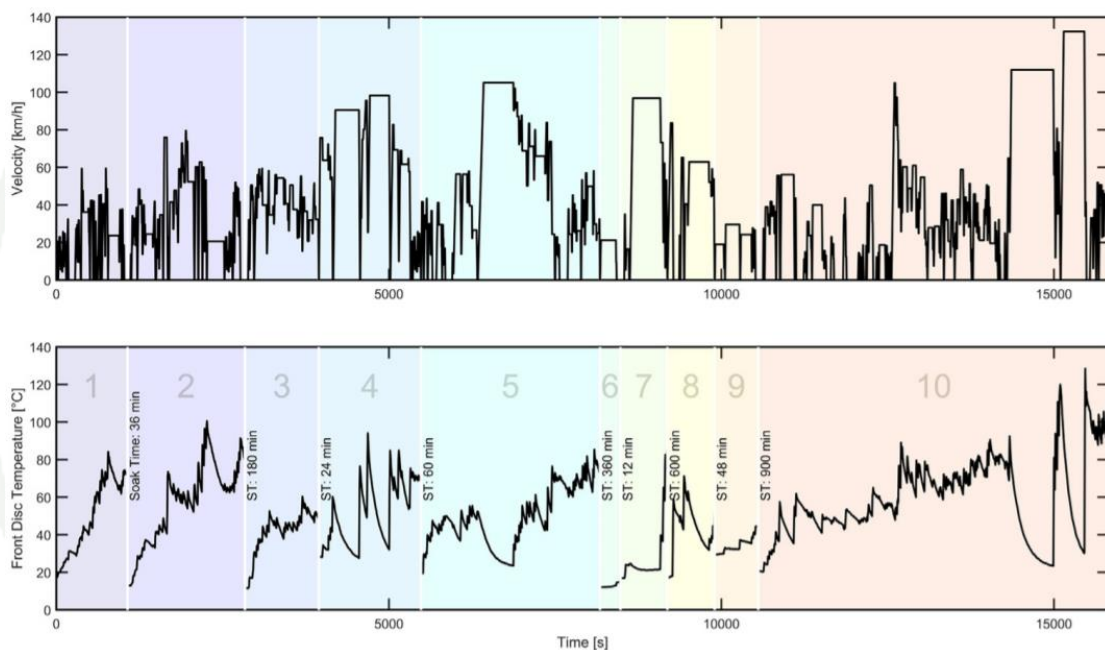
Figure 12 Top: Proposed novel brake cycle schedule (velocity vs time). Bottom: Brake disc temperature (front left)
Source: (Mathissen et al., 2018)

It is possible that the high temperature generated during braking can cause some of brake pad materials fall-out. The next chapter will discuss on effects of braking temperature on brake wear PM emissions.

Effects of braking temperature on brake wear PM emissions

High brake power resulting in high friction initiate to high brake temperature are consistent with **Figure 13**, shows comparatively the tribological behavior of materials M1, M2 and M6 as the test temperature was externally increased from room temperature to 300 °C. The expected transition from mild to severe wear occurred at disc temperatures between 180°C and 250°C, depending on the material, this testing is done by brake dynamometer. The composition of M1, M2 and M6 as shown in **Table 8**. It is clear that M1 consists of the highest amount of hard abrasives (Al_2O_3 and SiC) accompanied by mild abrasives (MgO and $(Fe, Mg)Cr_2O_4$). The M1 formulation is considered to have the most abrasive character while the abrasive effect of this friction material is balanced mainly by the presence of graphite and metal lubricants SnS_2. M2 friction material consists of obviously high amounts of ZrO_2 and low amounts of Al_2O_3 and the abrasive character of this formulation is balanced mainly by the presence of graphite, $K_2Ti_6O_{13}$ and also $BaSO_4$. The M6 formulation is the typical one for non-asbestos organic (NAO) friction materials.
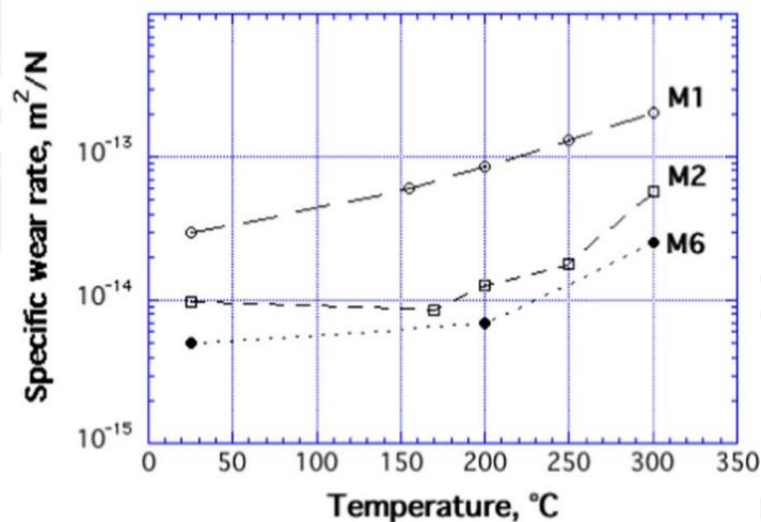
Figure 13 Specific wear rate for M1, M2 and M6 materials from pin-on-disc tests as a function of the disc temperature (external heating)
Source: (Perricone et al., 2018)

Table 8 The composition of brake pad

Phase (%Wt)	M1	M2	M6
Zinc – Zn	14.31	9.68	5.08
Graphite – C	39.28	26.51	31.98
Copper – Cu	11.16	16.03	9.00
Silicates–(K,Na)(Mg;Fe) $(AlSi_3O_{10})(OH)_2$	6.93	1.17	9.42
Potassium Hexatitanate–$K_2Ti_6O_{13}$	0.75	11.07	8.37
Barite – $BaSO_4$	0.00	7.85	22.88
Baddeleyite – ZrO_2	0.00	23.16	9.85
Fe-alfa – Fe	3.52	3.67	0.93
Moissanite – SiC	1.80	0.00	0.00
Chromite – $(Fe, Mg)Cr_2O_4$	5.61	0.00	0.00
Zincite – ZnO	2.25	0.15	0.00
Berndtite – SnS_2	2.46	0.00	1.13
Periclase – MgO	5.89	0.00	0.00
Sphalerite – (Zn,Fe)S	1.71	0.45	0.00
Corundum – Al_2O_3	4.33	0.26	1.36
Stibnite – Sb_2S_3	0.00	0.00	0.00

Source: (Perricone et al., 2018)

(Verma et al., 2016) tested the relationship of temperature and pin/disc brake, the experiment set up as in the **Figure 14**. The tests were carried out with a laboratory high temperature pin-on-disc rig, at the following controlled disc temperatures, starting from room temperature (25°C), 170°C, 200°C, 250°C and 300°C. A test was also conducted at 350°C but stopped before completion, the other conditions of the tests were: sliding speed of 1.31 m/s (corresponding to 500 rpm), applied pressure of 2 MPa and actual sliding distance of 4000 m, for a total duration of 50 min per test. The results are shown in **Figure 15**.
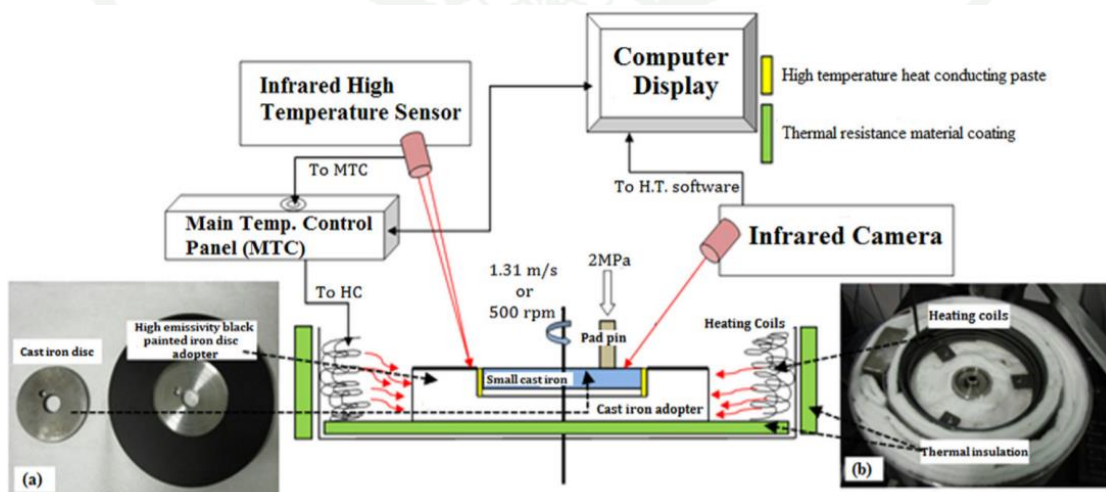
Figure 14 Schematic closed loop feedback high temperature wear test setup.
Source: (Verma et al., 2016)
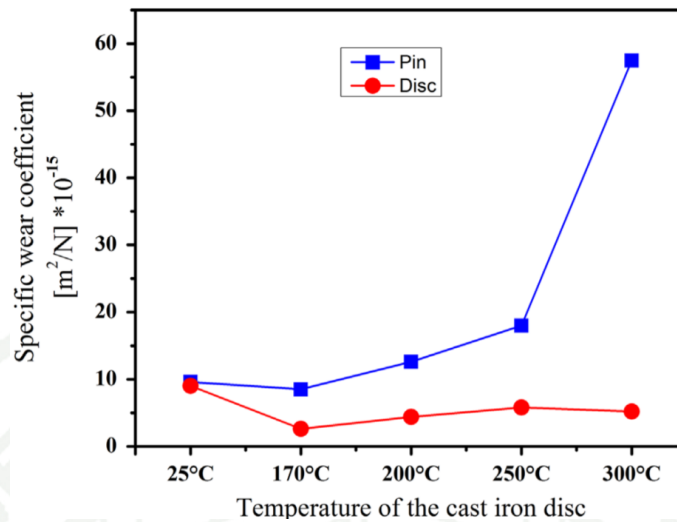
Figure 15 Specific wear behavior of pin and cast-iron disc at different temperatures.
Source: (Verma et al., 2016)

For temperatures up to 170 °C, a nearly constant wear coefficient is recorded, with values that are typical of a mild wear regime. Above this temperature, a sharp change in the wear coefficient, corresponding to a sharp increase in the wear rate, drives the system into a severe wear regime. As expected, no significant change in the wear behavior of the disc is observed over the considered temperature range. The specific wear coefficient, K_a, was calculated using the following expression **(1)** (Hutchings, 1992) and specific wear volume, W, was calculated from the following relation, Equation **(2)** (Verma et al., 2016).

$$K_a = \frac{V}{sF_N} \tag{1}$$

where V is the measured wear volume, s is the sliding distance and F_N is the applied load. The estimated wear rates (given by: W=V/s).

$$W = \frac{W_1 - W_2}{\rho d} \tag{2}$$

where W_1 and W_2 are the weights of the pin before and after each test respectively, ρ is the density of the friction material and d is the sliding distance.

(Vainio, 2021) observe the braking temperature to investigate a behavior of PN (Particle number) by brake enclosure design as shown in **Figure 16**. Where the brake temperature reached 150°C and high PM emissions were observed as shown in **Figure 17** (grey line is brake event, red line is brake temperature, yellow line is eFilter current, blue line is ELPI+, and orange line is Condensation Particle Counter).
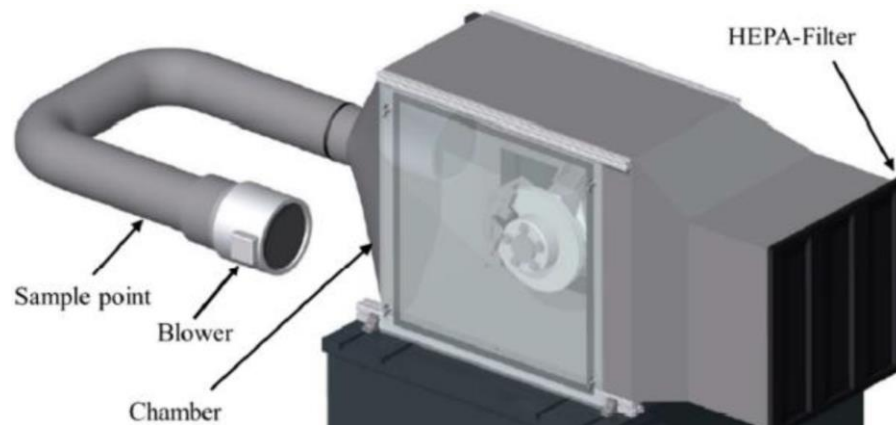
Figure 16 Brake enclosure measurement
Source: (Hesse et al., 2021)
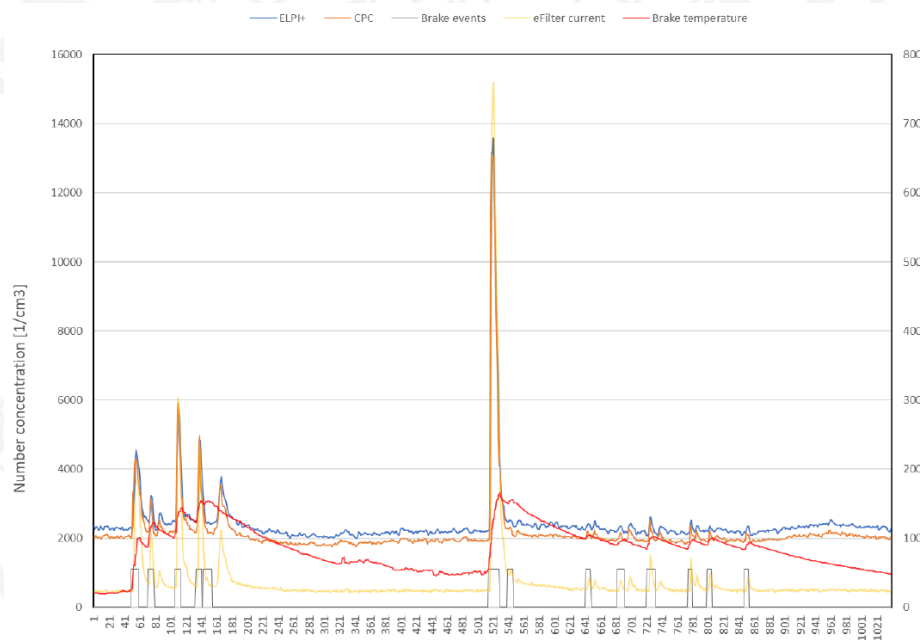
Figure 17 PN concentration (ELPI and CPC), eFilter, brake events and brake
temperature
Source: (Vainio, 2021)

Based on the reviews, it is clear that brake temperature rises when braking force increases. The following chapter will discuss about influence of payloads on brake wear PM emissions.

Influence of payloads on brake wear PM emissions

It can be hypothesized that Brake wear should be influenced by vehicle weight. Research by (Garg et al., 2000) distinguishes between brake emissions from small cars, large cars and large pickup trucks. They found that the brakes of large cars emit 55% more TSP, PM_{10} and $PM_{2.5}$ than small cars. Large pickup trucks were found to emit more than double the amount of particulates compared to small cars. The estimated emission factors for all other categories of vehicles (between light-duty and heavy-duty) were derived by linearly interpolating the rates between light-duty and combination heavy-duty vehicle classes by their respective weights as shown in the **Figure 18**. This is based on a rather simple engineering hypothesis that the relative brake emissions are proportional to the weight of the vehicle classes relative to light-duty and heavy-duty vehicles. The hypothesis is based on the assumption that relative mass of the vehicles is proportional to the relative energy required to stop the vehicles. **Figure 18** shows the relative mass of light- and heavy-duty vehicles. The corresponding emission rates are in **Table 9**.
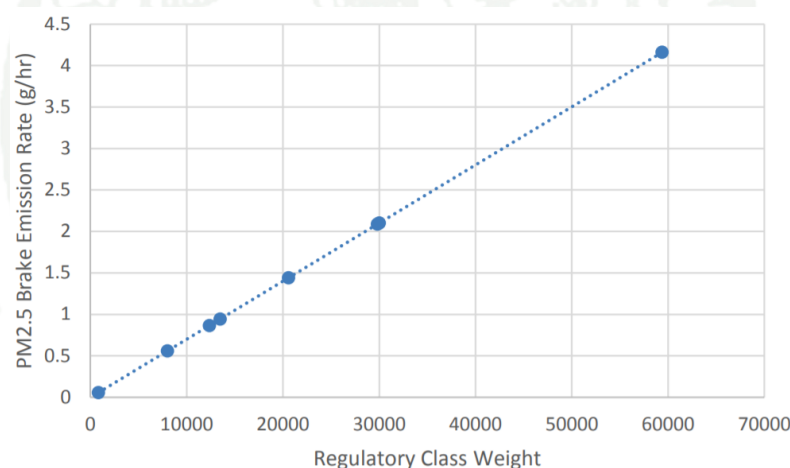
Figure 18 Interpolated Brake $PM_{2.5}$ Emission Rates by Regulatory Class Weight. Passenger Cars and Combination Heavy duty Trucks Define the Slope.
Source: (U.S. Environmental Protection Agency, 2014)

Table 9 Scaling Emission Rates to their vehicle class.

	regclasswt in lbs.	g/hr
MC	830	0.056
LDGV	8000	0.56
LDT	13,474	0.94
HD<=14k	12,358	0.87
HD>14k	20,575	1.4
MHDD	29,808	2.1
HHDD	59,369	4.2
Urban Bus	30,000	2.1

Source: (U.S. Environmental Protection Agency, 2014)

(Ekathai, Chalermpol, & Worawat, 2021) focuses on investigating of non-exhaust PM emissions emitted from a Hybrid Electric Vehicle (HEV) during a braking sequence. The test is done by using a PM Mobile onboard measuring equipment attached directly onto a moving vehicle at the spot nearby the center cap bore of the front wheel as shown in **Figure 19**.

Figure 19 Measurement setup with instruments
Source: (Ekathai et al., 2021)

Based on this experiment (**Figure 20** and **Figure 21**), the additional payloads of 60-70 kg increase the amount of non-exhaust $PM_{2.5}$ and PM_{10} emissions almost 25%. The effects of increasing payloads on $PM_{2.5}$ and PM_{10} emissions can be clearly observed as a linear relationship. However, for PM_1 emissions, when increasing payloads, a certain cut point is observed at the payload of 130 kg. Adding payloads more than 130 kg do not affect the amount of PM_1 emissions.
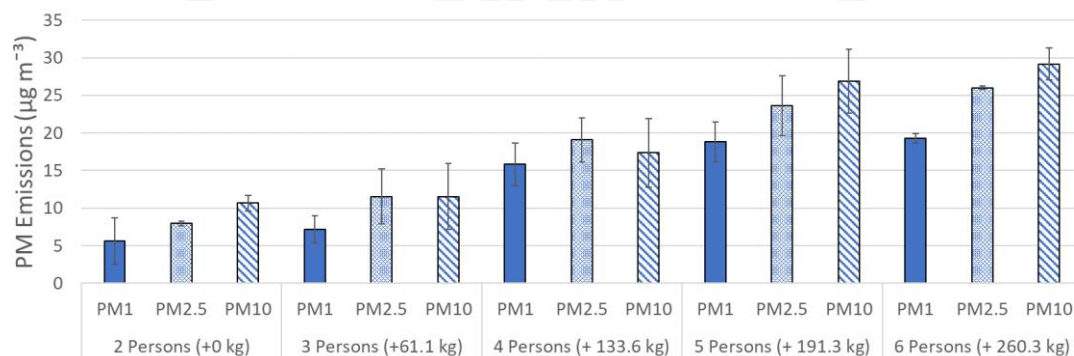
Figure 20 Effects of payloads on non-exhaust PM_1, $PM_{2.5}$, and PM_{10} emissions
Source: (Ekathai et al., 2021)
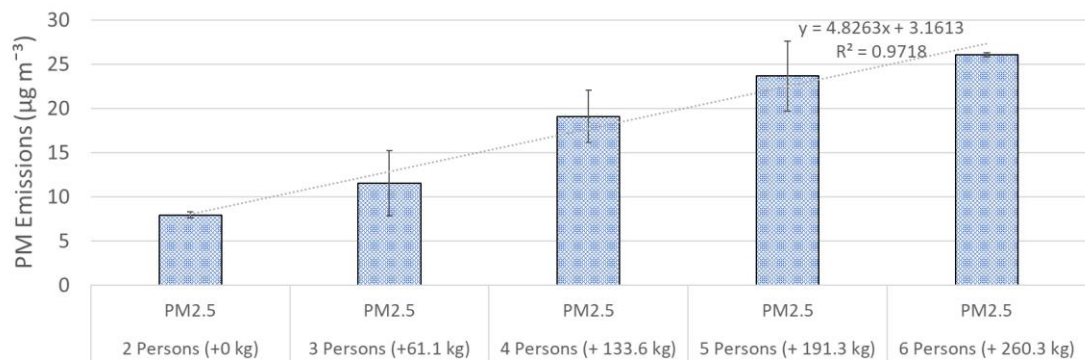
Figure 21 Non-exhaust PM$_{2.5}$ emissions under various payloads, with the dotted line indicating a linear relationship
Source: (Ekathai et al., 2021)

Vehicle weight was expected to play a role in brake wear emission factors, since brake wear is affected by weight. Several studies provided evidence that there is indeed a positive correlation between weight and brake wear emissions.

Influence of type of vehicle on brake wear PM emissions

(Hagino et al., 2015) investigate the airborne brake wear particles and evaluate the resuspension regarding $PM_{2.5}$ and PM_{10} through real-time particle mass measurements using dust monitors of three vehicles. The airborne brake wear particles emission was measured using a brake dynamometer (**Figure 22**) established with an engine dynamometer, an enclosure (chamber), and a constant volume sampling system. This system allows measuring and investigating airborne brake wear particles. The real-time mass emission measurements were performed under constant driving, different initial wheel speeds and acceleration/deceleration conditions. Braking is deceleration the vehicle from 60 km/h to 0 km/h in 17 seconds and driving is acceleration the vehicle from 0 km/h to 60 km/h in 29 seconds.
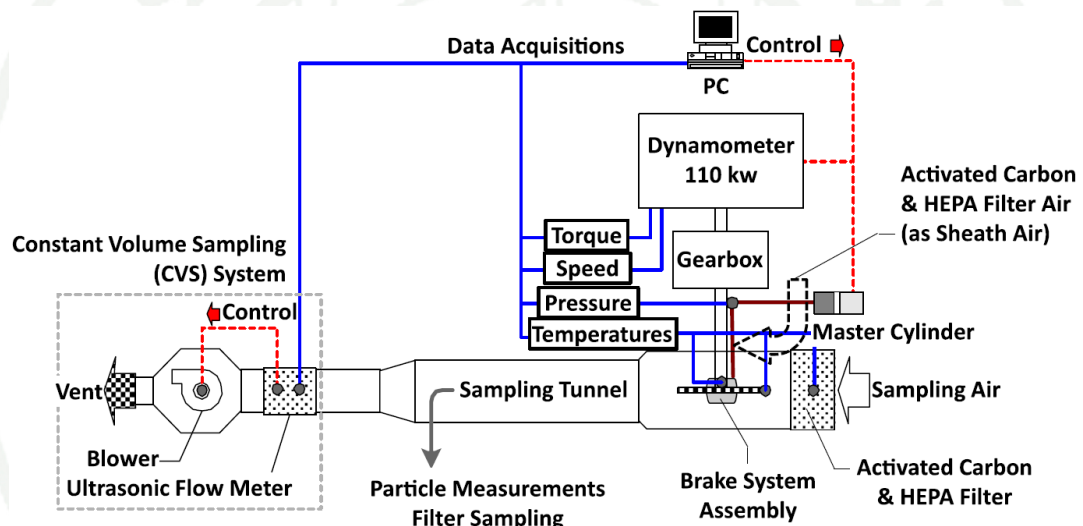
Figure 22 Scheme of the brake dynamometer assembly and measurement instruments.
Source: (Hagino et al., 2015)

Figure 23 shows the temporal profiles of the vehicle speed and the mass concentration (mg/s) of $PM_{2.5}$ and PM_{10} during a deceleration of 1.5 m/s^2 and an initial speed of 60 km/h. Three types of commercially available brake assemblies, widely found in Japanese two-passenger cars and trucks in 2005–2010, were used for the abrasion tests. The two-passenger cars (Vehicles I and Vehicle II) had disc brake systems, while the middle truck (Vehicle III) had a drum brake system.
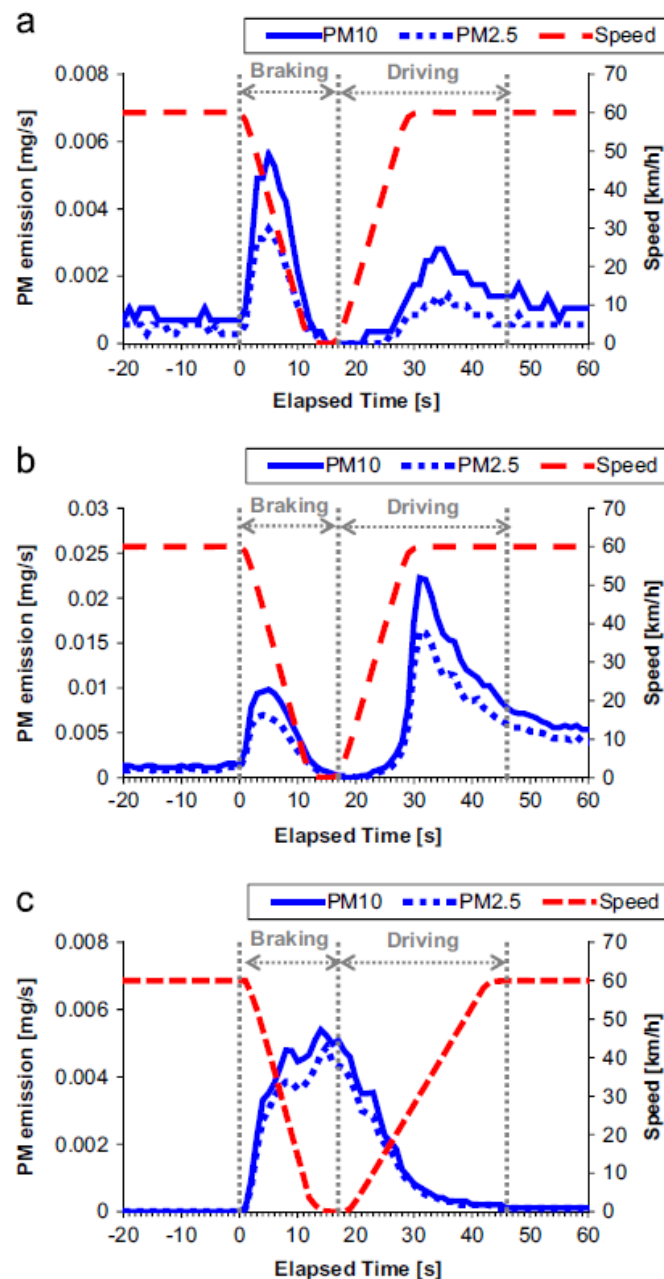
Figure 23 Time series profiles of brake dust particle mass emissions obtained during the measurement of particle mass concentrations as PM_{10} and $PM_{2.5}$ for vehicles I, II, and III.

Source: (Hagino et al., 2015)

For the braking event (only deceleration), the emissions for the disk brake systems (vehicles I and II) tended to increase with the initial speed for the same deceleration (e.g., 1.5 m/s²) (**Figure 24** (a) and (c)). For the same initial speed (e.g., 60 km/h), the mass emissions tended to increase with increasing deceleration. Oppositely, the mass emissions for the drum brake system (vehicle III) tended to increase with increasing initial speed but showed no significant difference with deceleration. These tendencies were also observed for the total (deceleration and acceleration) $PM_{2.5}$ and PM_{10} mass

emissions. For an initial speed of 60 km/h and a deceleration of 3 m/s^2 (1.5 m/s^2 for vehicle III), the mass fractions of PM$_{2.5}$ to PM$_{10}$ were 57% (vehicle I), 72% (vehicle II), and 85% (vehicle III), respectively. The emission weight of the fine particles (2.5 µm) was then more significant than that of the coarse particles (2.5–10 µm). No significant changes were reported in previous studies, with a unimodal mass size distribution of brake wear particles and a mass weighted mean diameter of 2 – 6 µm (Iijima et al., 2007), (Iijima et al., 2008), (Sanders et al., 2003) and (Garg et al., 2000).
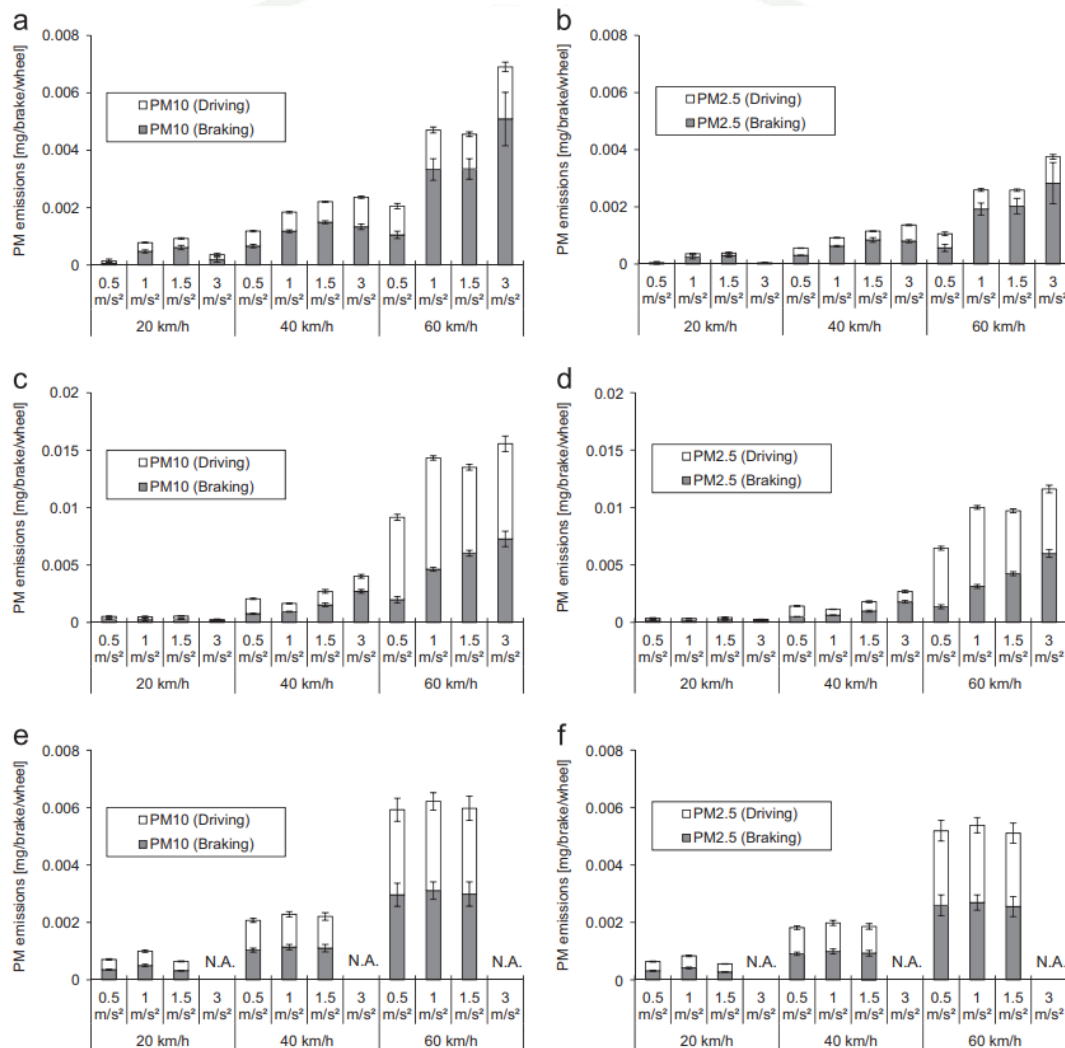
Figure 24 Averaged brake dust emissions as PM$_{10}$ and PM$_{2.5}$ for each braking and driving event for vehicles I, II, and III. N.A: not available. (a, b) is vehicle I. (c, d) is vehicle II. (e, f) is vehicle III.
Source: (Hagino et al., 2015)

HYPOTHESIS OF RESEARCH

The research gap analysis from past literatures is as the follows:

1.) Effects of braking behavior on brake wear PM emissions and braking temperature -> Braking behavior influences emissions coupled with brake temperature?
2.) Influence of type of vehicle on brake wear PM emissions -> Different vehicle effects on brake wear when driving in real-word test?
3.) Influence of payloads on brake wear PM emissions -> Weight of vehicle effects on brake wear PM emissions?
4.) PM formation from brake wear mechanism -> The amount of Carbon content (IC/OC) direct measure from braking?
5.) Effect of braking temperature on brake wear PM emissions -> Where is the cut-point temperature. How does it influence for PM characteristics and morphology?

It is obvious from all the above-referenced literatures that: 1.) driving cycle (braking behavior), 2.) braking temperature, 3.) payloads and 4.) types of vehicles contribute to concentration, characteristics, and morphology (chemical and physical compositions) of brake wear particles. Furthermore, most of the above studies were performed using brake dynamometers to measure brake wear (simulation in laboratory). While this research develops a new method to determine more accurate brake wear PM emissions from real-world driving as well as identifies factors that contribute to brake wear PM emissions.

The expected or anticipated benefit gains from this research is as the follows:

1.) Capability to identify factors affecting PM formation from vehicle braking system.
2.) Understanding the physical and chemical properties of PM from brake wear (from factors that found in 1.)).
3.) Fundamental understanding(s) of PM formation mechanism from vehicle braking system.

MATERIALS AND METHODS

Tested vehicles

This research work is performed by using two types of vehicles (passenger car and SUV). All these vehicles use semi-metallic brake pad. Details of the selected vehicles are as the follows:

1. Mid-size passenger car

Mid-size passenger car is commonly used in Thailand. The specification of the tested vehicle is shown in **Table 10**.

Table 10 Specifications of Mid-size passenger car

Parameter	Index
Engine	
Type	SOHC 4 Cylinder 16 valve i-VTEC
Capacity (cc.)	1,997
Max. Power (kw (ps) / rpm)	114 (155) / 6,500
Max. Torque (Nm (kg-m) / rpm)	190 (19.4) / 4,300
Braking system	
Front	Ventilated Disc
Rear	Disc
Dimension (mm.)	
Length * Width * Height	4,870 * 1,850 * 1,465
Ground clearance	141
Weight (kg.)	1,525
Wheel size	17 * 7.5J
Tyre size	225 / 50 R17

2. Subcompact crossover SUV

Subcompact crossover SUV in this segment typically have limited off-road capabilities with the majority adopting front-wheel-drive layout. This tested vehicle is use internal combustion engine like a passenger car, but the weight of vehicle is less than passenger car with higher ground clearance. The specification of the tested vehicle is shown in **Table 11**.

Table 11 Specifications of Subcompact crossover SUV

Parameter	Index
Engine	
Type	DOHC 4 Cylinder 16 valve VTi-TECH
Capacity (cc.)	1,498
Max. Power (kw (ps) / rpm)	84 (114) / 6,000
Max. Torque (Nm / rpm)	150 / 4,500
Braking system	
Front	Ventilated Disc
Rear	Disc
Dimension (mm.)	
Length * Width * Height	4,323 * 1,809 * 1,653
Ground clearance	170
Weight (kg.)	1,290
Wheel size	17
Tyre size	215 / 55 R17

Sampling system

The choked flow condition as a compressible fluid reaches the speed of sound (i.e., has a Mach number of 1), pressure changes can no longer be communicated upstream as the speed of which these pressure changes are propagated is limited by the speed of sound. In a nozzle or restriction this has the effect of isolating the upstream side from the downstream side at the throat. Because of this effect any reduction in downstream pressure will have no effect on the flow rate, as the increased pressure differential is not 'felt' upstream of the restriction.

The establishment of choked flow can be identified as the point at which the ratio of the minimum fluid pressure to inlet pressure falls below the critical pressure ratio in the fluid. It should be noted that while downstream changes in pressure will not affect the mass flow rate when the flow is choked, changes in the upstream pressure may still have an effect as it will affect the local speed of sound at the throat, and thus change the mass flow rate at which the system becomes choked (Miller, 1996).

The principal standard for direct measurement of local particle mass flux in most gas-solid flows is provided by the isokinetic sampling system. The isokinetic sampling principle requires that the sampling probe which is aligned with the flow (iso axial) extracts airborne particulates at the sampling velocity matching the original undisturbed local flow velocity. In practice, the isokinetic sampling is closely approached but almost impossible to be rigorously realized. Several problems as the determination of flow velocity in the presence of significant amount of particles, the elimination of intrusive effect of the sampling probe, the interactions between particles and carrying fluid, the loss of particles to the wall deposition and particle bounce/reentrainment in the sampling tube are frequently observed. By these reasons, three types of sampling (e.g. **Figure 25**) can be carried out: isokinetic (sampling velocity=stream velocity) or two kind of an isokinetic sampling: over-sucking (sampling velocity>stream velocity), under-sucking (sampling velocity<stream velocity) (Gil, Ramos, Arauzo, & Román, 2009).
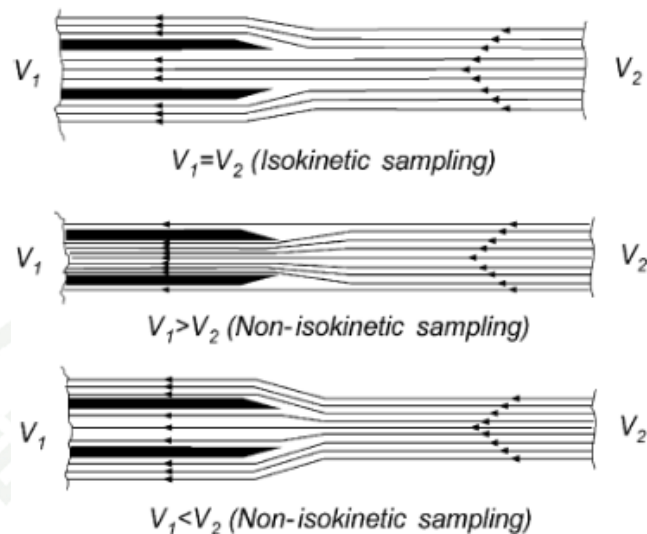
Figure 25 Isokinetic and non-isokinetic sampling
Source: (Diez-Lazaro, Hitchman, & Littlejohn, 2005)

The schematic of the current PM sampling system is shown in **Figure 26**. Brake wear particles from a semi-metallic disc brake of a test vehicles is drawn via the 17-inch left front wheel of the tested vehicle. For stable flow conditions, the air flow of the system is driven constantly by a vacuum pump at the end of the sampling system. A choked flow condition at the flow rate of 10 m^3/h is chosen and met by an orifice of 5 mm diameter. A cylinder chamber that has a diameter of 3 inch is installed to ensure the isokinetic sampling, the same velocity of the sampling point comparing to the required flow rate of PM measuring devices. This sampling system has been under patent registered (more details are shown in **Appendix Figure 1**).
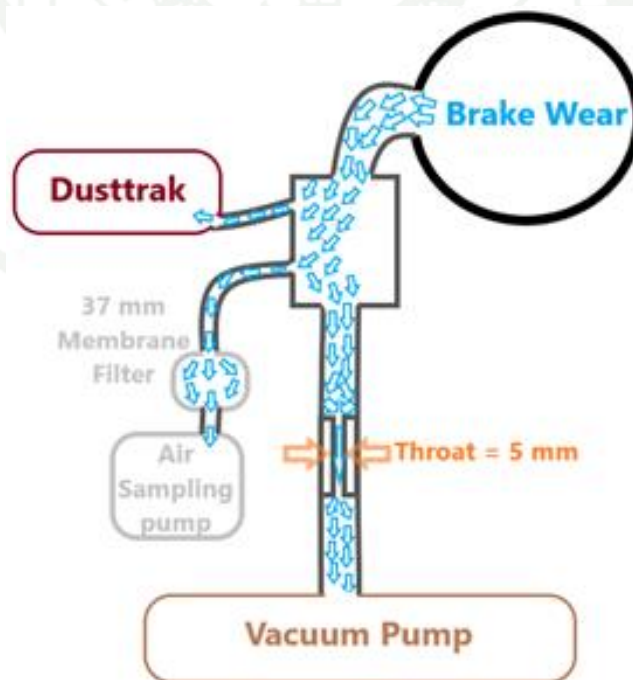
Figure 26 Schematic of test vehicle with the current experimental setup

The measurement concept is based on the Constant Volume Sampling system (CVS) to ensure the isokinetic sampling and choked flow conditions. PM is collected downstream of the experimental setup for gravitational analysis. Isokinetic sampling techniques are adopted to prevent skewed particulate concentration measurements due to inertial effects of particles as they enter a sampling nozzle. The idea is to sample at the same velocity of the gas stream so that the streamlines in the vicinity of the nozzle are straight (Sloley, 2012). Turning in the streamlines near the nozzle can cause heavier particles to miss the nozzle, thus skew the measured value of concentration (Brockmann, Lucero, Romero, & Pentecost, 1993). For the current setup, (Ilea & Iozsa, 2018) found out that in the study of aerodynamic of flow around a wheel of a vehicle, the velocity of vehicle is about 3 times of the fluid flow velocity around the wheel. Since the average velocity of the current study's conditions is around 30 km/h, thus the velocity of fluid flow around the wheel should be at 10 km/h. The area of the gap inside the wheel is 0.001 m^2 (comes from measurement). Therefore, the flow rate is chosen as 10 m^3/h. This value is based on the vehicle velocity ranging from 0 - 60 km/h, the experimental matrix for the current study under tested driving cycle and ISO 21994:2007 standard.

The apparatus is use in sampling system are as follows:

1. Vacuum pump

The high negative pressure of the vacuum pump (DSS-6E) (placed it in the vehicle) is shown in **Figure 27**. The specifications of DSS-6E appear in **Table 12** and the graph of performance is shown in **Figure 28**.

Figure 27 Vacuum pump inside vehicle

Table 12 Specification of vacuum pump (DSS-6E)

Parameter	Index
Normal Speed (rpm)	1,450
Discharge Capacity (l/m)	450
Usual Exhaust Pressure	0.5 kg/cm^2
Pipe Orifice	3/4 inches PT
Motor Rating	3 Phase 0.75 kw 4P
Dimension (Length * Width * Height) (mm.)	560 * 270 * 265
Weight (kg.)	27
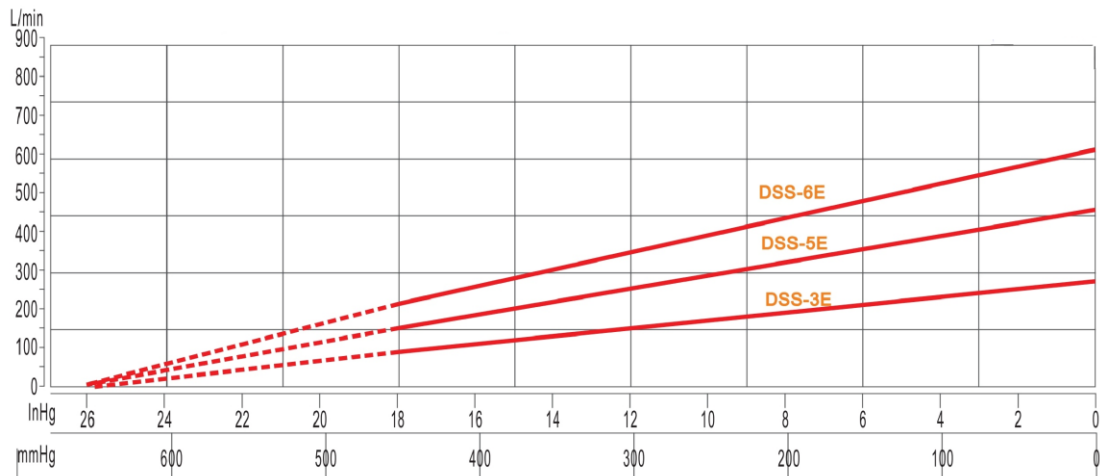
Figure 28 graph performance of DSS-5E

For stable flow conditions, the flow rate of the inlet tube must be equal in every test condition, that is, this experiment is set up to maintain choked flow conditions (Nertrium, 2015). If pressure downstream of the throat (or the restriction) is decreased until equation **(3)** reaches choked flow conditions, the mass flow rate is constant. Equation **(4)** demonstrates the mass flow rate at choked flow conditions.

$$\frac{P_T}{P_0} \leq \left(\frac{2}{\gamma+1}\right)^{\gamma/(\gamma-1)} = 0.528, \, @ \, \gamma = 1.4 \tag{3}$$

$$\dot{m}_{air} = \frac{C_D A_T P_0}{\sqrt{RT_0}} \gamma^{1/2} \left(\frac{2}{\gamma+1}\right)^{(\gamma+1)/2(\gamma-1)} \tag{4}$$

Where: C_D is discharge coefficient,

　　　　　A_T is throat area (minimum flow area or restriction area) (mm^2),

　　　　　P_0 is upstream pressure (Pa),

　　　　　T_0 is upstream temperature (k),

　　　　　P_T is pressure downstream of the throat (or the restriction) (Pa),

　　　　　γ is specific heat ratio,

　　　　　R is gas constant

In the current setup, the geometrical flow area of the restrictor is 19.63 mm^2 (A_T) @ $D_T = 5$ mm and flow rate is 10 m^3/h. **Figure 29** indicates the choked flow condition by adjusting a vacuum pump until the flow rate is stable.
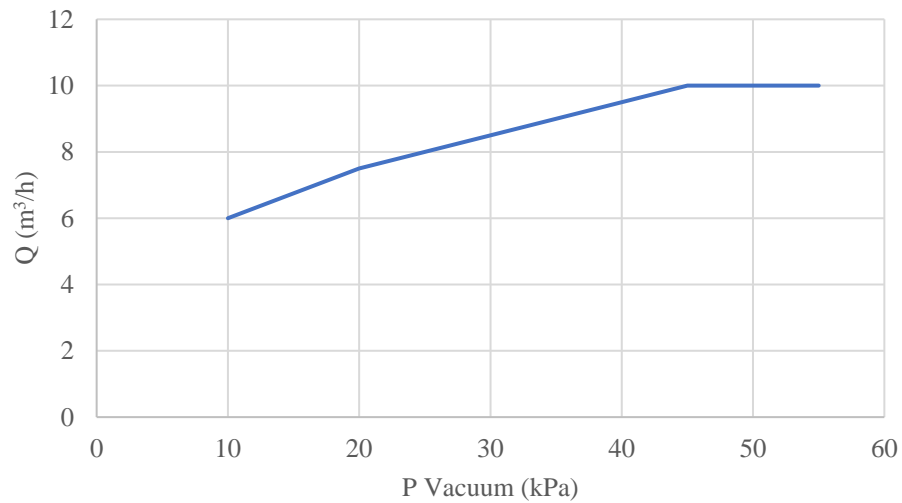
Figure 29 Choked flow condition setup in this experiment ($D_T = 5$ mm.)

2. Electrical System

This vacuum pump is a 220 Volts electrical appliance. Therefore, installations of a 6,000 Watts inverter and a 200 Ah / 12 Volts battery are applied.

3. Thermocouple type K

Thermocouple type K (Testo 176 T4 with 3 m Omega thermocouple wire type K) is installed nearby the left front disc brake to record brake temperatures during braking sequences as shown in **Figure 30**.
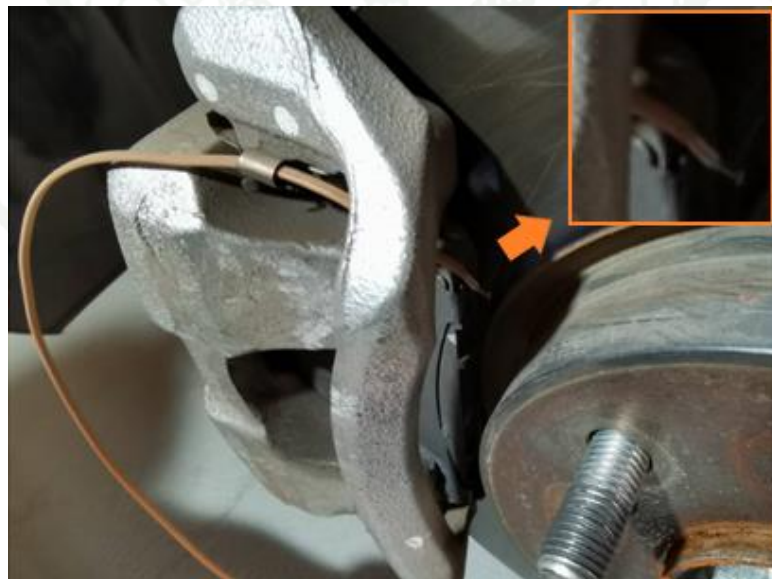
Figure 30 Thermocouple type K setup nearby a disc brake

PM measuring device

PM is sampled from 3-inch cylinder chamber to DustTrak DRX Aerosol Monitor 8533 where real-time PM concentration is measured by the light scattering method and to Gilian Gilair-5 Air Sampling Pumps where PM is collected for the gravitational analysis. The filter used in the current study is a Mixed Cellulose Ester (MCE) filter with 0.8 µm pore size and 37 mm diameters. This type of filter is selected due to (Kukutschová & Filip, 2018). This literature suggested PM size distributions from a Semi-metallic brake wear are mostly larger than 0.8 µm. More details of PM measuring device are as follow:

1. DustTrak DRX Aerosol Monitor 8533

DustTrak DRX monitors (as shown in **Figure 31**) are laser photometers that simultaneously measure five size segregated mass fraction concentrations. The desktop with external pump and handheld monitors are continuous, real-time, 90°, light-scattering laser photometers (as shown in **Figure 32**) that simultaneously measure size-segregated mass fraction concentrations corresponding to PM_1, $PM_{2.5}$, Respirable (PM_4), PM_{10}, and Total PM fractions (PM_{15}). They combine both particle cloud (total area of scattered light) and single particle detection to achieve mass fraction measurements. The benefit of this device is real-time mass concentration and size fraction readings, as well as data-logging allow for data analysis during and after sampling. The selected response time of this device in the current study is 1 second.

Figure 31 DustTrak DRX Aerosol Monitor 8533
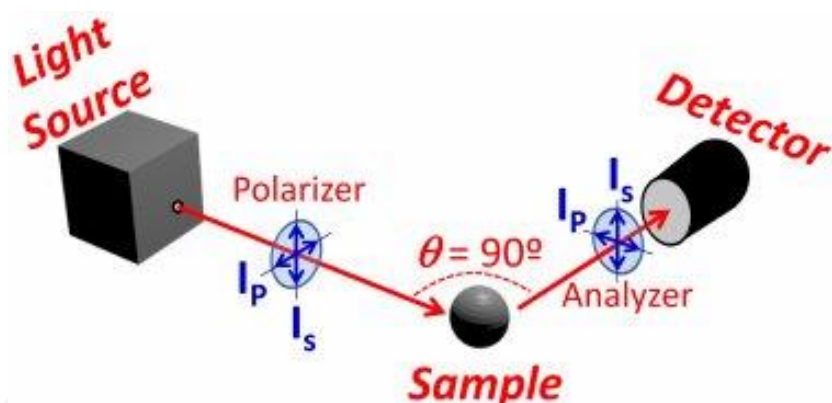
Figure 32 Configuration for performing right-angle light-scattering measurements
Source: (Barreda, Sanz, & González, 2015)

This size-segregated mass fraction measurement technique is superior to either a basic photometer or Optical Particle Counter (OPC). It delivers the mass concentration of a photometer and the size resolution of an OPC. Typically, photometers can be used at high mass concentration, but they do not give any size information (unless used with size selective inlet conditioners) and significantly underestimate large particle mass concentrations. OPC's provide size and count information; however, they do not provide any mass concentration information and cannot be used in high mass concentration environments. The DustTrak DRX can do both. The specifications are shown in **Table 13**.

Table 13 Specifications of DustTrak DRX Aerosol Monitor 8533

Parameter	Index
Sensor Type	90° light-scattering
Particle Size Range	0.1 to 15 µm
Aerosol Concentration Range	0.001 to 150 mg/m^3
Resolution	± 0.1% of reading or 0.001 mg/m^3
Flow Rate	3.0 L/min
Time Constant	User adjustable 1 to 60 seconds
Dimension (Length * Width * Height) (mm.)	135 * 216 * 224

2. Gilian Gilair-5 Air Sampling Pumps

The GilAir-5 (as shown in **Figure 33**) has one of the largest user bases of any air sampling pump worldwide. This reliable 5 liter per minute air sampling pump. Setting the flow rate on the GilAir-5 is a simple process that requires no special adjustment tool, so it spend less time configuring pumps.

Figure 33 Gilian Gilair-5 Air Sampling Pumps

Automatic constant flow - the most important feature of any sampling pump is standard on all GilAir-5 pumps. Flow is maintained within 5% of the initial set point, even with varying backpressures from flow restrictions or buildup of material on the filter. GilAir-5 pumps are suitable not only for conventional pull-through sampling media but also for bag sampling and other pressure applications. The specifications are shown in **Table 14**.

Table 14 Specifications of Gilian Gilair-5 Air Sampling Pumps

Parameter	Index
Flow Range	0.001 – 5 L/m
Constant Flow Control	± 5% of set flow at 1 – 5 L/m
Run time	8 hours minimum
Flow fault	If flow changes exceed 5%, fault icon appears.
Dimension (Length * Width * Height) (mm.)	51 * 100 * 90

PM is collected by Gilian Gilair-5 Air Sampling Pump, using a Mixed Cellulose Ester (MCE) filter with 0.8 µm pore size and 37 mm diameters (as shown in **Figure 34**). The schematic diagram of Gilian Gilair-5 Air Sampling Pumps (ASP) with MCE filter paper is shown in **Figure 35**.
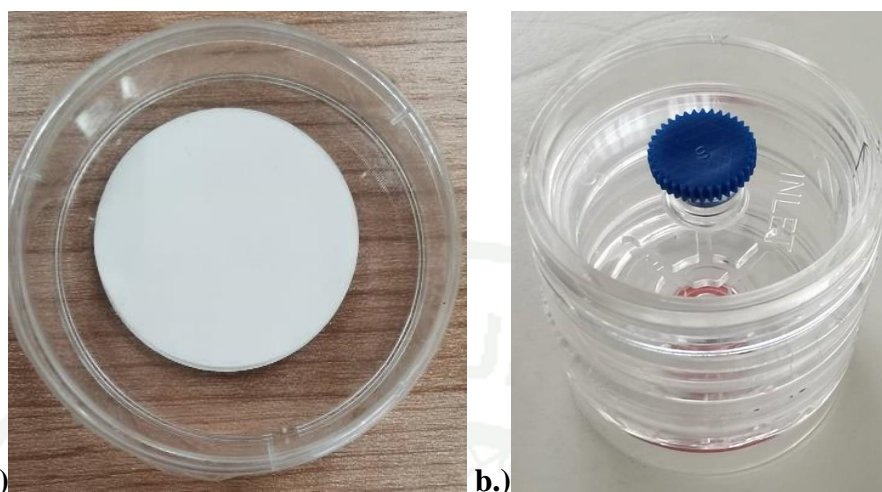
Figure 34 a.) MCE filter with 0.8 µm pore size and 37 mm diameters, b.) 37 mm filter holder

Figure 35 Schematic Diagram of Gilian Gilair-5 Air Sampling Pumps with MCE filter paper

The chemical compositions, by Energy Dispersive x-ray Spectroscopy (EDS), of blank MCE filter paper is shown in **Table 15** (Wt% is percentage by weight and At% is percentage by atomic). There are Oxygen (O), Carbon (C), and Nitrogen (N) sorted in weight in descending orders. All carbon component (TC) is organic carbon (OC) as shown in **Figure 36** (by TC/OC method).

Table 15 Chemical compositions of blank MCE filter paper

Element	Wt%	At%
C	37.11	43.49
N	09.41	09.45
O	53.48	47.05
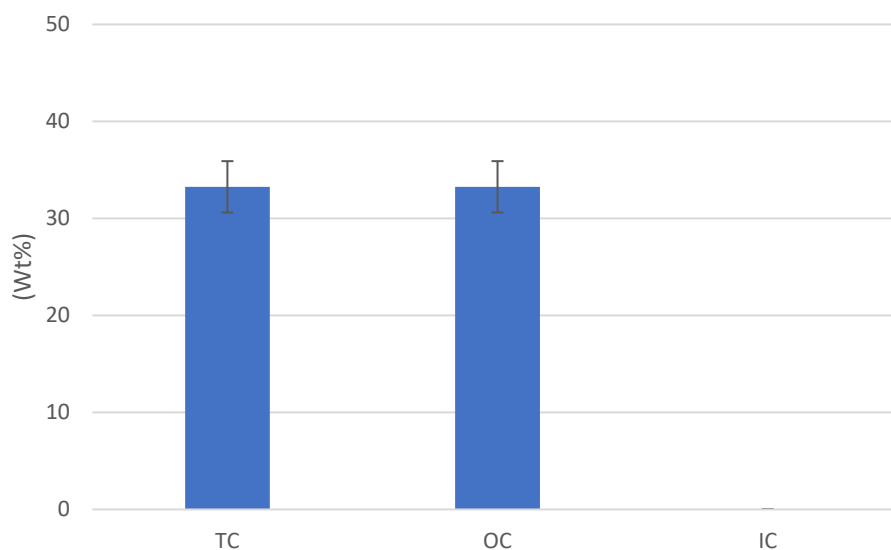
Figure 36 Carbon component of blank MCE filter paper

The microstructure of blank MCE filter paper is shown in **Figure 37** (by Scanning Electron Microscope (SEM) magnifying power 20,000x). The texture of filter is characterized by mesh fibers interconnected.
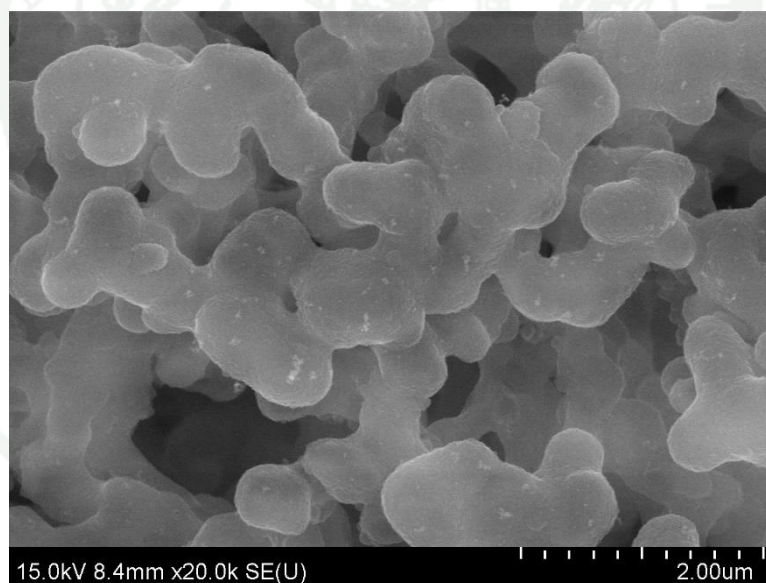
Figure 37 Microstructure of blank MCE filter paper

Measurement technique

This experiment using on-road measurement sampling to analyze the PM mass concentration, chemical compositions, and physicals of PM from brake wear. More details are as follow:

1. PM Mass concentration

PM Mass concentration are measured by Gilian Gilair-5 Air Sampling Pump with 4.5 L/min, captured in 37 mm membrane filters to perform gravimetric analysis by a six-digit microelectronic balance (shown in **Figure 38**); [except for the tests in passenger car, a four-digit microelectronic balance is used] and DustTrak 8533, using Light Scattering Laser Photometer method with 2.25 L/min. Mass concentration for both methods can be calculated by equation **(5)** (adapted from (Hearl, 1998)).

Figure 38 Microelectronic balance

$$C = \frac{(W2 - W1)}{V} \times 10^3 \qquad\qquad \textbf{(5)}$$

Where:　　　　C　　　is the concentration of total particulate (mg/m³),

　　　　　　　V　　　is the air volume sampled (L)

　　　　　　　W_1　　is tare weight of filter before sampling (mg),

　　　　　　　W_2　　is post-sampling weight of sample-containing filter (mg)

Particulate matter characteristics from brake wear are further studied in their chemical and physical compositions. The filter from brake wear is cut-off 1 x 1 cm at the center of the filter (with carbon coat), then placed onto the measuring devices, i.e., Scanning Electron Microscope (SEM) and Energy Dispersive X-ray Spectrometer (EDS). Parallelly, brake pad is also cut into small pieces (as shown in **Figure 39**) and analyzed.

Figure 39 Small pieces of brake pad

The size distributions of brake wear PM emissions are obtained using DustTrak 8533 light scattering laser photometer analyzer. This apparatus can detect particle sizes range from 0.1 to 15 µm and automatically segregated mass fractions PM_1, $PM_{2.5}$, Respirable (PM_4), PM_{10} and total PM (PM_{15}).

2. Chemical compositions

The specific characteristics of brake wear PM emissions are examined in a Scanning Electron Microscope (SEM) equipped with an Energy Dispersive X-ray Spectrometer (EDS). This EDS is capable in identifying both qualitative analysis and quantitative analysis chemical compositions of the collected PM emissions. The operational principle of this EDS is shown in **Figure 40**. Kα born from the electron of L layer is replace the electron of K layer. Kβ born from the electron of M layer is replace the electron of K layer. Lα born from the electron of M layer is replace the electron of L layer. Lβ born from the electron of N layer is replace the electron of L layer and so on.
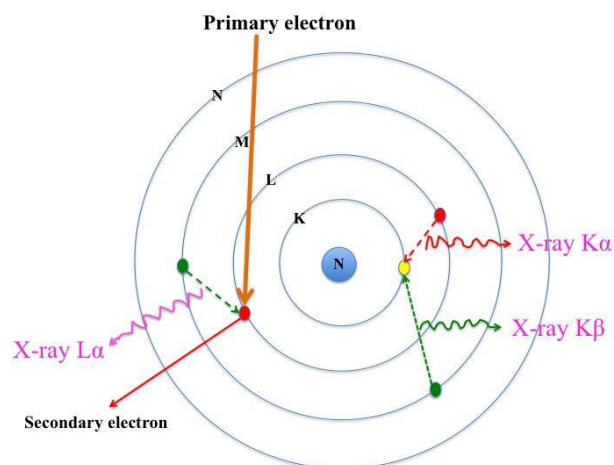
Figure 40 The operational principle of this EDS

Carbon compounds are known to be key components in PM. In analyzing these key carbon compounds, Total Carbon/Organic Carbon (TC/OC) method (SSM-5000A as shown in **Figure 41**) is used to measure the amount of Total Carbon (TC), Organic Carbon (OC) and Inorganic Carbon (IC), another name is EC.

Figure 41 SSM-5000A

The principle of operation is shown in **Figure 42**. The sample is delivered to the combustion furnace, which is supplied with purified air. There, it undergoes combustion through heating to 900°C with a platinum catalyst. It decomposes and is converted to carbon dioxide. The carbon dioxide generated is cooled and dehumidified and then detected by the NDIR. The concentration of TC (total carbon) in the sample is obtained through comparison with a calibration curve formula (1)). Furthermore, by subjecting the oxidized sample to the sparging process, the IC (inorganic carbon) in the sample is converted to carbon dioxide and the IC concentration is obtained by detecting this with the NDIR (2)). The TOC concentration is then calculated by subtracting the IC concentration from the obtained TC concentration (3)).
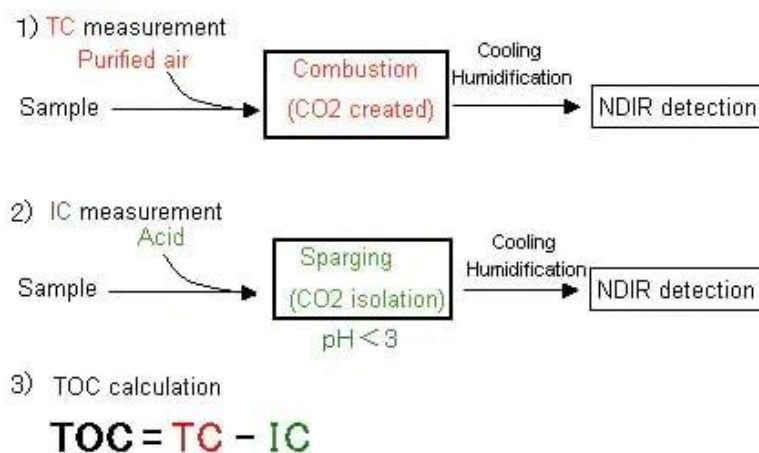
Figure 42 Principle of operation of TOC
Source: (Shimadzu, 2021)

3. Physicals of PM from brake wear

The physicals PM from brake wear are examined in a Hitachi: SU8020 for SEM as shown in **Figure 43**. The Scanning Electron Microscope (SEM) uses a focused beam of high-energy electrons to generate a variety of signals at the surface of solid specimens. The signals that derive from electron-sample interactions reveal information about the sample including external morphology (texture). The schematic diagram of SEM as shown in **Figure 44**.

Figure 43 Hitachi: SU8020 for SEM
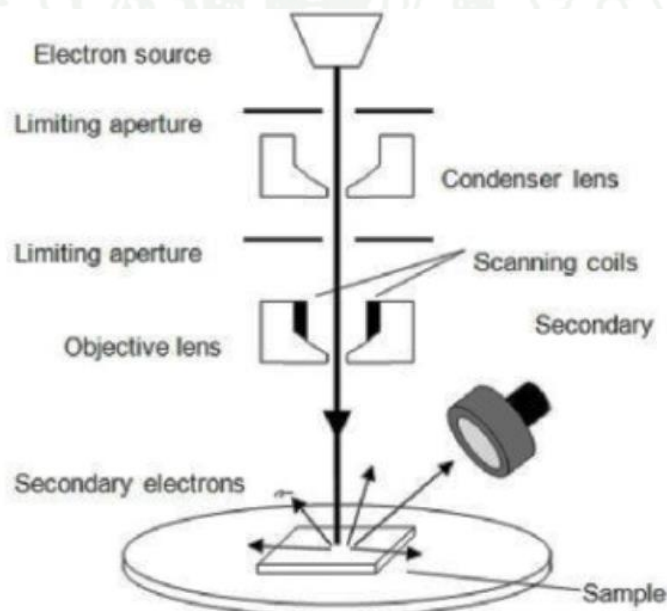
Figure 44 Schematic diagram of SEM
Source: (Mukhopadhyay, 2015)

In a typical SEM, a stream of electron beam is emitted from a cathode either thermionically or by electric field. The electrons are emitted from a field emission cathode. After emission, the electrons are accelerated by applying a gradient of

electric field. The beam passes through two electromagnetic lenses, which are called condenser lens (**Figure 44**). Finally, the beam passes through an electromagnetic scanning coil and is focused onto the sample. The scanning coil deflects the beam in the x and y directions (in the plane of the sample) so that it scans in a raster fashion over a rectangular area of the sample surface. When high energetic electron beam interacts with the sample, different types of electrons are emitted or scattered from the sample due to the elastic and inelastic collision of accelerated electrons with the electrons present near the sample surface. The scattered electrons include secondary electrons, backscattered electrons, Auger electrons. The energy is also emitted in the form of characteristic X-rays and visible light (cathodo-luminescence). The secondary electrons are produced by inelastic scattering of incident electrons with the atoms of the sample. In a typical SEM, the secondary electrons are detected by a detector. An image of the sample surface is constructed by comparing the intensity of these secondary electrons to the scanning primary electron beam. Finally, the image is displayed on a monitor (Mukhopadhyay, 2015).

Experimental matrix

        In the current study, the variables contributing to PM emissions are as the follows:

    1. Tested vehicles

        The Mid-size passenger car and Subcompact crossover SUV in this experiment are use semi-metallic brake pad as shown in **Figure 45** and **Figure 46**, respectively.
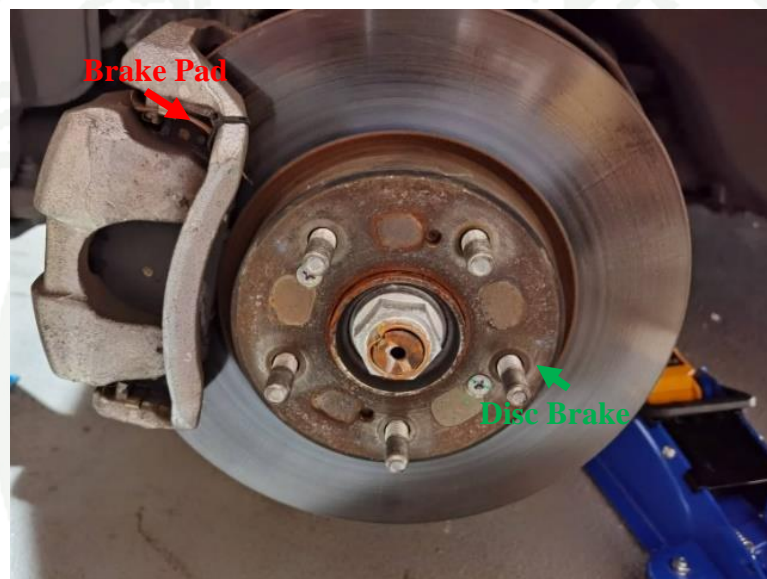
Figure 45 Semi-metallic brake of Mid-size passenger car
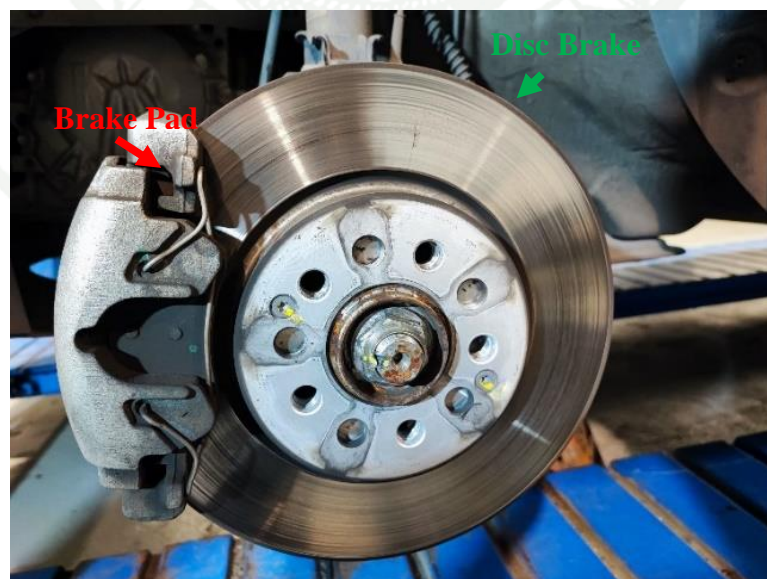
Figure 46 Semi-metallic brake of Subcompact crossover SUV

        Test vehicles (Mid-size passenger car and Subcompact crossover SUV) with the current experimental setup are shown in **Figure 47** and **Figure 48**, respectively.

Figure 47 Passenger car with the current experimental setup

Figure 48 SUV with the current experimental setup

2. Braking behavior

    In the current study, driving cycle of on road test conditions are observed for PM emissions during braking sequences. The driving cycle is called the Real Driving Conditions (RDC) as shown in **Figure 49** which lasts almost 4,000 second in a selected closed road.   These transient driving cycles are composed of both deceleration and acceleration phases (Hagino et al., 2015) and employed to mimic RDC under congested traffic areas. Before every test, the vehicle is parked inside a close building overnight at room temperature.
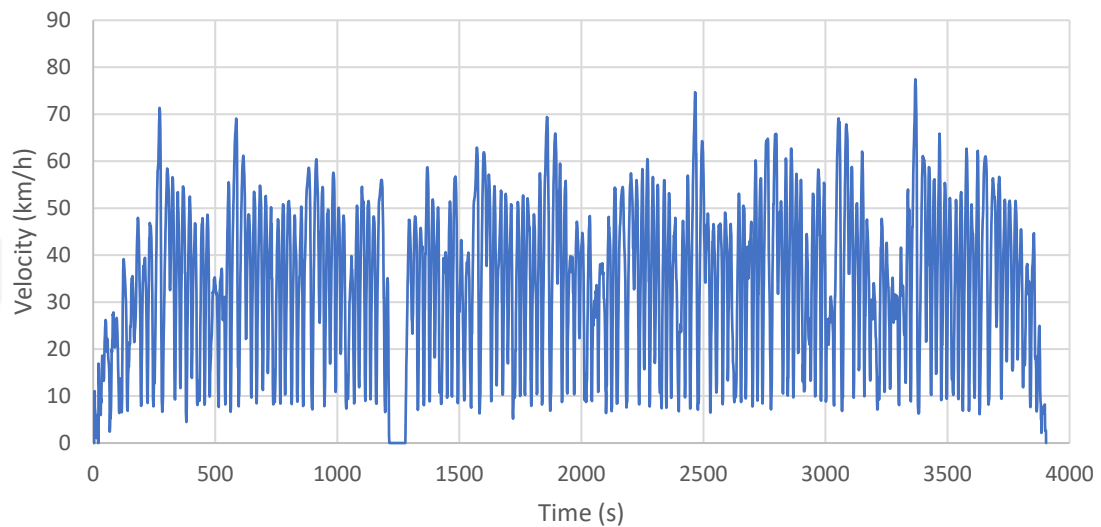
Figure 49 An example of the real driving conditions (RDC) in the current study

3. Brake temperature

    High brake power resulting in high friction can initiate high temperature of the brake pad. It is possible that this can also increase brake particle wear (Perricone et al., 2018).   In the real driving conditions test vehicle is parked overnight, the measuring temperature is closed to room temperature. The temperature is divided into two regions referred to as cold test (temperature nearby the disc brake less than 130°C) and hot test (temperature nearby the disc brake more than 130°C). Temperature ranging is done because of the trend in particle emissions observed in the study (using DustTrak 8533) as shown in **Figure 50**. More discussions will be presented in the following section.
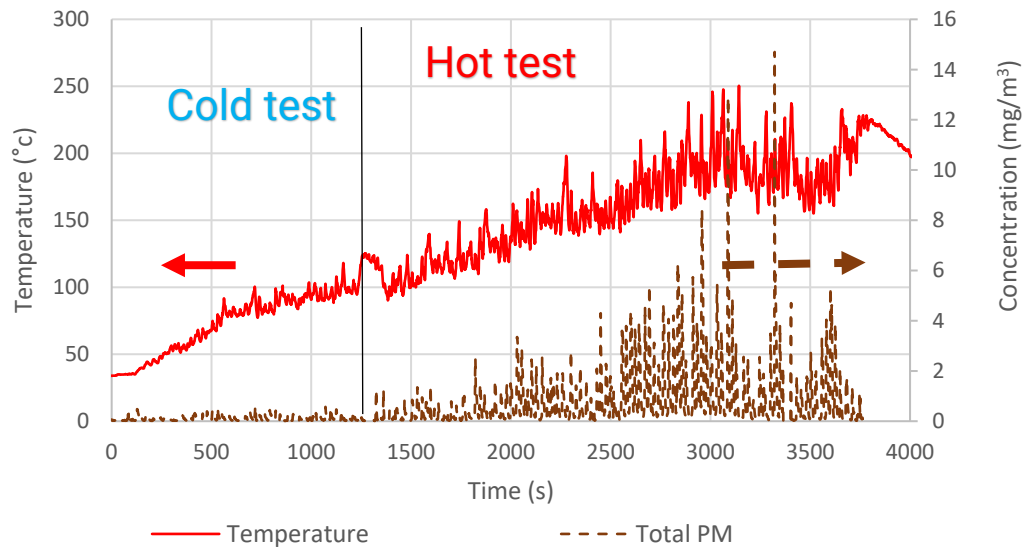
Figure 50 PM emissions and temperature nearby the disc brake during normal driving pattern

The maximum, minimum, and averaged values of measuring brake temperature on all tests are shown in **Figure 51**.
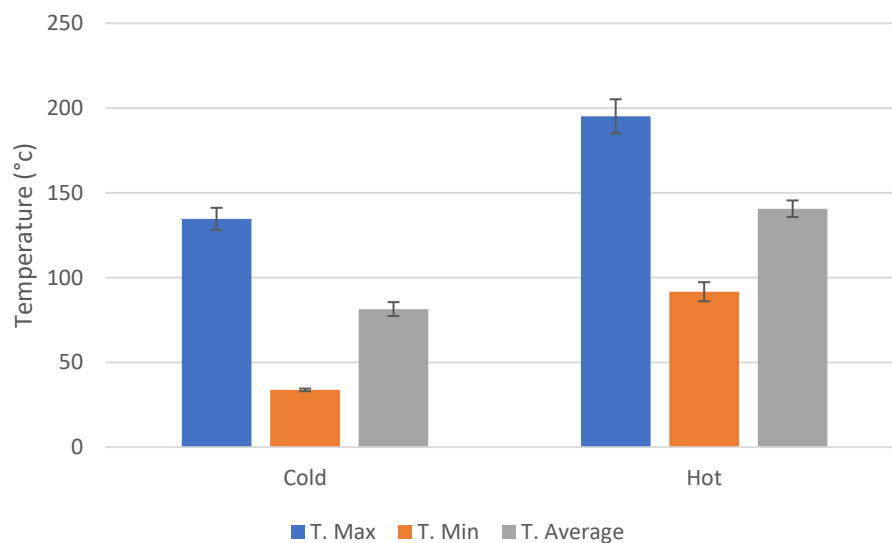
Figure 51 Maximum, Minimum, Averaged Temperature nearby the disc brake during cold and hot tests

4. Payloads

Many literatures indicate that brake wear particle emissions are influenced by vehicle weights (Timmers & Achten, 2016). In this experiment, the so-called "light total weight" of each tested vehicle included the standard factory weight plus one driver (70 kg body weight) and testing devices (95 kg) comparing to "the heavy total weight" with 200 kg additional weights ranged between (1) 1,690 and 1,890 kg, (2)

1,455 and 1,655 kg of Mid-size passenger car and Subcompact crossover SUV, respectively.

　　　　Figure 52 – 54 demonstrates time durations, distance, and maximum/averaged velocity of all tests in real driving conditions, respectively. Each test data is presented in overall (cold + hot), cold, and hot tests. **Figure 52** and **Figure 53** show that the time and distance of cold test is less than hot test because of the temperature rapidly reached 130°C. Studies on time duration, distance and maximum/averaged velocity can be performed repeatedly (with only a minor error bar) from each test conditions.
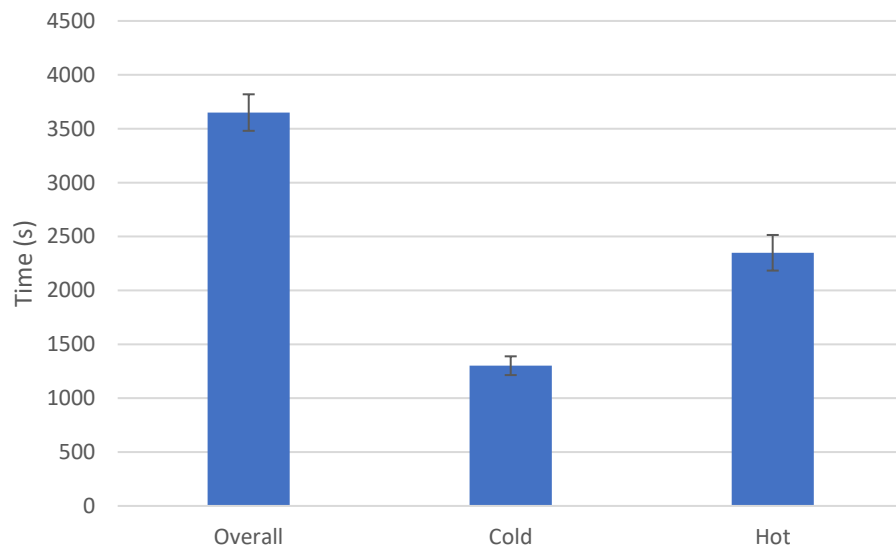
Figure 52 Time durations of all tests in real driving conditions
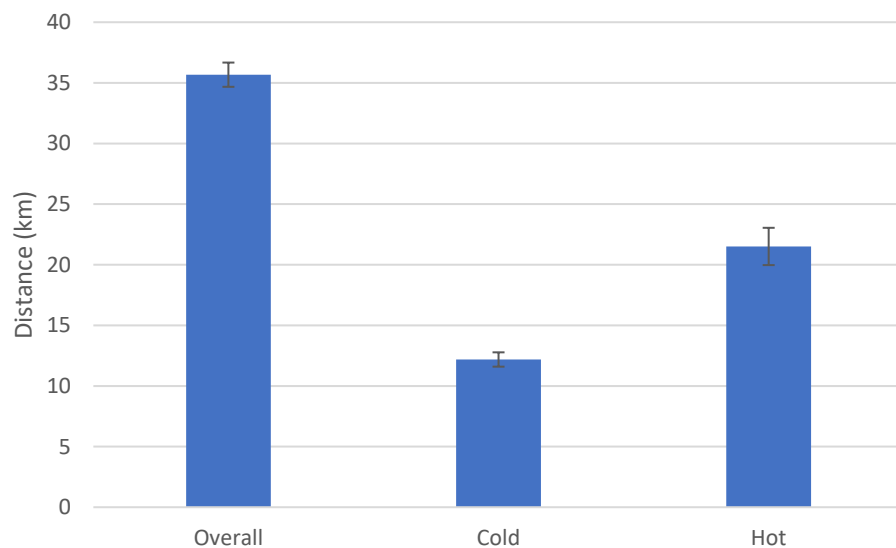
Figure 53 Distance of all tests in real driving conditions
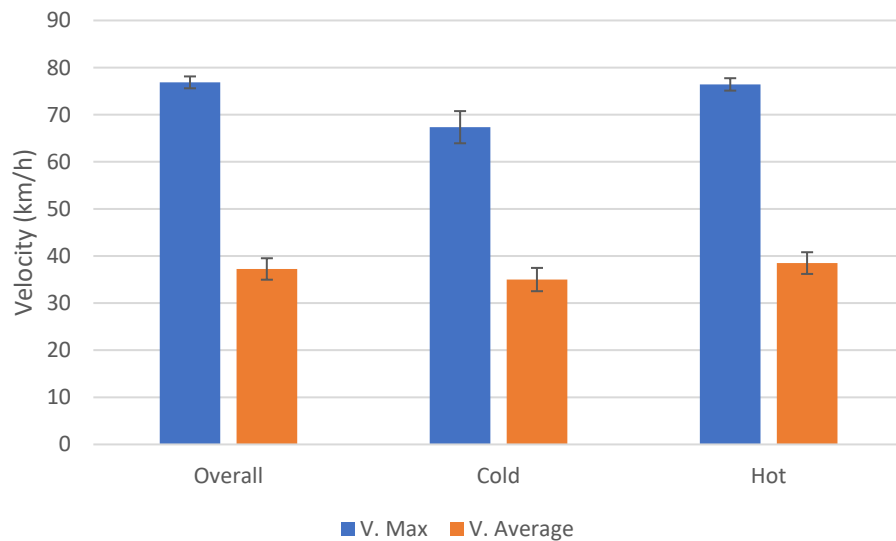
Figure 54 Maximum/averaged velocity of all tests in real driving conditions

PM concentration of backgrounds from this tested route is around 10 – 25 µg/m3 measured by Dusttrak 8533 as shown in **Figure 55**. They are considered relatively low and thus, is neglected in the current study.
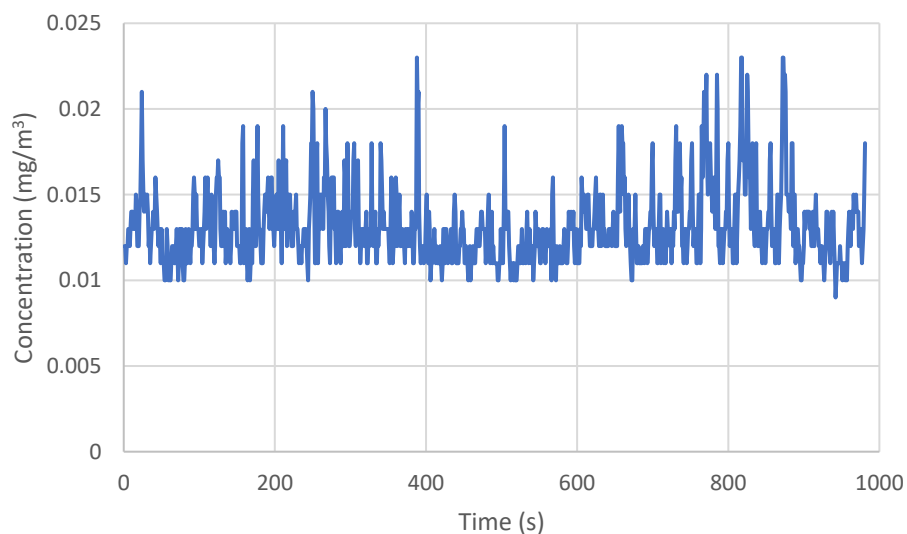
Figure 55 PM concentration of backgrounds from this tested route

The experimental procedures of this research are shown in **Figure 56** (each testing is repeated 2 - 3 times). Firstly, the tested vehicle is selected considering its ground clearance. Secondly, the two braking behaviors (i.e., RDC and ISO21994:2007 standard) are performed. Thirdly, brake tests are performed based on - I) light payloads (which included: 1. standard factory vehicle weight, 2. one driver's body weight of 70 kg and 3. testing devices weigh 95 kg) and II) heavy payloads (light payloads plus 200 kg additional weight). Lastly, studies on brake wear PM emission, investigating PM characteristics and morphology.
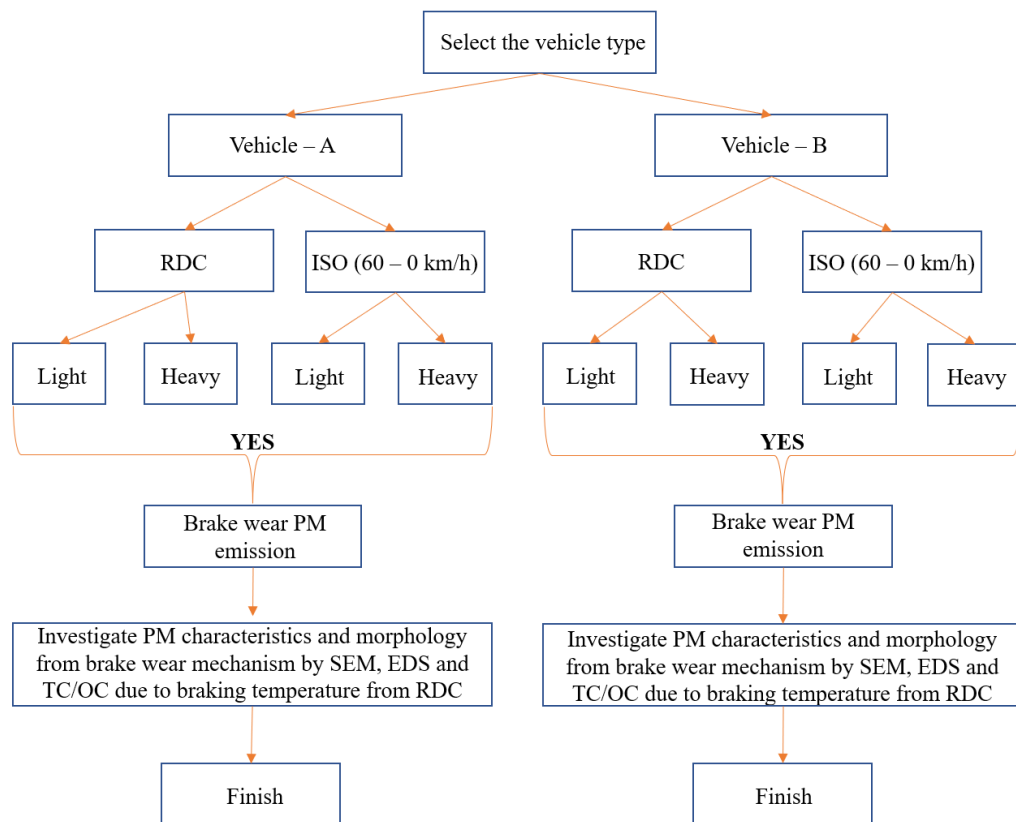
Figure 56 Flowchart for experimental procedures

RESULTS AND DISCUSSION

Overview of Brake wear PM emissions during Real Driving Conditions (RDC)

The real-time brake wear PM emissions are measured by DustTrak 8533, while temperature is measured nearby the disc brake during RDC by thermocouple type K. Brake wear particles are captured in 37 mm membrane filters by DustTrak 8533 and Gilian Gil-Air 5 to perform gravimetric analysis. PM concentrations are calculated based on the sampling flow rate and collection time.

The absolute value results of passenger car and SUV are shown in **Appendix Table 1 - 3**. the concentration of filter can calculate by equation (**5**).

Definitions:

- Light = light payloads
- Heavy = light payloads plus 200 kg additional weight
- Cold = brake temperature under 130˚C
- Hot = brake temperature above 130˚C.
- Cold or hot filter tests are performed using ASP Gilian Gil-air5 (flow rate is 4.5 l/min)
- Cold + hot filter tests are performed using TSI8533 (flow rate is 2.25 l/min)

Figure 57 shows real-time brake wear PM emissions in light payload passenger car. The x-axis indicates a time, the blue line is a velocity related to left y-axis, and the brown line is a PM concentration related to right y-axis. During the first 1,300 seconds, PM emissions are unnoticeable and can be neglected in terms of mass concentrations. However, after that, PM emissions are detected and gradually increased. And later at some points, they can be as high as 5 mg/m^3.
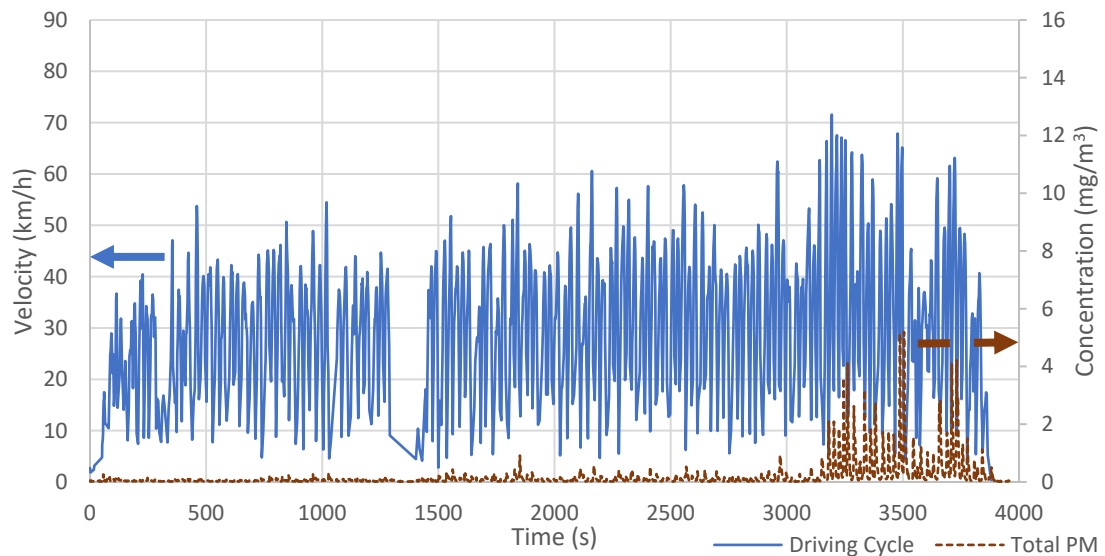
Figure 57 An example of brake wear PM emissions during RDC of light payload passenger car

Figure 58 (heavy payloads) shows similar trends as **Figure 57** (light payloads). However, in after 1,250 seconds, PM emissions are detected and significantly increased. And later at some points, they can be as high as 15 mg/m³. This trend of PM emissions corresponds to (Hagino et al., 2016).
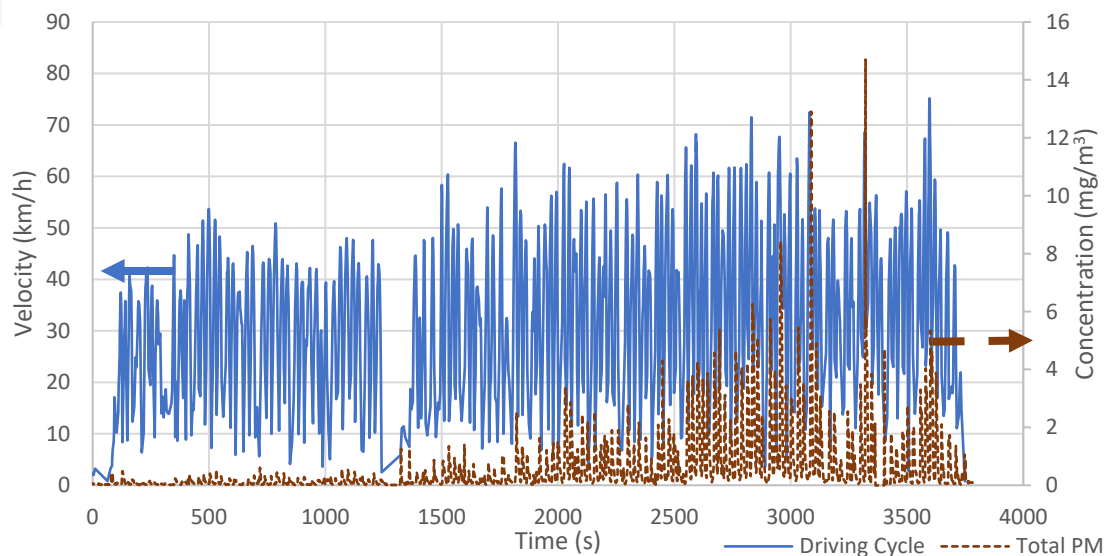
Figure 58 An example of brake wear PM emissions during RDC of heavy payload passenger car

Figure 59 and **Figure 60** (SUV) show similar trends as **Figure 57** and **Figure 58** (passenger car). In light payloads, it can be seen from the results that the longtime of driving cycle have a slight effect to the PM concentration. Most of the peak PM

concentration at each point is around 1 mg/m^3. While, in the heavy payload at some points, PM concentration can be as high as 10 mg/m^3 and the average peak at each point are higher than light payloads.
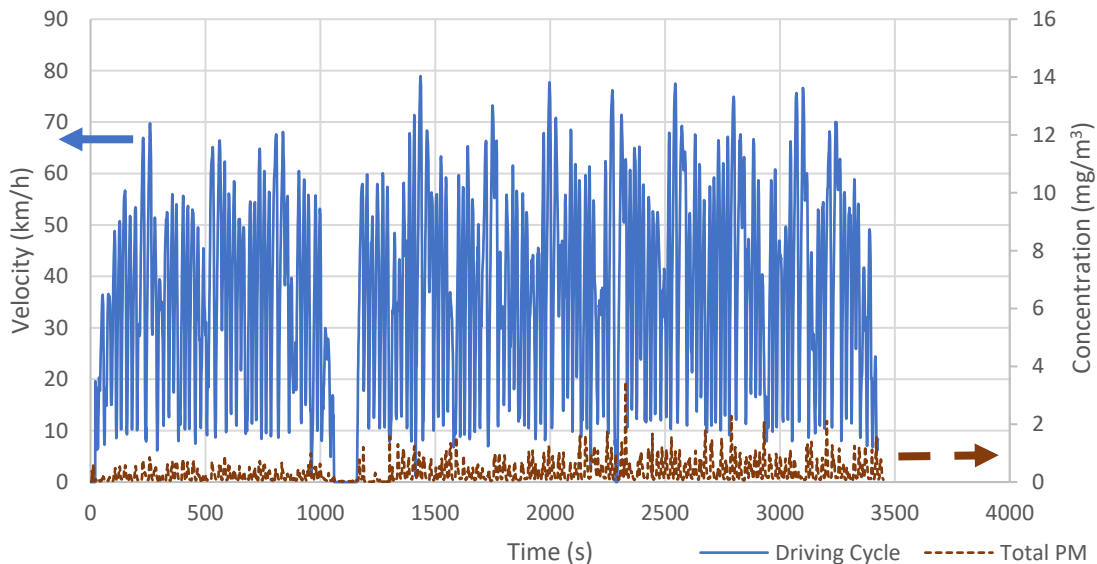
Figure 59 An example of brake wear PM emissions during RDC of light payload SUV
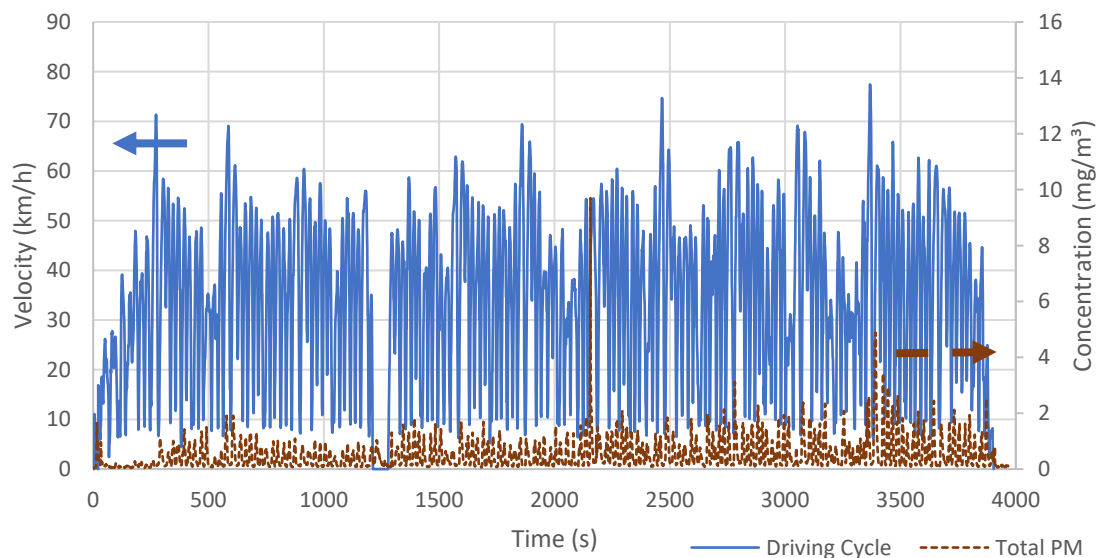
Figure 60 An example of brake wear PM emissions during RDC of heavy payload SUV

From the previous results, PM concentration from brake wear emissions is influenced by not only driving cycle test, but also the brake temperature. Next part will describe PM emissions from brake wear due to braking temperature.

As known, temperature of the brake pad increases with the braking time and frequency (from **Figure 12**) and thus increases the amount of brake pad material fall-out as PM (from **Figure 13** and **Figure 15**). **Figure 61** (red line indicates brake

temperature related to right y-axis) shows real-time temperature measuring nearby the disc brake during RDC of heavy payload passenger car and **Figure 62** (red line indicates brake temperature related to left y-axis and brown line indicates PM concentration related to right y-axis) shows the relation between brake temperature and PM mass concentration. It is clearly seen from the results that PM emissions are significantly related to the brake temperature. At the beginning, since the vehicle is parked overnight, the measuring temperature is closed to room temperature. Once the test is undertaken, the temperature is increased and reached 250˚C towards the end of the test. The relationship between temperature and PM concentrations are shown in (**Figure 62**). Based on this data, the brake temperature of 130˚C is chosen as the cut-point between cold and hot tests to differentiate brake wear particle behaviors. After 130˚C the PM concentrations are clearly increased. And later at some points, they can be as high as 15 mg/m^3 when the temperature is reaches to 250˚C.
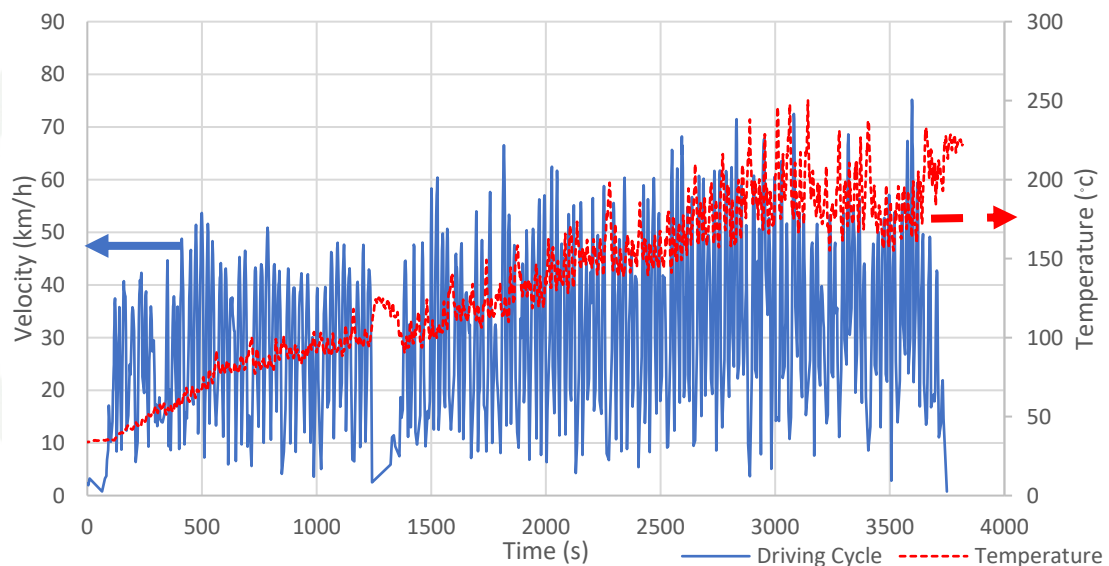
Figure 61 An example of temperature measurement nearby the disc brake during RDC of heavy payload passenger car
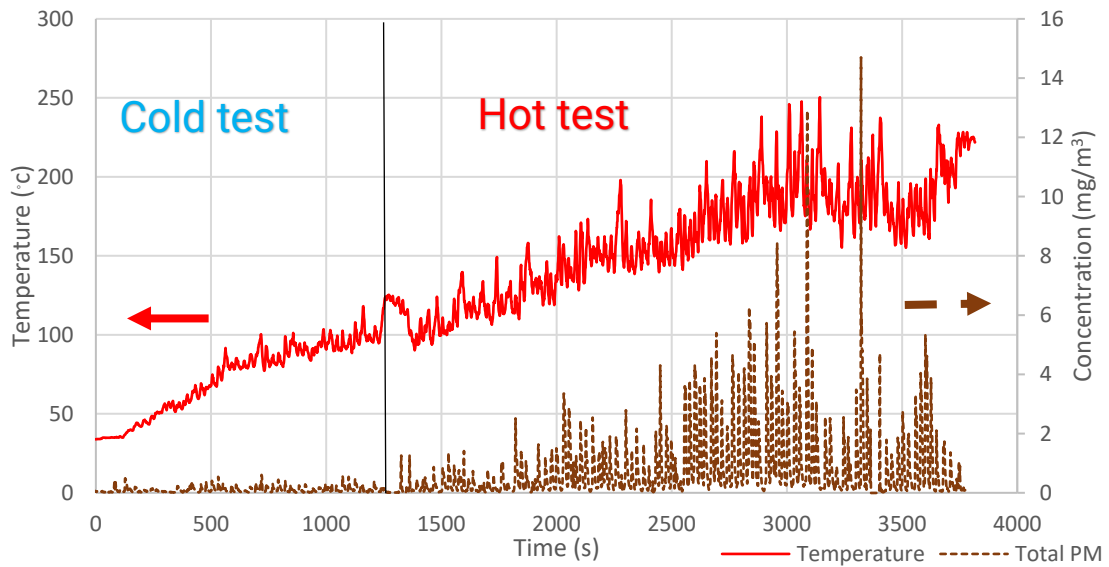
Figure 62 An example of PM emissions and temperature nearby the disc brake during RDC of heavy payload passenger car

In the same way of light payload. **Figure 63** and **Figure 64** show the temperature is increased and reached 220°C towards the end of the test. During the first 1,300 seconds, PM emissions are unnoticeable and can be neglected in terms of mass concentrations. However, until 150°C, PM emissions are detected and significantly increased. And later at some points, they can be as high as 5 mg/m³ (This trend is correspond to (Vainio, 2021) where the brake temperature reached 150 °C and high PM emissions are observed).

Figure 63 An example of temperature measurement nearby the disc brake during RDC of light payload passenger car

Figure 64 An example of PM emissions and temperature nearby the disc brake during RDC of light payload passenger car

While, in SUV both the light and the heavy payload the temperature is only increases to 200°C (**Figure 65** and **Figure 66**) that's because the high ground clearance of SUV resulting in the good ventilation. From **Figure 67** and **Figure 68** it can see that the PM concentrations in the hot test are rather than the cold test.
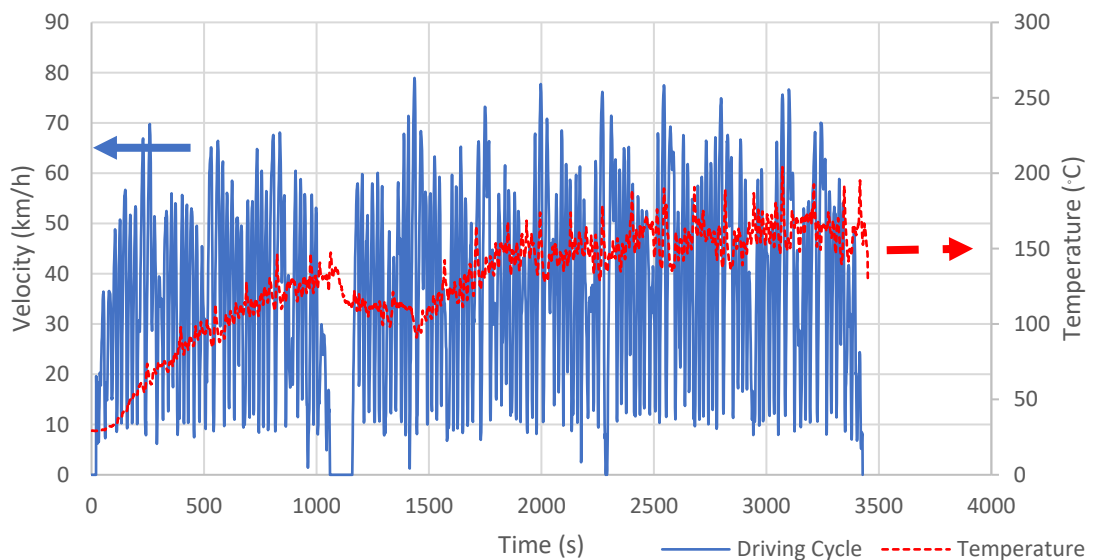
Figure 65 An example of temperature measurement nearby the disc brake during RDC of light payload SUV
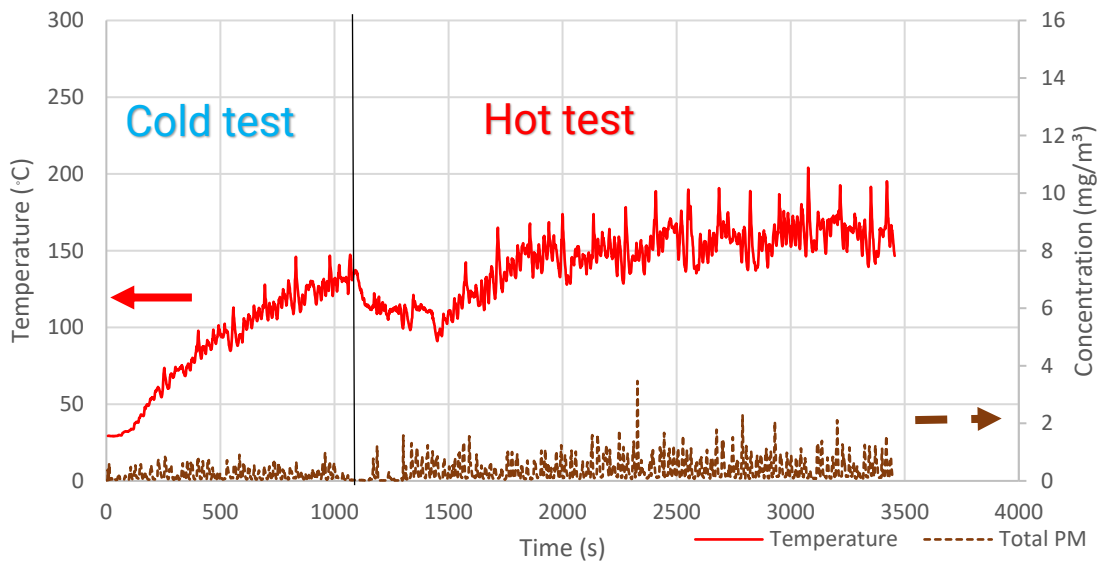
Figure 66 An example of PM emissions and temperature nearby the disc brake during RDC of light payload SUV
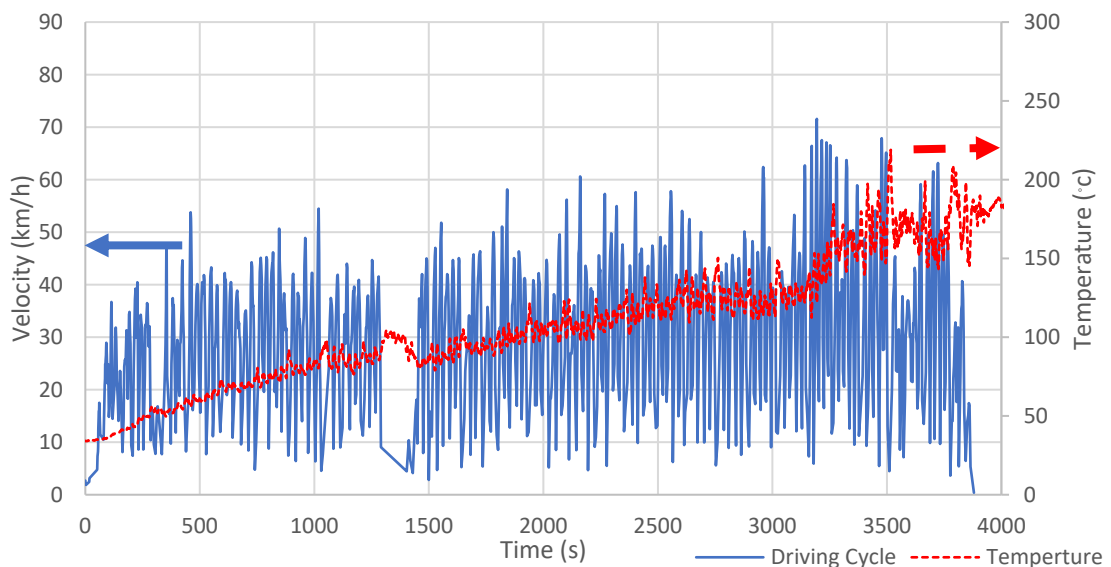

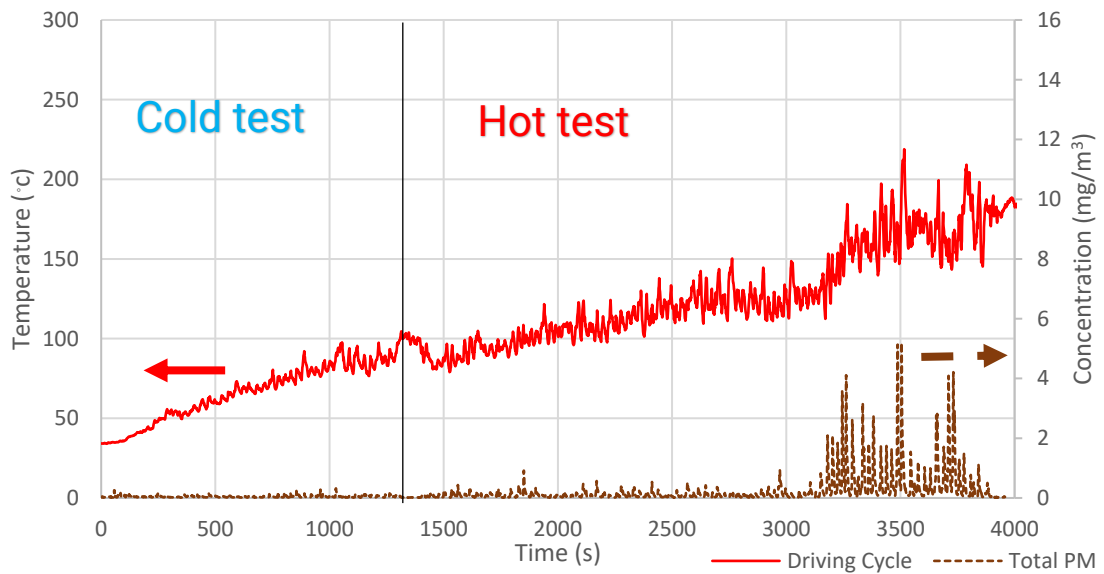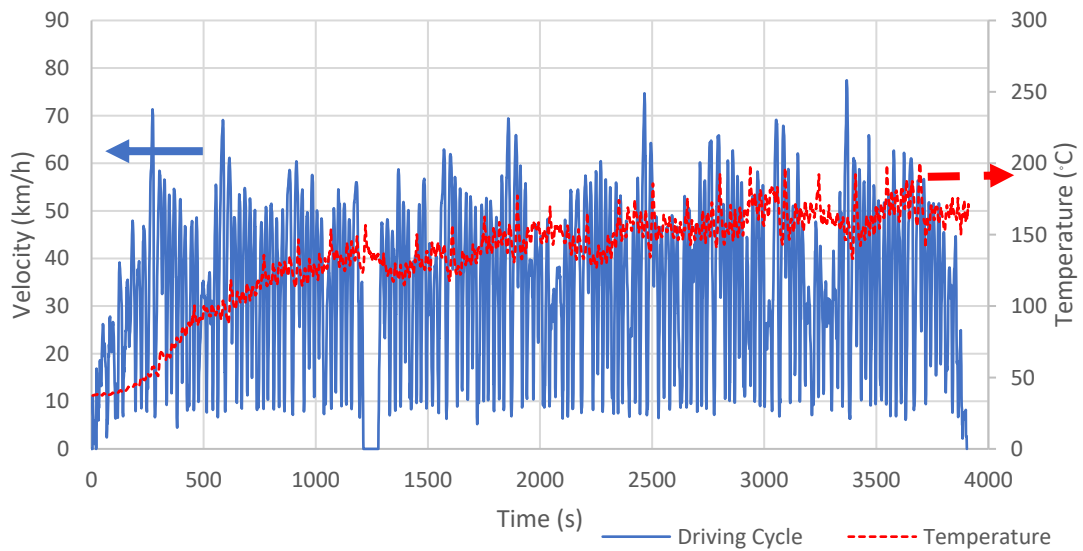**Figure 67** An example of temperature measurement nearby the disc brake during RDC of heavy payload SUV
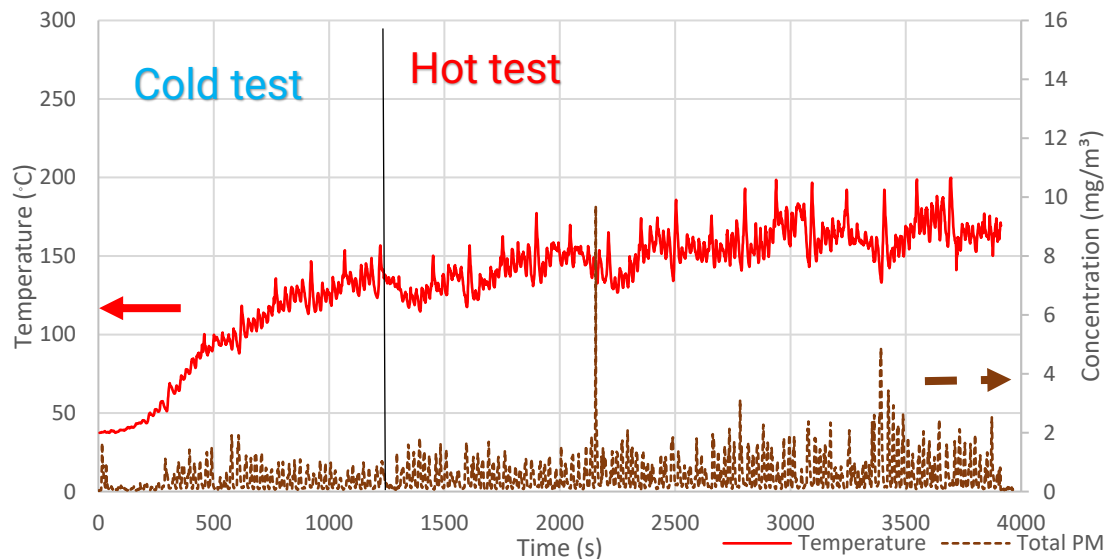
Figure 68 An example of PM emissions and temperature nearby the disc brake during RDC of heavy payload SUV

These two vehicles (passenger car and SUV) can show the PM concentrations measured in real-time by DustTrak 8533 and averaged to overall cold and hot tests. PM is classified into PM_1, $PM_{2.5}$, PM_4, and PM_{10}. Including Gilian Gilair-5 Air Sampling Pump to perform gravimetric analysis during cold and hot tests.

Figure 69 and **Figure 70** shows the PM concentration between cold and hot test of DustTrak 8533 and Gilian Gilair-5, respectively. Results are shown into two different Temperatures. Similar trend to the DustTrak 8533 and Gilian Gilair-5 is observed. However, the absolute value of PM concentration between two equipment are significantly different due to the detection limit of microelectronic balance.
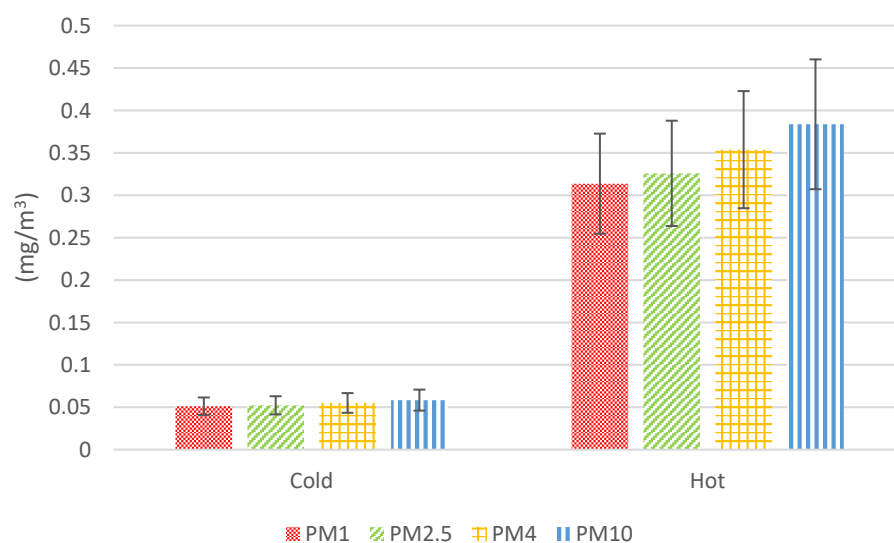
Figure 69 PM concentration of cold and hot passenger car by DustTrak 8533
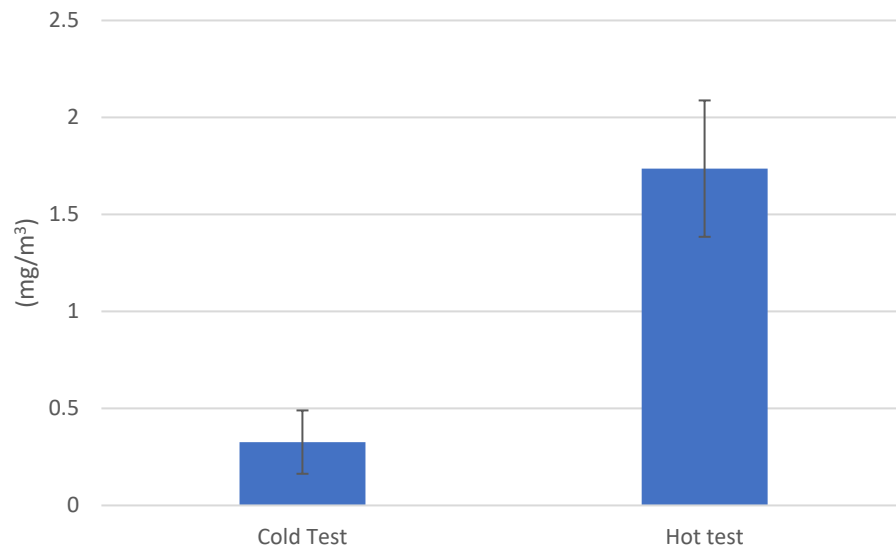
Figure 70 PM concentration of cold and hot passenger car by Gilian Gilair-5

Based on the data in **Figure 69** and **Figure 70** the amounts rise 6 – 8 times in hot test as compared with the cold test.

Figure 71 and **Figure 72** shows an average of PM size distribution from brake wear particle concentrations (by DustTrak 8533) in the form of a pie chart for the cold and the hot tests condition. It can be clearly seen that most of particles are classified as PM_1 which is around 88% and 81%, respectively.
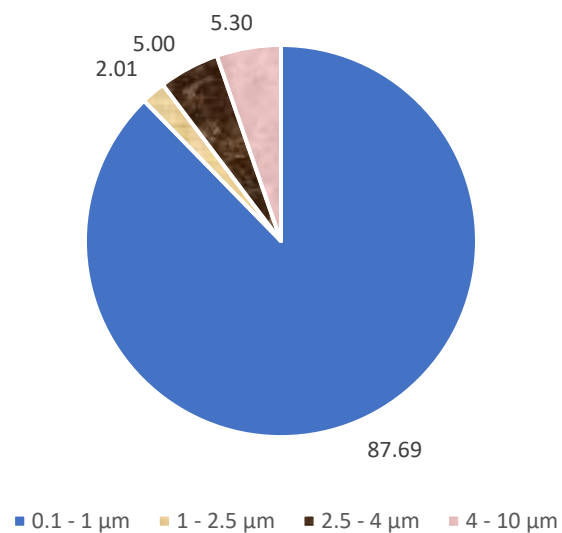
Figure 71 PM size distribution from brake wear particles (cold test in passenger car)

8.13
7.74
3.41
80.72

■ 0.1 - 1 µm   ■ 1 - 2.5 µm   ■ 2.5 - 4 µm   ■ 4 - 10 µm
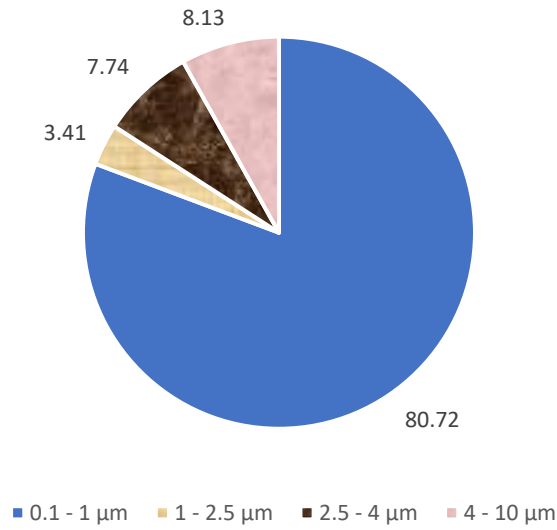
Figure 72 PM size distribution from brake wear particles (hot test in passenger car)

Considering in SUV, **Figure 73** and **Figure 74** shows the results of the average PM concentrations due to cold and hot tests by DustTrak 8533 and Gilian Gilair-5 (Similar trend and absolute value of PM concentration between two equipment). These results show the average PM concentration in hot test more than cold test.
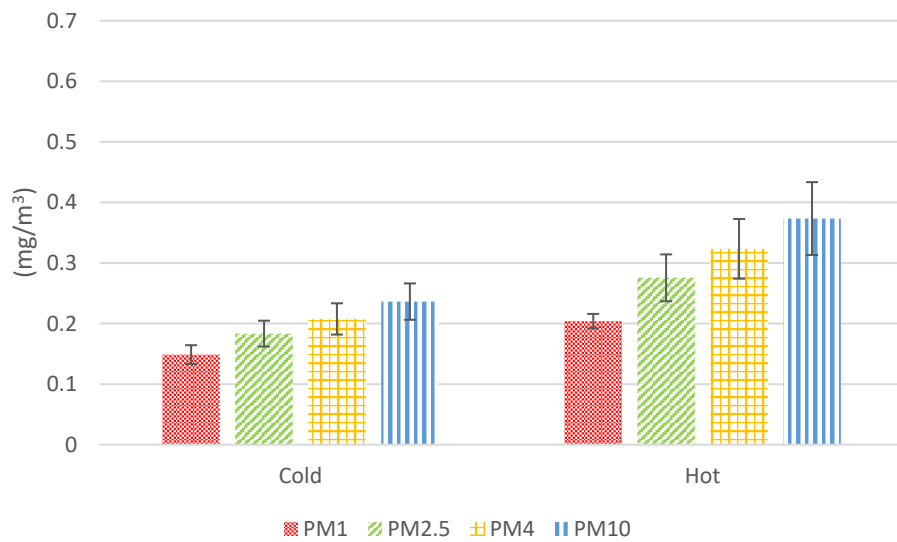
Figure 73 PM concentration of cold and hot SUV by DustTrak 8533
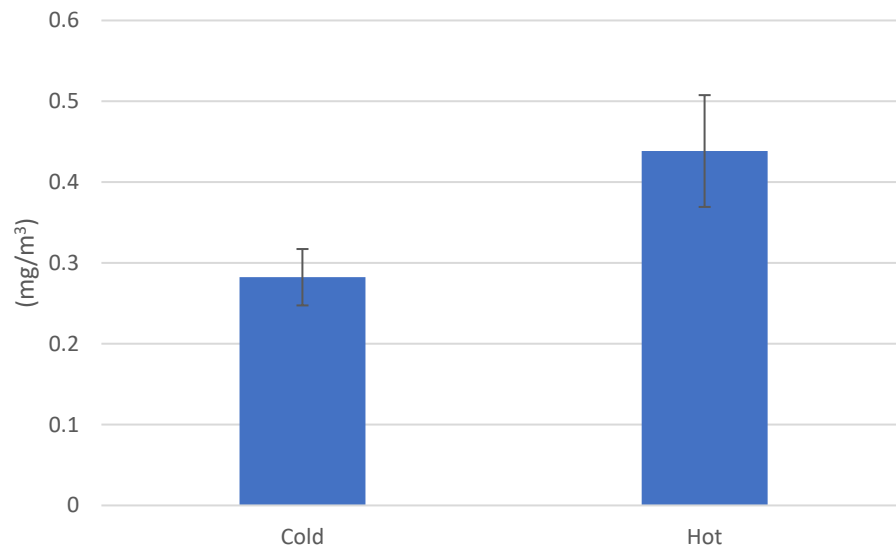
Figure 74 PM concentration of cold and hot SUV by Gilian Gilair-5

Figure 75 and **Figure 76** shows an average of PM size distribution from brake wear particle concentrations (by DustTrak 8533) in the form of a pie chart for the cold and the hot tests condition. In cold and hot tests most of particles are classified as PM_1 which is around 64% and 57%, respectively.
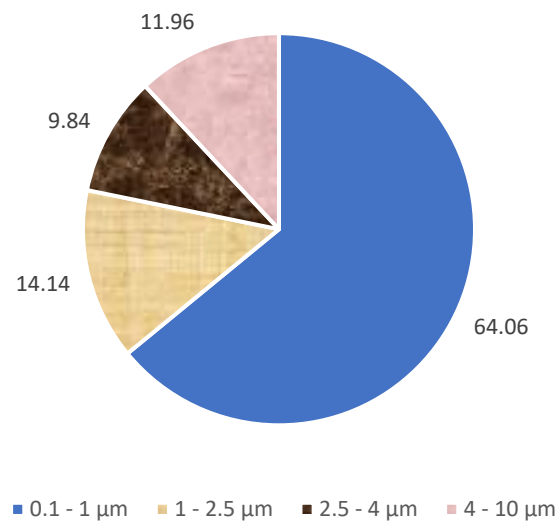
Figure 75 PM size distribution from brake wear particles (cold test in SUV)
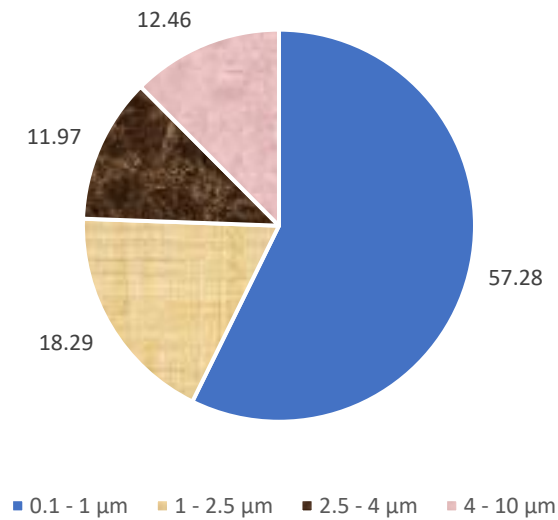
Figure 76 PM size distribution from brake wear particles (hot test in SUV)

In term of PM size distribution (**Figure 71** – **72** and **Figure 75** – **76**), increasing brake temperature can cause bigger the PM. Considering the two types of vehicles, PM size distribution of SUV is bigger than the PM of passenger car. It is possible that brake temperature of SUV increased faster than Passenger car. This assumption is obtained by SEM.

When comparing passenger car and SUV, brake temperature of SUV increased faster than passenger car until 150°C. Thereafter in SUV, the temperature increased gradually to 200°C, while in passenger car the temperature rapidly rises to 250°C. The main causes of brake temperatures are mainly due to ventilation of vehicles (air flow passing brake pads and discs). It is obvious that the PM concentration emitted from SUV is higher before 1,750 seconds; thereafter, PM concentration emitted from passenger car is remarkably higher. These results are shown in **Figure 77** and **Figure 78**.
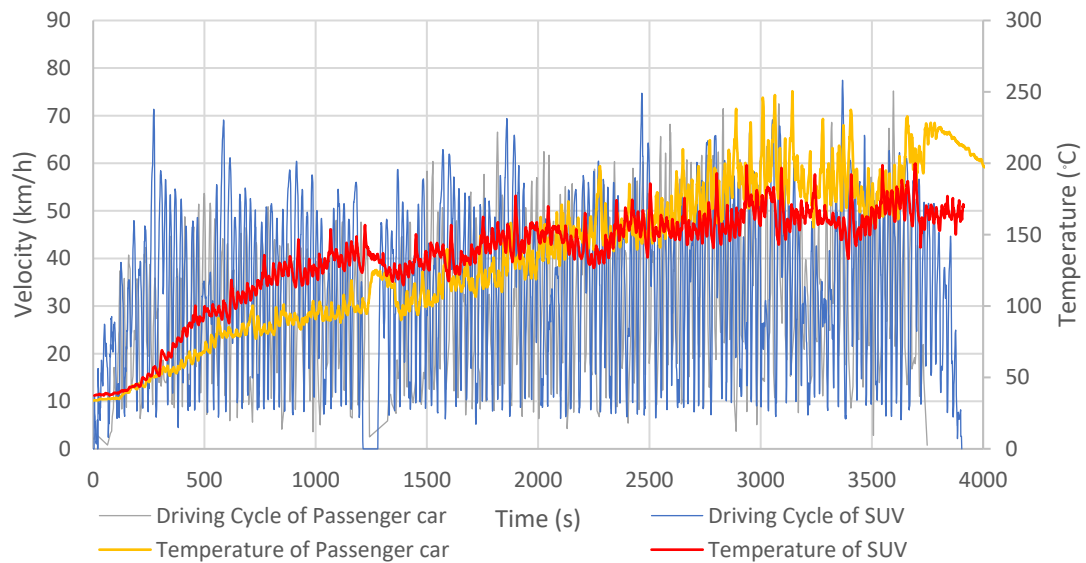
Figure 77 Comparison of Temperature between passenger car and SUV
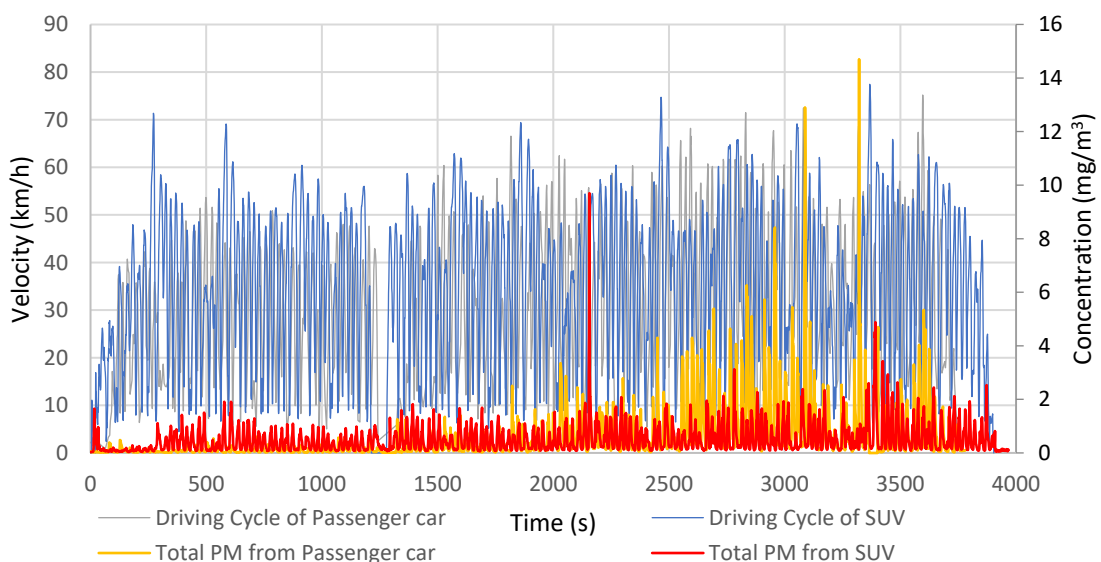
Figure 78 Comparison of PM concentration between passenger car and SUV

From **Figure 79** and **Figure 80** can be calculated to average absolute data in term of PM concentration and braking temperature are as the follows:

1.) The comparison of the PM concentration between passenger car and SUV as shown in **Figure 79**. PM mass concentration of SUV is higher than passenger car around 34.61%.

2.) The comparison of the average brake temperature between passenger car and SUV as shown in **Figure 80**. brake temperature of SUV is higher than passenger car around 17.27%
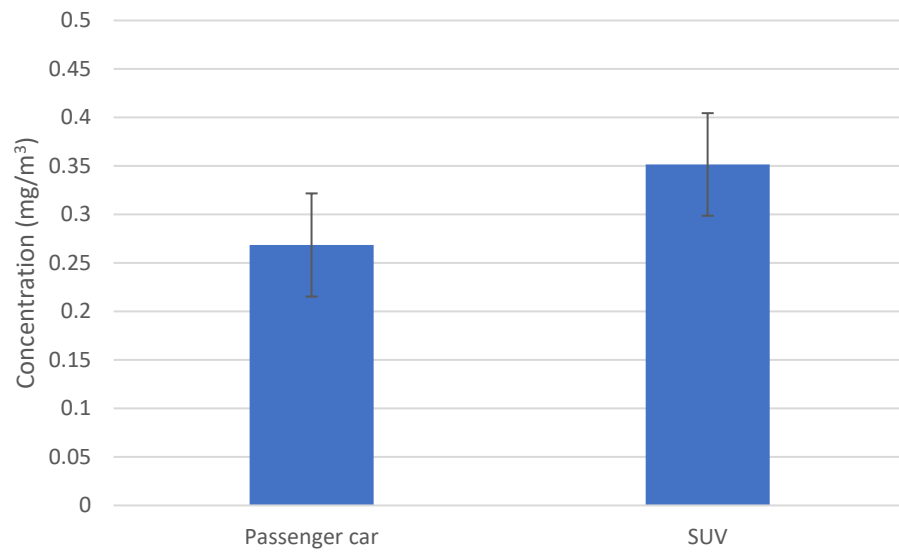
Figure 79 The comparison of PM concentration between passenger car and SUV
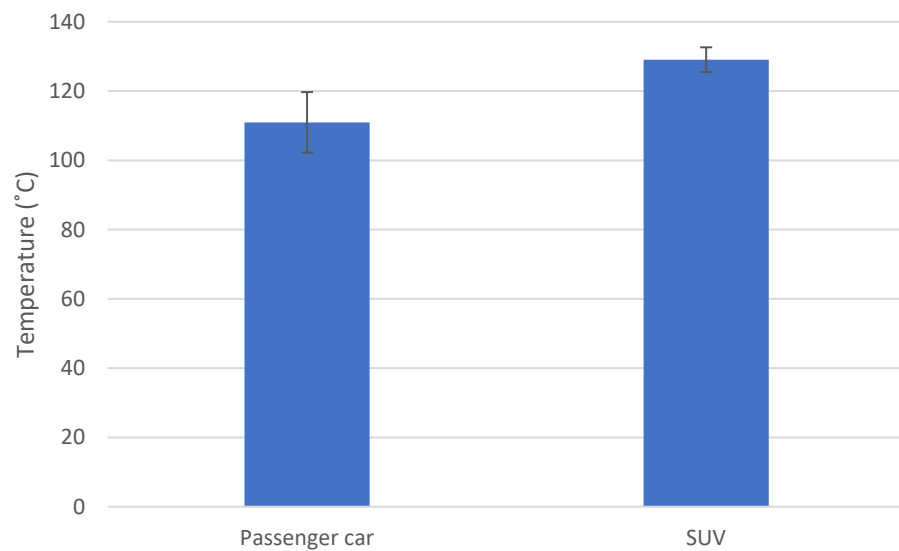
Figure 80 The comparison of braking temperature between passenger car and SUV

All the above results confirm that the brake temperature play an important role in increasing brake wear which directly turn to be PM emissions.

Effect of payloads on braking PM concentration

Figure 81 shows the PM concentrations of passenger car are measured in real-time by DustTrak 8533 and averaged to overall RDC (combining cold and hot tests). PM is classified into PM_1, $PM_{2.5}$, PM_4 and PM_{10}. Results are shown into two different payloads.
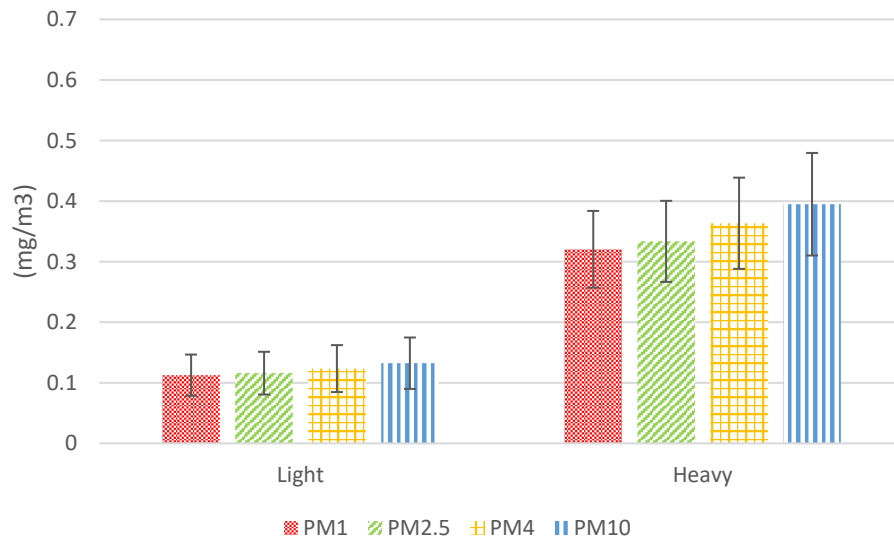
Figure 81 PM concentration of passenger car by DustTrak 8533

Figure 82 shows similar data seen in **Figure 81** but collected by 37 mm membrane filters by using DustTrak 8533 to perform gravimetric analysis. Results for both light and heavy payload conditions demonstrate the effects of increasing payloads on higher PM emissions (Timmers & Achten, 2016). Similar trend to the light scattering method is observed. However, the absolute value of PM concentration between two equipment are significantly different due to the detection limit of microelectronic balance.
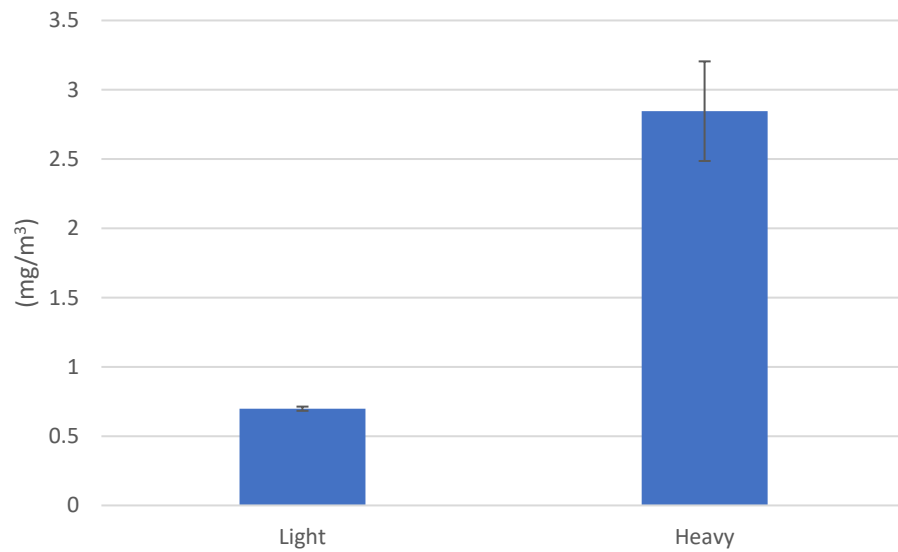
Figure 82 PM concentration of passenger car by gravimetric sampling method

Figure 83 shows an average of PM size distribution from brake wear particle concentrations (by DustTrak 8533) in the form of a pie chart for the light payload condition. It can be clearly seen that most of particles are classified as PM_1 which is around 86%. Heavy payload condition yields a similar trend as shown in **Figure 84**.

■ 0-1 μm   ■ 1-2.5 μm   ■ 2.5-4 μm   ■ 4-10 μm
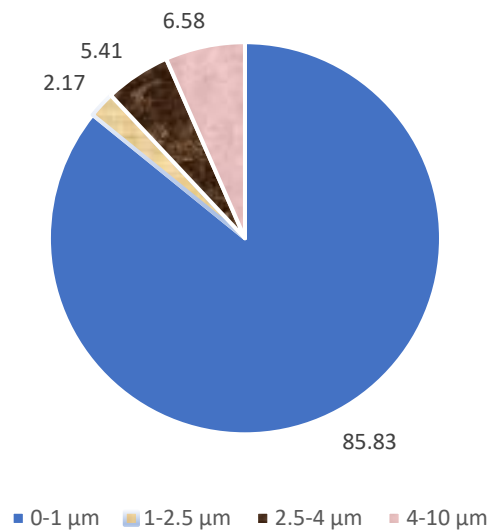
Figure 83 PM size distribution from brake wear particles (Light payload in passenger car)

7.29
7.08
3.14
82.48

■ 0-1 µm   ■ 1-2.5 µm   ■ 2.5-4 µm   ■ 4-10 µm
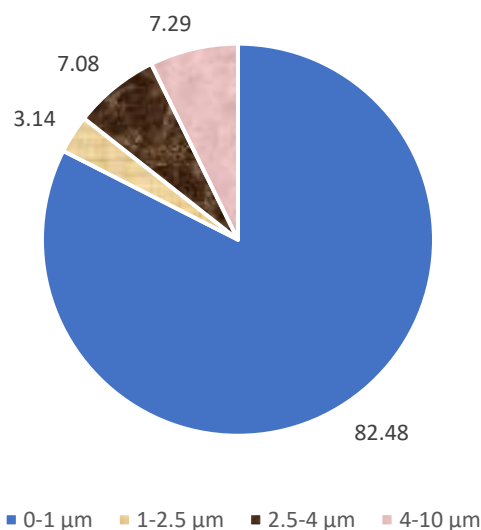
Figure 84 PM size distribution from brake wear particles (Heavy payload in passenger car)

In subcompact crossover SUV. **Figure 85** show the data similar seen in **Figure 81**. And **Figure 86** show the PM concentration collected by captured in 37 mm membrane filters by using DustTrak 8533 to perform gravimetric analysis. It is found out that the additional payloads of 200 kg increase the amount of brake wear PM concentration almost doubled and the absolute value of PM concentration between two equipment are similar value.

■ PM1   ■ PM2.5   ■ PM4   ■ PM10
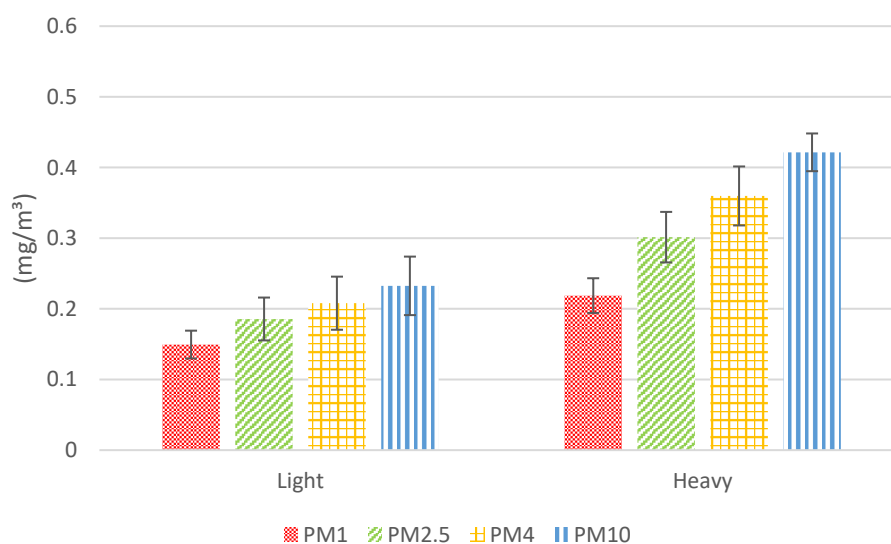
Figure 85 PM concentration of SUV by DustTrak 8533
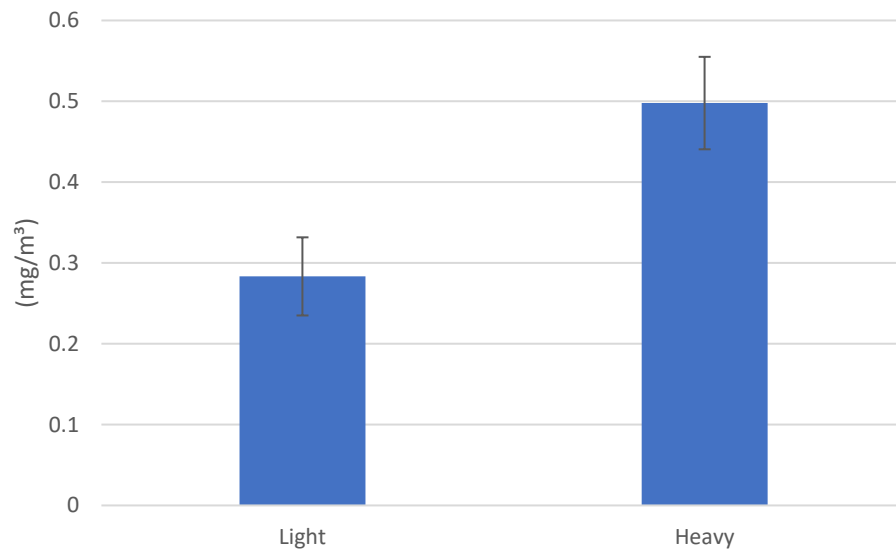
Figure 86 PM concentration of SUV by gravimetric sampling method

Figure 87 and **Figure 88** show PM size distribution of the light and the heavy payload, respectively. In the light payload, 65.63% of PM emissions from brake wear are considered as PM_1. While, in the heavy payload half of all is PM_1.
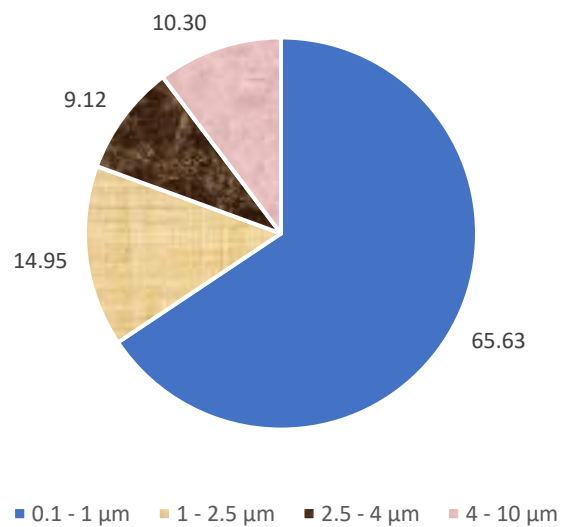
Figure 87 PM size distribution from brake wear particles (light payload in SUV)
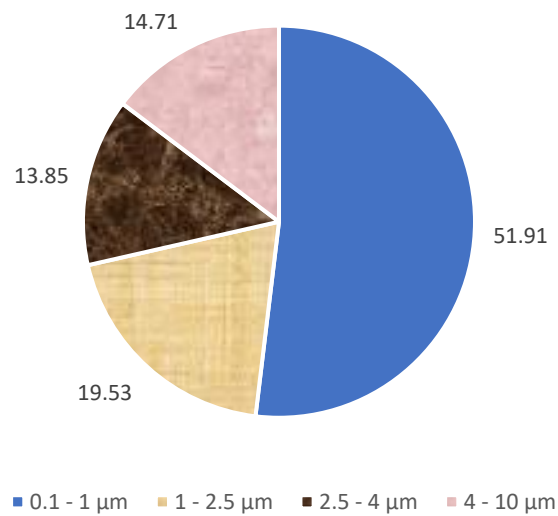
Figure 88 PM size distribution from brake wear particles (heavy payload in SUV)

High payloads are obvious that this can increase PM mass concentration. This conclusion is confirmed in ISO 21994:2007 standard. ISO 21944:2007 specifies an open-loop test method to determine the stopping distance of a vehicle during a straight-line braking manoeuvre, with the Anti-lock Braking System (ABS) fully engaged. The vehicle runs at the constant speed of 60 km/h. Brake is applied to reduce the vehicle speed to 0 km/h within 36.7 m (More details of the ISO 21994:2007 standard can be found in Ref. (ISO, 2007)) and the vehicle is accelerated (Driving) to the speed of 60 km/h again as shown in **Figure 89**. This test commencing when the temperature nearby disc brake is ranging from 150˚C - 170˚C.
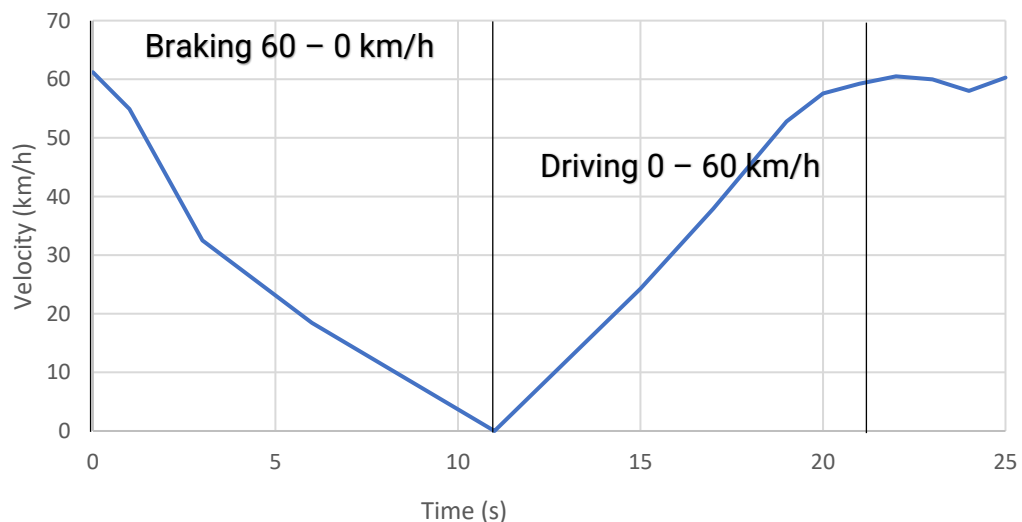
Figure 89 Braking from 60 to 0 km/h under ISO 21994:2007 standard

Results from two tests under the ISO 21994:2007 standard (**Figure 89**) of passenger car are found in **Figure 90** and **Figure 91**. For the case of light payload (**Figure 90**), only one peak of real-time PM concentrations while braking is observed. However, for the case of heavy payload (**Figure 91**), there are two peaks of PM concentrations. The first peak is observed during braking while the second peak comes during acceleration (sometimes called resuspension). On the other hand, in SUV, the results are only one peak when the vehicle stop as shown in **Figure 92** and **Figure 93** (the light and the heavy payload, respectively). This observation of passenger car corresponds to results found in (Hagino et al., 2015) which based on two tests from two passenger cars. It is speculated that this should be the cause of higher PM emissions due to increasing payloads (Ekathai et al., 2021).
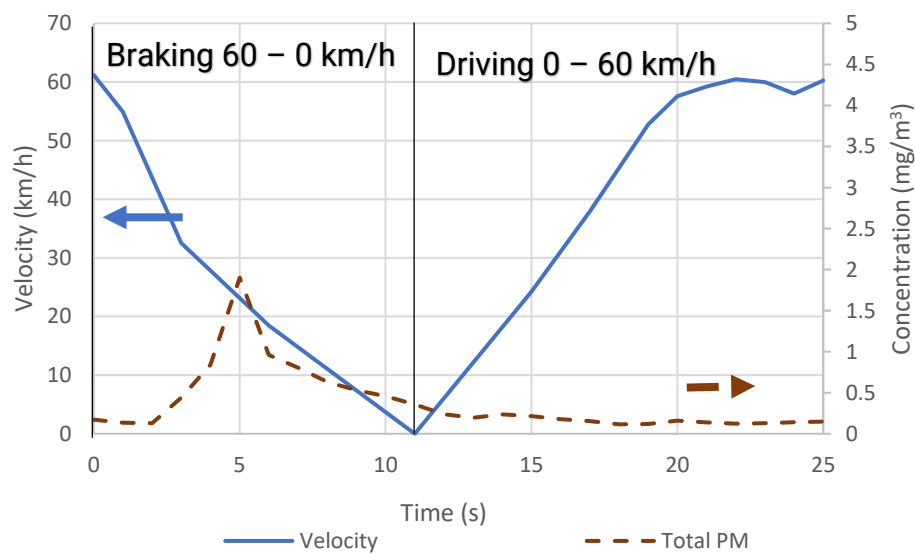
Figure 90 Real-time PM concentrations of light payload passenger car under ISO 21994:2007 standard test
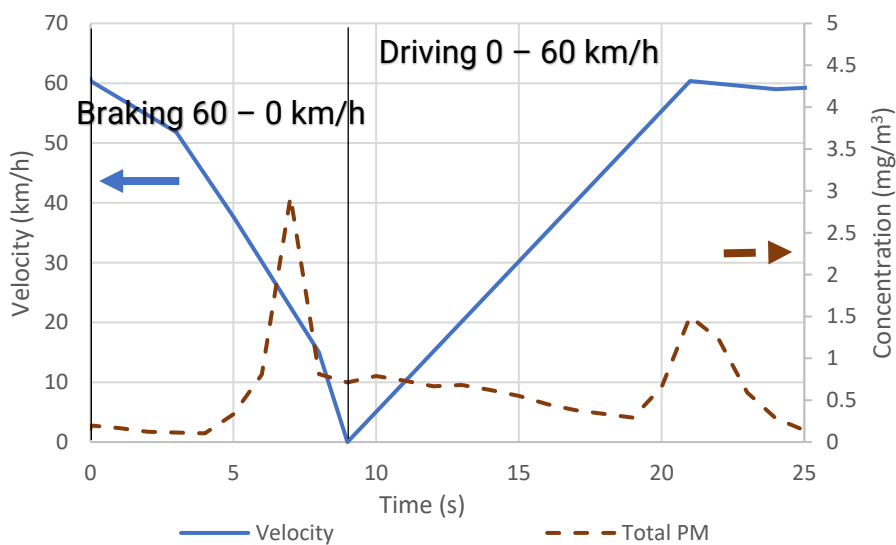
Figure 91 Real-time PM concentrations of heavy payload passenger car under ISO 21994:2007 standard test
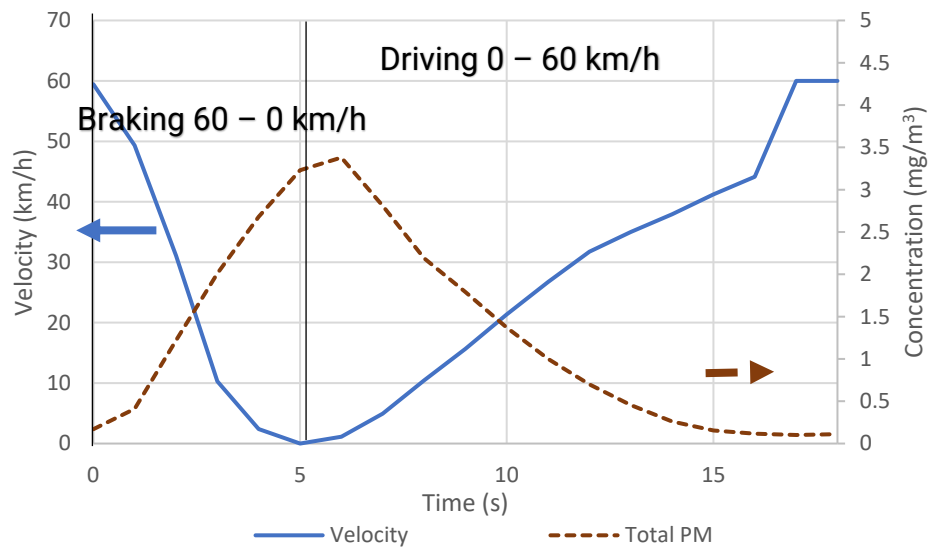
Figure 92 Real-time PM concentrations of light payload SUV under ISO 21994:2007 standard test
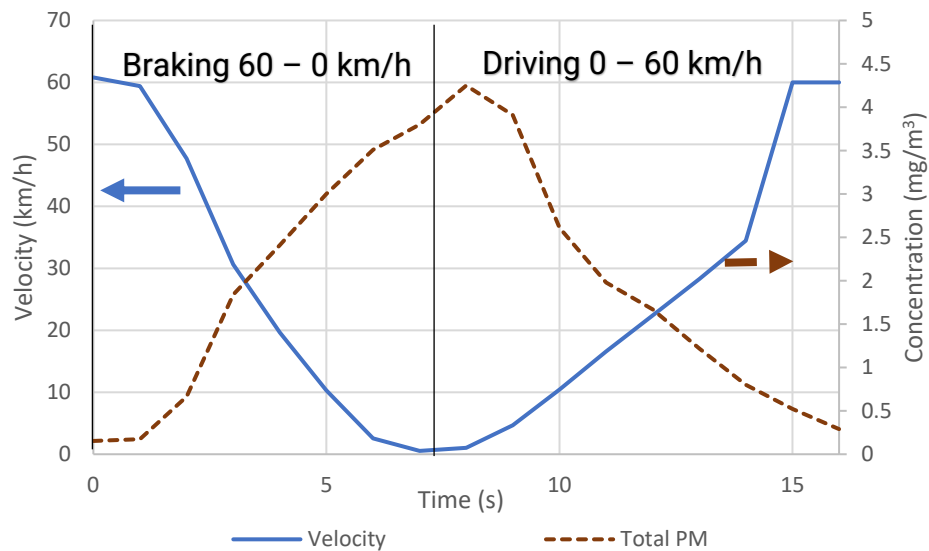
Figure 93 Real-time PM concentrations of heavy payload SUV under ISO 21994:2007 standard test

Figure 90 – **93** can lead (by average and calculate each test) to **Figure 94**. It shows PM mass concentration during ISO21994:2007 standard test. The mass PM concentration per stop is ranging from 0.71 – 2.12 mg/m^3. Higher payloads (200 kg additional), the PM can be increased more than twice.
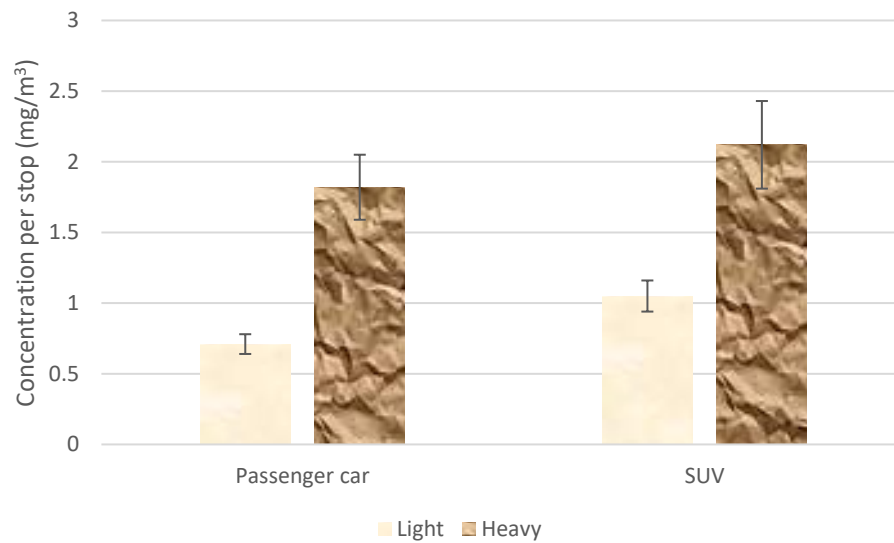
Figure 94 PM concentration under ISO 21994:2007 standard test

From the previous results, amounts of brake wear PM emissions of PM emissions are significantly related to payloads. These results correspond to (Ekathai et al., 2021). All the tested results can be found in **Appendix Figure 2 - 49**.

Particulate Matter characteristic and morphology from brake wear due to braking temperature

This part is focused on the effect of braking temperatures in cold test (brake temperature less than 130°C) and hot test (brake temperature above 130°C) on brake wear PM characteristics and morphology. The PM is collected on MCE filter 37 mm from Gilian Gilair-5 air sampling pump and brake pad of test vehicles to analyze the chemical compositions and morphology using Energy Dispersive x-ray Spectrometer (EDS), Total Carbon/Organic Carbon (TC/OC), and Scanning Electron Microscope (SEM).

Characteristic and morphology of brake pad material from passenger car

The microstructure and chemical compositions of the semi-metallic brake pad from mid-size passenger car are shown in **Figure 95** (SEM) (brake pad material structure is consistent with **Figure 3**), **Figure 96** (EDS), and **Table 16** (Chemical compositions). **Figure 96** and **Table 16** show the main components of brake pad, i.e., Carbon (C) which is distributed in black surface areas around 41.9 % by weight, Oxygen (O) which is spread around in brake pad about 21.15 % by weight. The metal components (sorted in weight in descending orders and diffuse in semi-metallic brake pad) are: 1.) Barium (Ba) which is used to fill up the empty spaces between the other components of brake pad, 2.) Iron (Fe) and 3.) Titanium (Ti) which are used to modify (increase or decrease) the coefficient of friction, 4.) Silicon (Si) is a fibrous material which improves the binder's mechanical properties (increases brake pad's strength), 5.) Copper (Cu) for improves thermal conductivity, 6.) Calcium (Ca), 7.) Aluminum (Al), and lastly 8.) Magnesium (Mg).
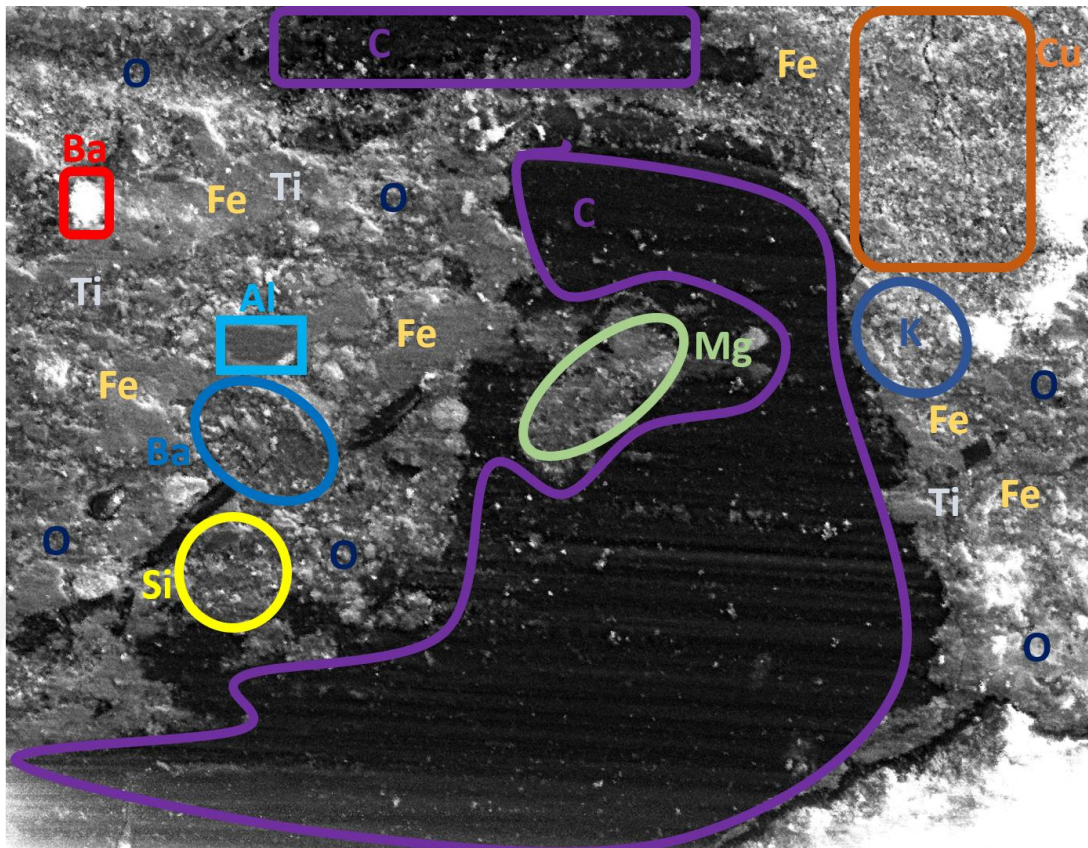
Figure 95 Microstructure of the semi-metallic brake pad from passenger car
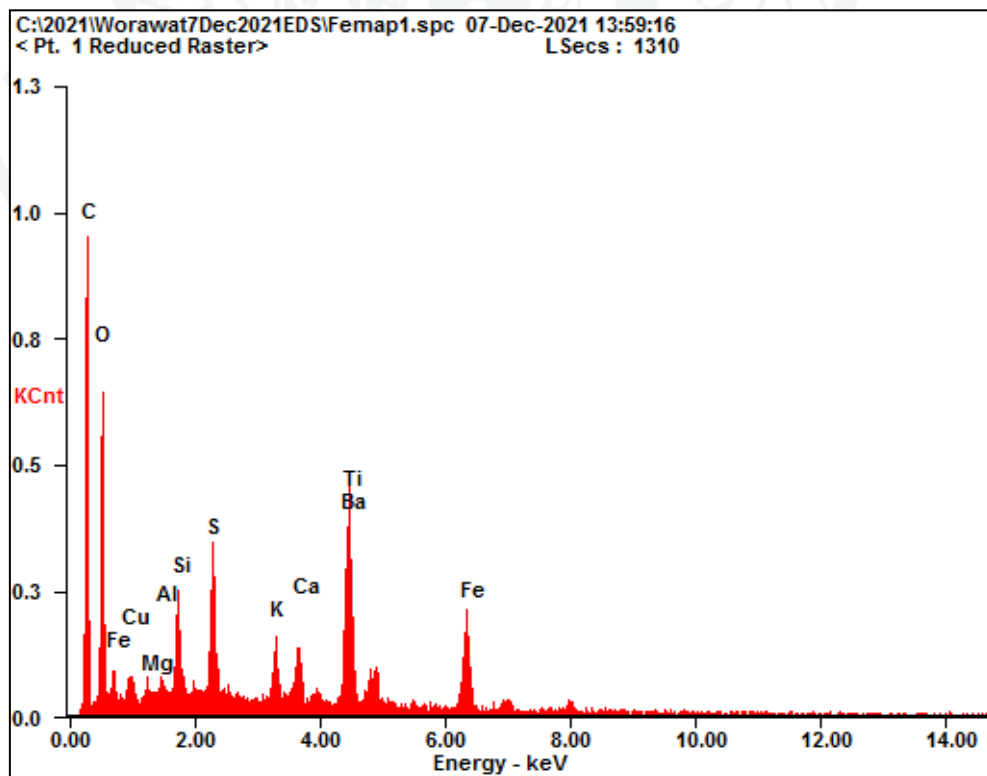
Figure 96 EDS of the semi-metallic brake pad from passenger car

Table 16 Chemical compositions of the semi-metallic brake pad from passenger car

Element	Wt%	At%
C	41.90	63.78
O	21.15	24.17
Cu	02.04	00.59
Mg	00.33	00.25
Al	00.39	00.27
Si	02.38	01.55
S	03.11	01.77
K	01.55	00.73
Ca	01.56	00.71
Ba	12.80	01.70
Ti	05.42	02.07
Fe	07.37	02.41

Characteristic and morphology of brake wear from passenger car

The MCE filters from brake wear of passenger car are shown in **Figure 97** it can be clearly seen that the hot test's filter (right) has a darker appearance than the cold test's filter (left) due to higher PM mass concentration. All samples collected in the MCE filters are analyzed using EDS, TC/OC, and SEM.

Figure 97 MCE filter (Left: cold test's filter and Right: hot test's filter) from passenger car

In the cold test, the chemical compositions of brake wear are Oxygen, Carbon and Nitrogen as shown in **Figure 98** and **Table 17**.
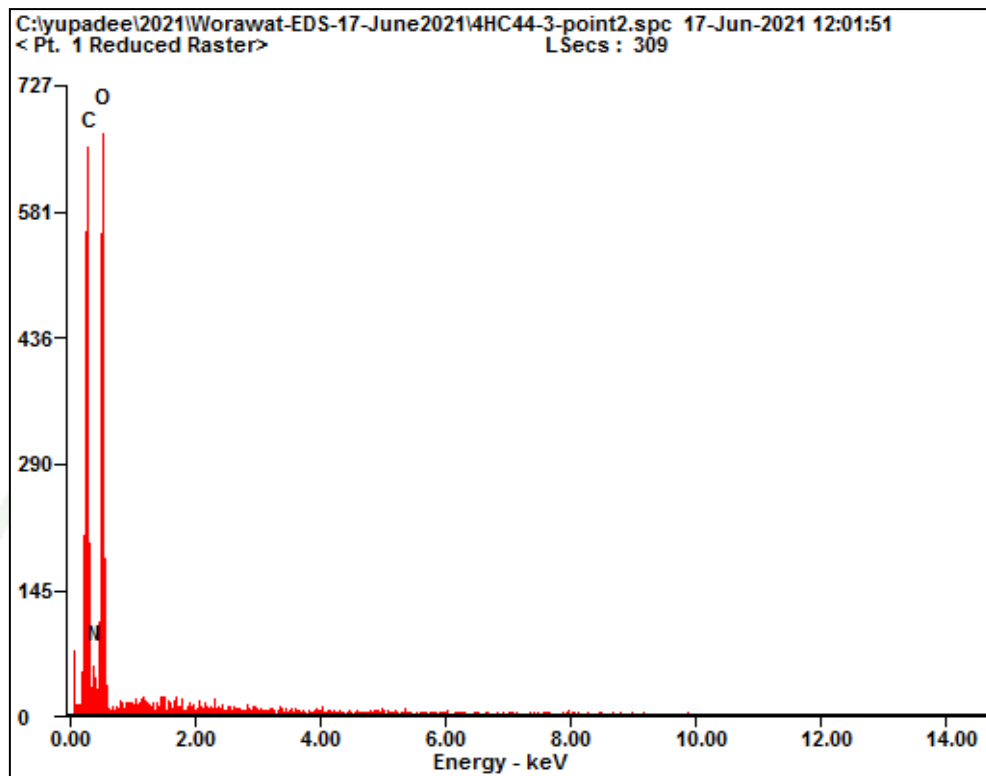
Figure 98 EDS of cold test's filter from passenger car

Table 17 Chemical compositions of cold test's filter from passenger car

Element	Wt%	At%
C	40.32	46.79
N	09.80	09.75
O	49.88	43.46

The chemical compositions of brake wear in the hot test are shown in **Figure 99** and **Table 18** with additional metal components, i.e., Iron (Fe), Platinum (Pt), Silicon (Si), Aluminum (Al), Magnesium (Mg) and Zinc (Zn), respectively. It can be noticed that Platinum and Zinc which are found in the brake wear came from the disc brake, whose coating with Platinum and Zinc in the first layer for wear resistant and heat resistant (Aranke, Algenaid, Awe, & Joshi, 2019), (Antamba, Azanza, Reyes, Remache, & Ruiz, 2020).
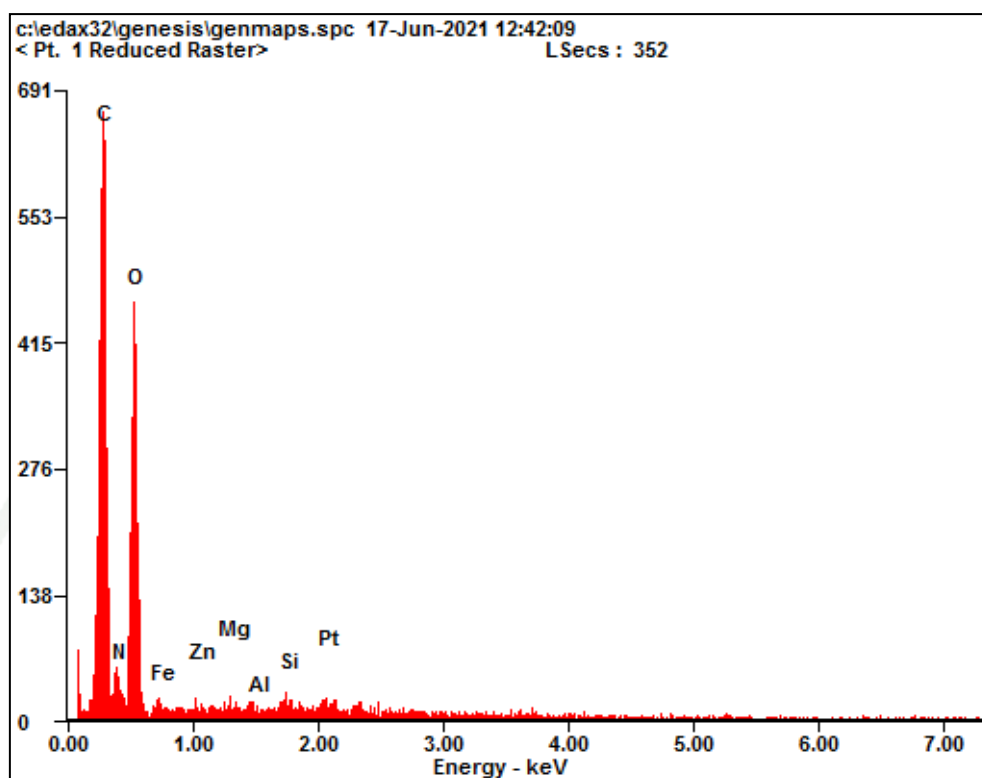
Figure 99 EDS of hot test's filter from passenger car

Table 18 Chemical compositions of hot test's filter from passenger car

Element	Wt%	At%
C	37.48	55.61
N	09.43	09.88
O	34.93	32.06
Fe	06.90	01.03
Zn	00.61	00.14
Mg	01.22	00.14
Al	02.48	00.26
Si	03.18	00.62
Pt	03.78	00.28

From cold and hot test filters, there are Carbon in large quantities. TC/OC method is used to further analyze an Organic Carbon (OC) and Inorganic Carbon (IC). **Figure 100** shows the Total Carbon (TC), IC and OC of the cold and the hot tests. The total carbon quantity from TC/OC method are almost equal to amount of carbon from EDS (**Table 17** and **Table 18**). In the cold test, all carbon component is organic carbon. In the hot test, a carbon composition is divided to organic carbon around 38 % (by weight) and inorganic carbon around 0.02 % (by weight).
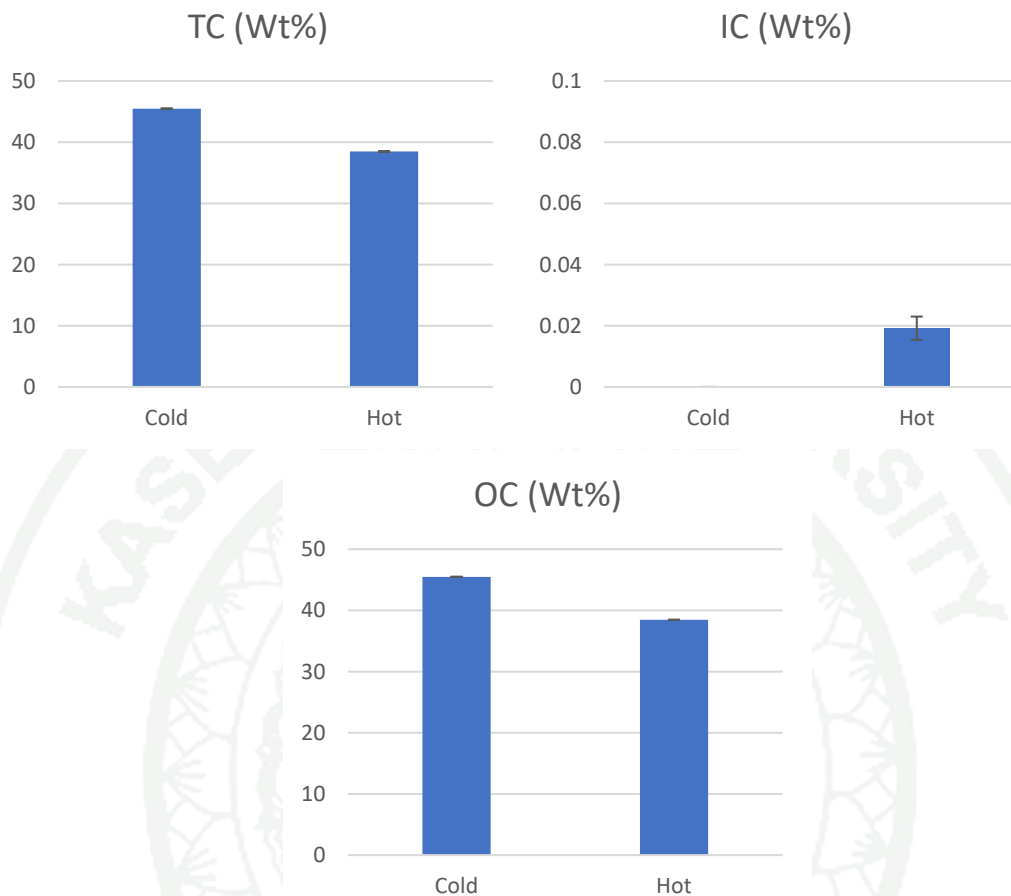
Figure 100 TC/OC of cold-hot test's filter from passenger car

From the previous part (**Figure 71** and **Figure 72**), the PM size distribution of the cold and the hot tests from brake wear particle concentrations in passenger car, it can be seen that in both the cold and the hot tests, most of particles are classified as PM_1 (around 87.69% and 80.72%, respectively). The PM characteristic and morphology from both the cold and the hot tests can be further analyze using SEM.

Figure 101 shows the microstructure of brake wear PM emission in 1,000x, 5,000x, 10,000x and 20,000x, in descending orders (from top to bottom of the figure). It can be seen that, the particle found in the cold test is spherical in shape similar to the shape of carbon and oxygen (Y. Kim et al., 2014). Whereas in the hot test, the texture of the PM emission is rougher (spherical covered with wavy shape) (Miler, 2021), due to the additional metallic compositions (which are not found in PM from the cold test).

Figure 101 SEM microstructure of brake wear from passenger car (left: cold test and right: hot test)
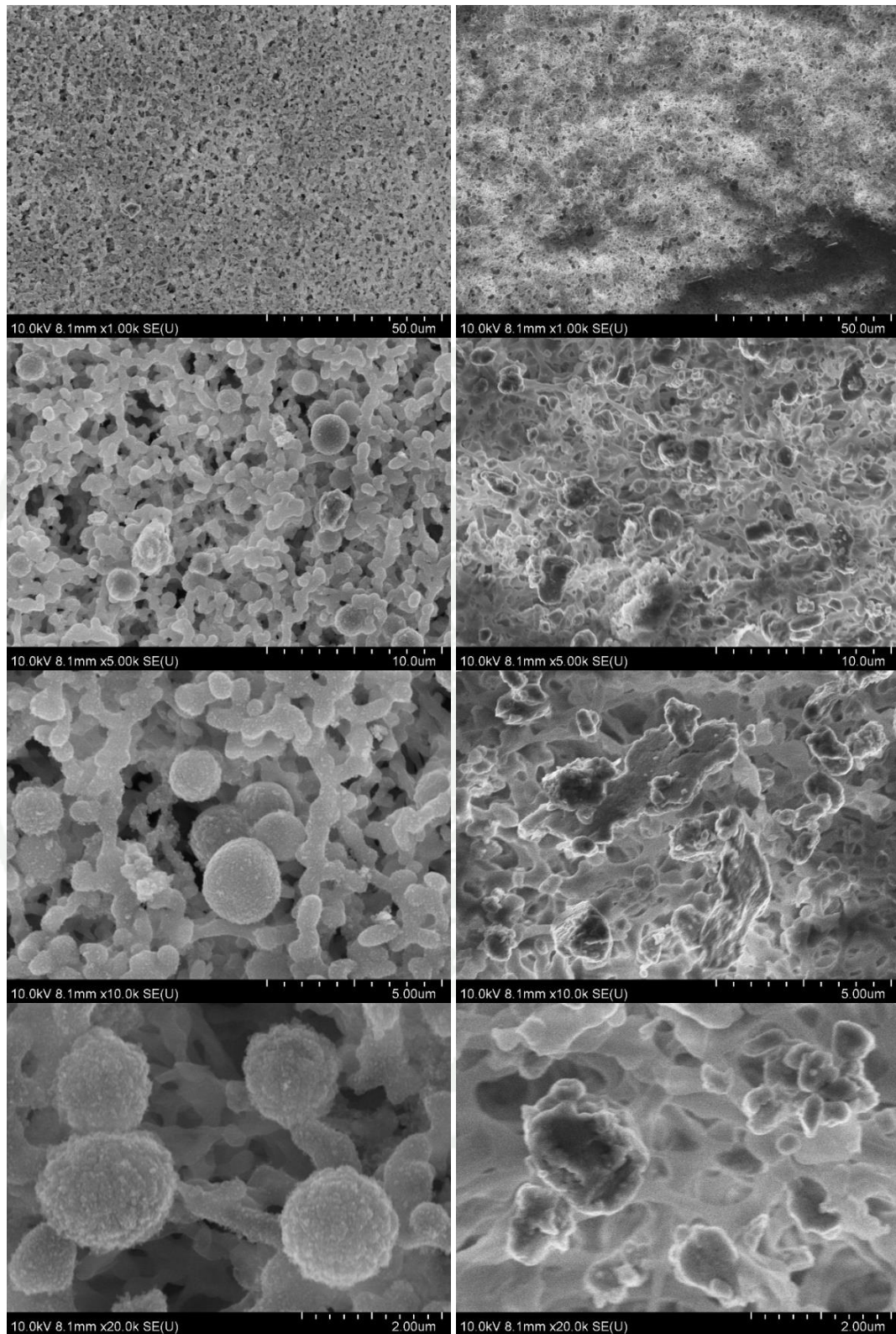
Characteristic and morphology of brake pad material from SUV

The results of particulate matter characteristics and morphology from studies in SUV repeated the same finding in passenger car (from all the studies above). The microstructure and chemical compositions of the semi-metallic brake pad from Subcompact crossover SUV are shown in **Figure 102** (SEM) (brake pad material structure is consistent with **Figure 3**), **Figure 103** (EDS) and **Table 19** (Chemical compositions). It shows the main components of brake pad, i.e., Carbon (C) which is distributed in black surface areas around 41.89% by weight, Oxygen (O) which is spread around in brake pad about 18.39% by weight. The metal components are Barium (Ba), Iron (Fe), Titanium (Ti), Silicon (Si), Aluminum (Al), Calcium (Ca), Magnesium (Mg), and Copper (Cu) sorted in weight in descending orders and diffuse in semi-metallic brake pad. They are fairly like semi-metallic brake pad of passenger car.
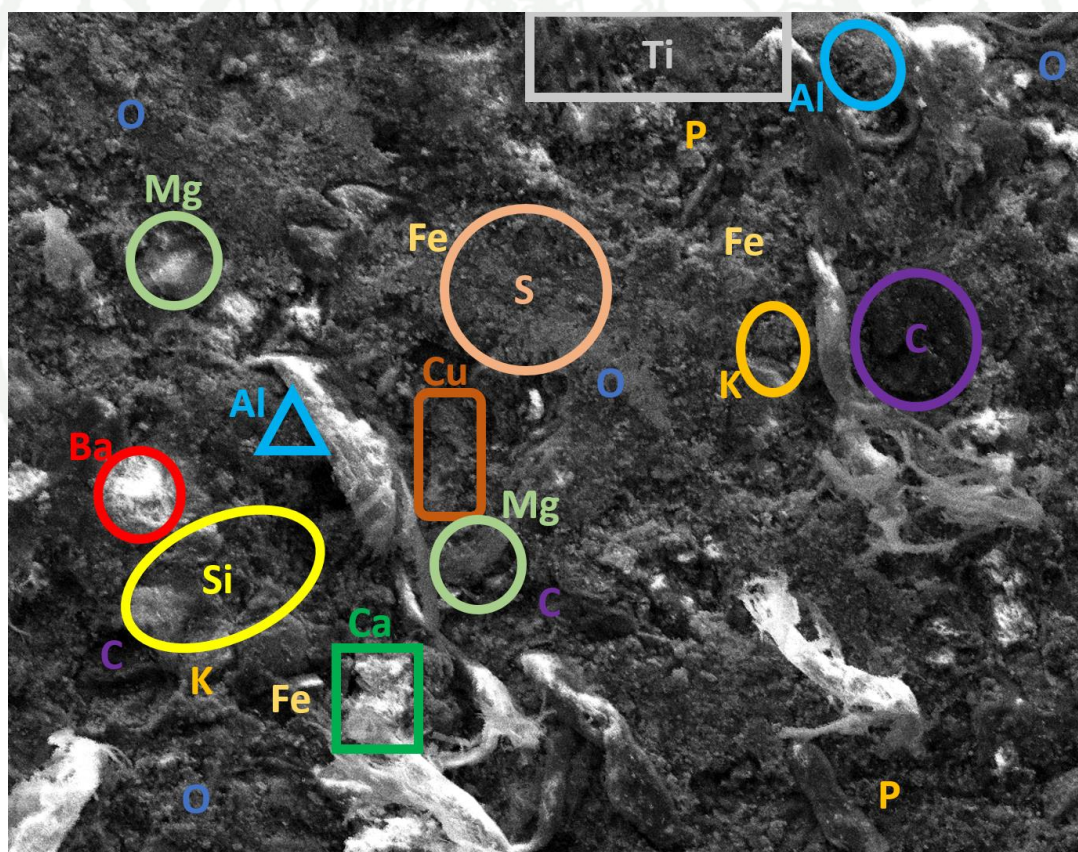
Figure 102 Microstructure of the semi-metallic brake pad from SUV
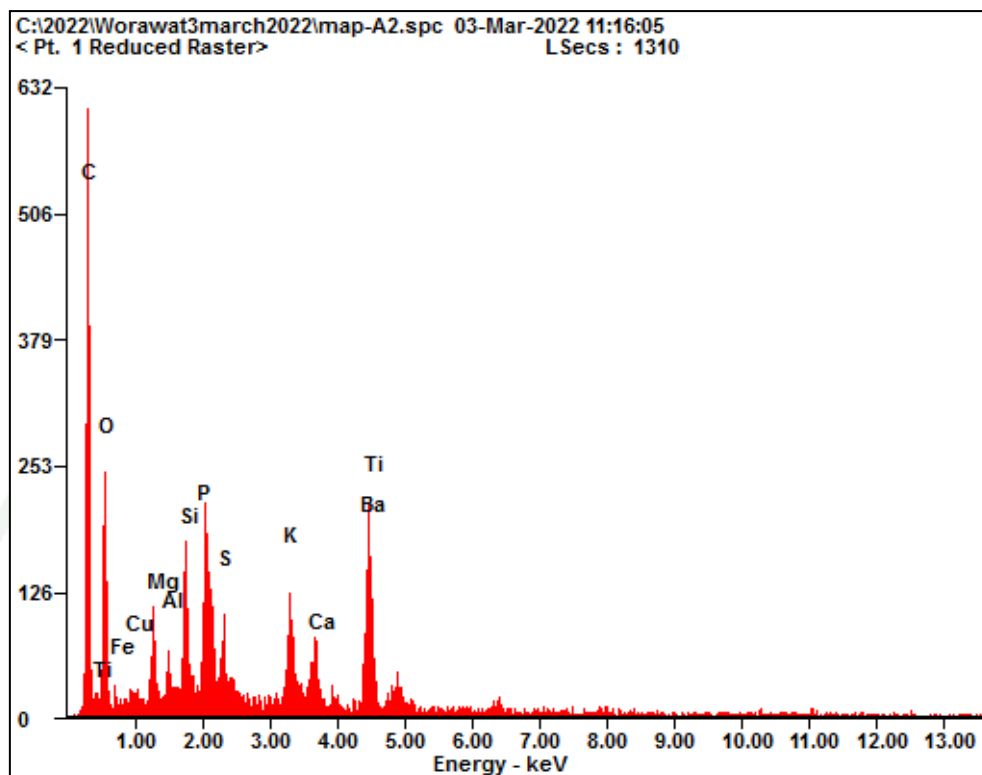
Figure 103 EDS of the semi-metallic brake pad from SUV

Table 19 Chemical compositions of the semi-metallic brake pad from SUV

Element	Wt%	At%
C	41.89	67.92
O	18.39	19.58
Fe	07.37	00.72
Cu	01.07	00.29
Mg	01.73	01.21
Al	02.68	00.43
Si	03.08	01.87
P	03.10	01.70
S	01.47	00.78
K	03.05	01.33
Ca	01.69	00.72
Ba	08.89	01.10
Ti	05.60	02.35

Characteristic and morphology of brake wear from SUV

The MCE filters from brake wear of passenger car are shown in **Figure 104**. The hot test's filter (right) has a darker appearance than the cold test's filter (left) due to higher PM mass concentration.

Figure 104 MCE filter (Left: cold test's filter and Right: hot test's filter) from SUV

Figure 105 and **Table 20** shows the chemical composition of cold test by EDS. The chemical compositions of brake wear are Oxygen, Carbon and Nitrogen and the percentage of weight of compositions are almost like in passenger as seen in **Figure 98** and **Table 17**.
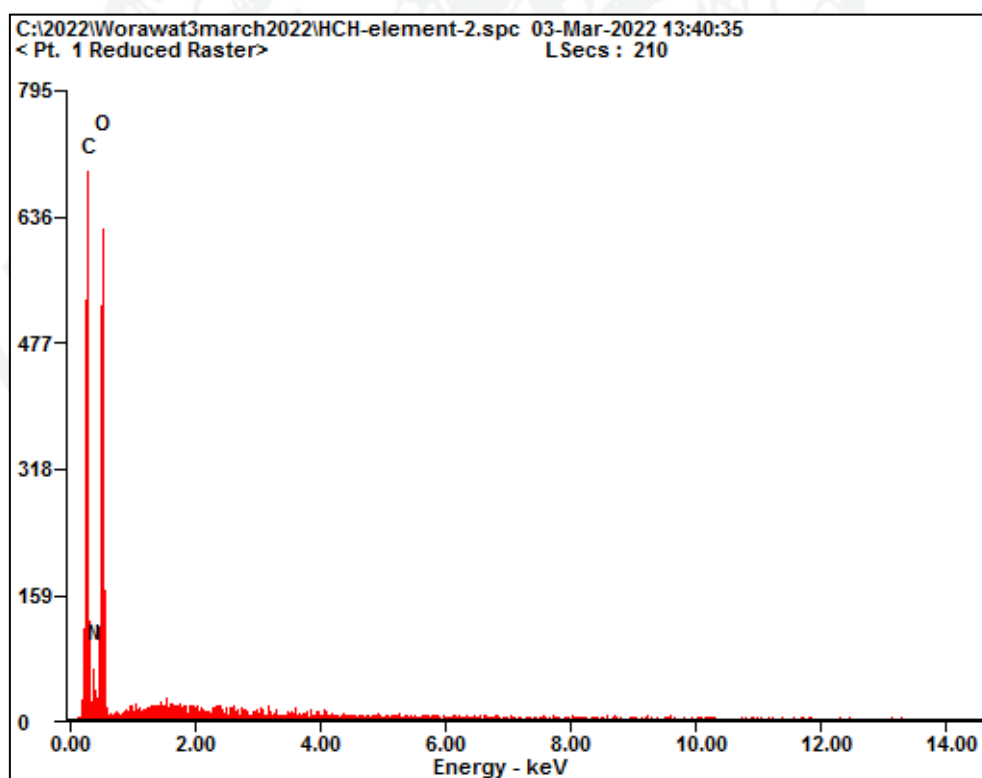
Figure 105 EDS of cold test's filter from SUV

Table 20 Chemical compositions of cold test's filter from SUV

Element	Wt%	At%
C	41.52	48.01
N	09.95	09.87
O	48.53	42.12

In hot test, the chemical compositions of brake wear are shown in **Figure 106** and **Table 21**. The main chemical compositions which additional from cold test is Iron. Also, Barium, Silicon, Aluminum and Copper are added as well. All Brake wear compositions in this test are related to the compositions of brake pad.
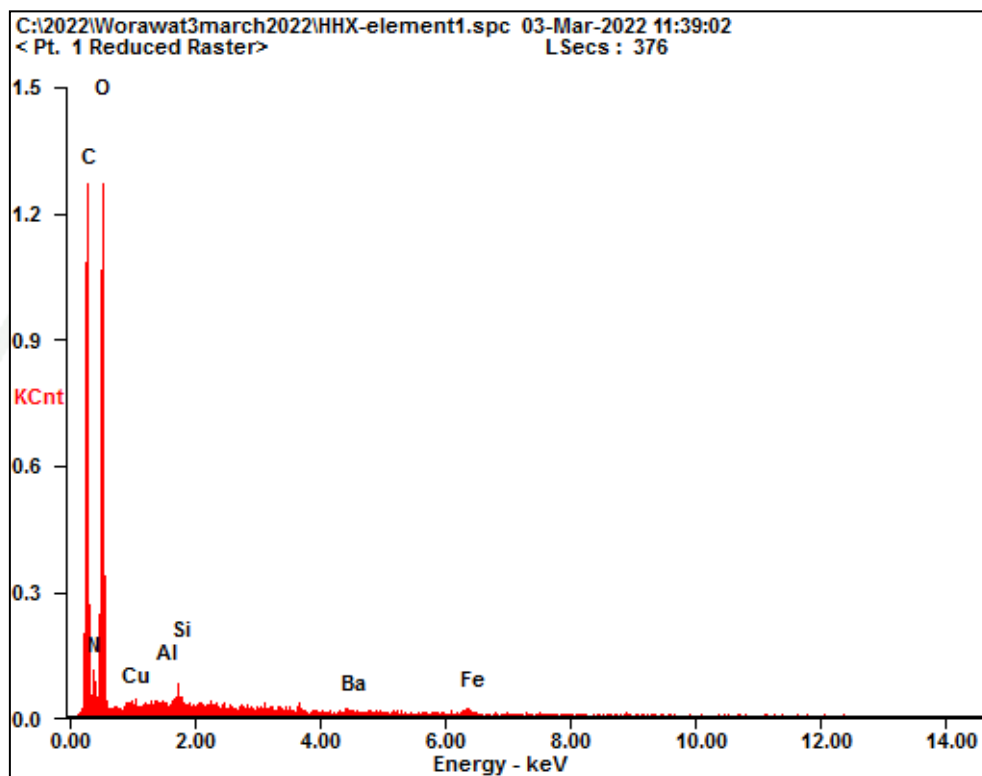
Figure 106 EDS of hot test's filter from SUV

Table 21 Chemical compositions of hot test's filter from SUV

Element	Wt%	At%
C	38.85	49.32
N	08.36	08.65
O	40.70	40.51
Cu	00.76	00.17
Al	01.25	00.13
Si	01.70	00.36
Ba	01.82	00.19
Fe	06.57	00.67

In respect of TC/OC, **Figure 107** shows TC, IC and OC of the cold and the hot tests. It can be concluded that, almost all carbon of brake wear is organic carbon due to the materials of semi-metallic brake is organic materials, as total organic carbon (Borawski, 2020).

TC (Wt%)

IC (Wt%)

TOC (Wt%)
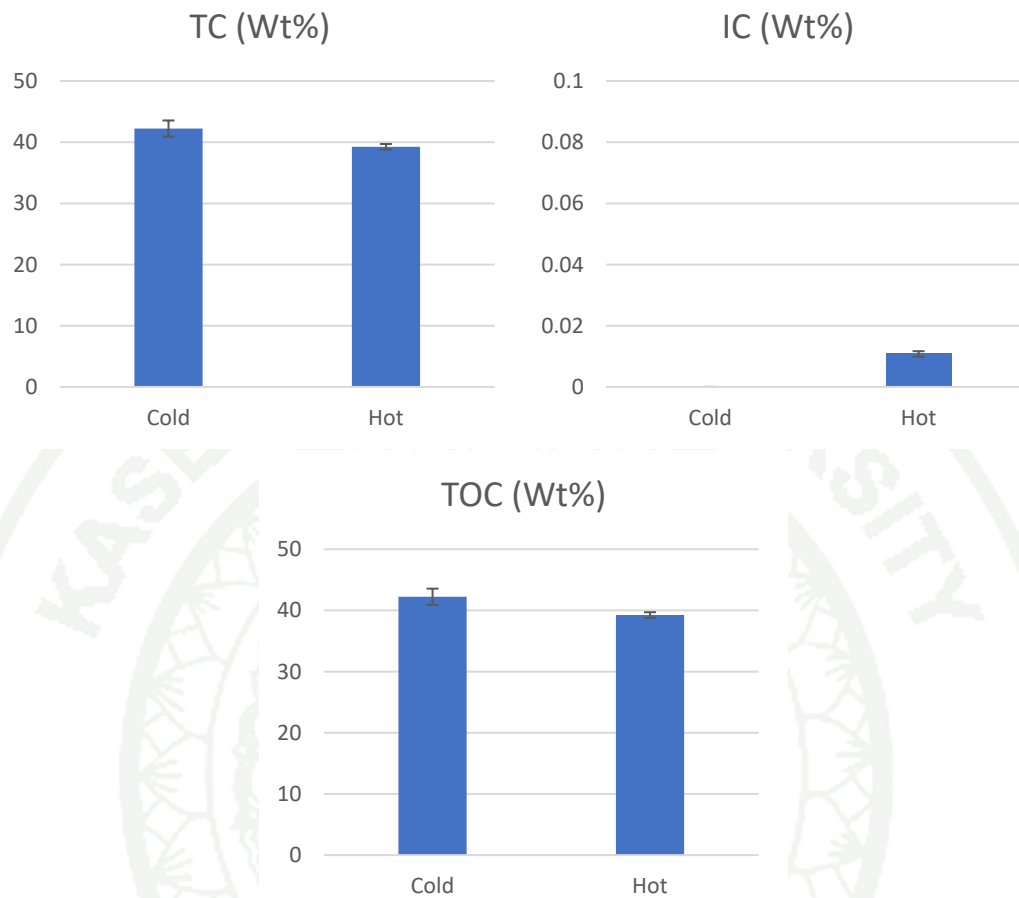
**Figure 107** TC/OC of cold-hot test's filter from SUV

Figure 108 shows the microstructure of brake wear PM emission in 1,000x, 5,000x, 10,000x and 20,000x, in descending orders (from top to bottom of the figure). Considering the particle found in the cold test is in spherical shape because there is not a metal component, while in the hot test the texture of the PM emission is quite rough due to the PM composition. Therefore, the particle in the hot test is deployed to do the mapping for find a cohesion of metal component on particle (as shown in **Figure 109**).
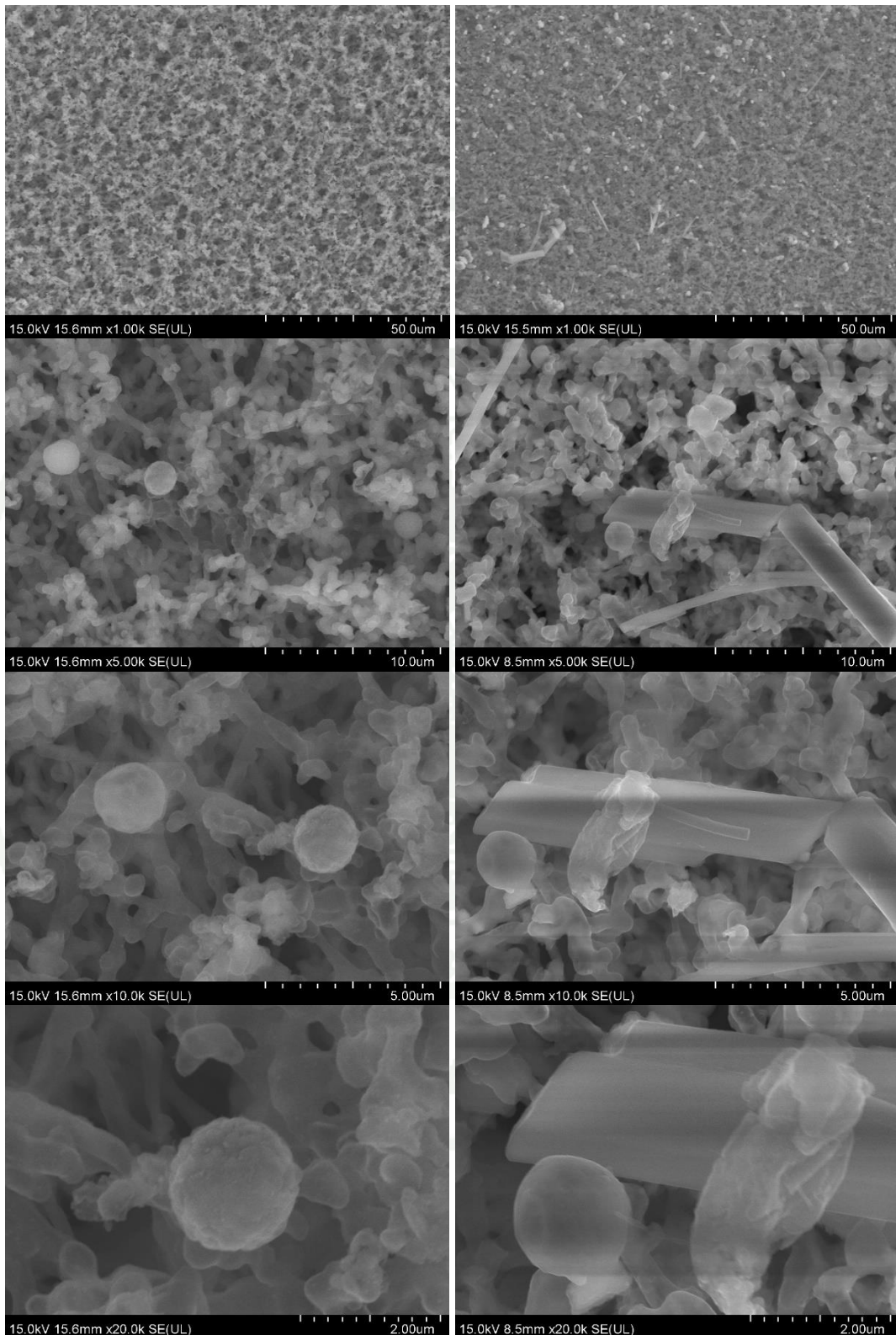
Figure 108 SEM microstructure of brake wear from SUV (left: cold test and right: hot test)

Figure 109 shows PM morphology, it can be seen that a carbon is spherical shape, oxygen and nitrogen which is spread around in filter, they are corresponds to

the cold test. However, the texture of the metal components (Fe, Ba, Si, Al and Cu) is quite rough that effect to the PM morphology in the hot test is spherical covered with wavy shape.
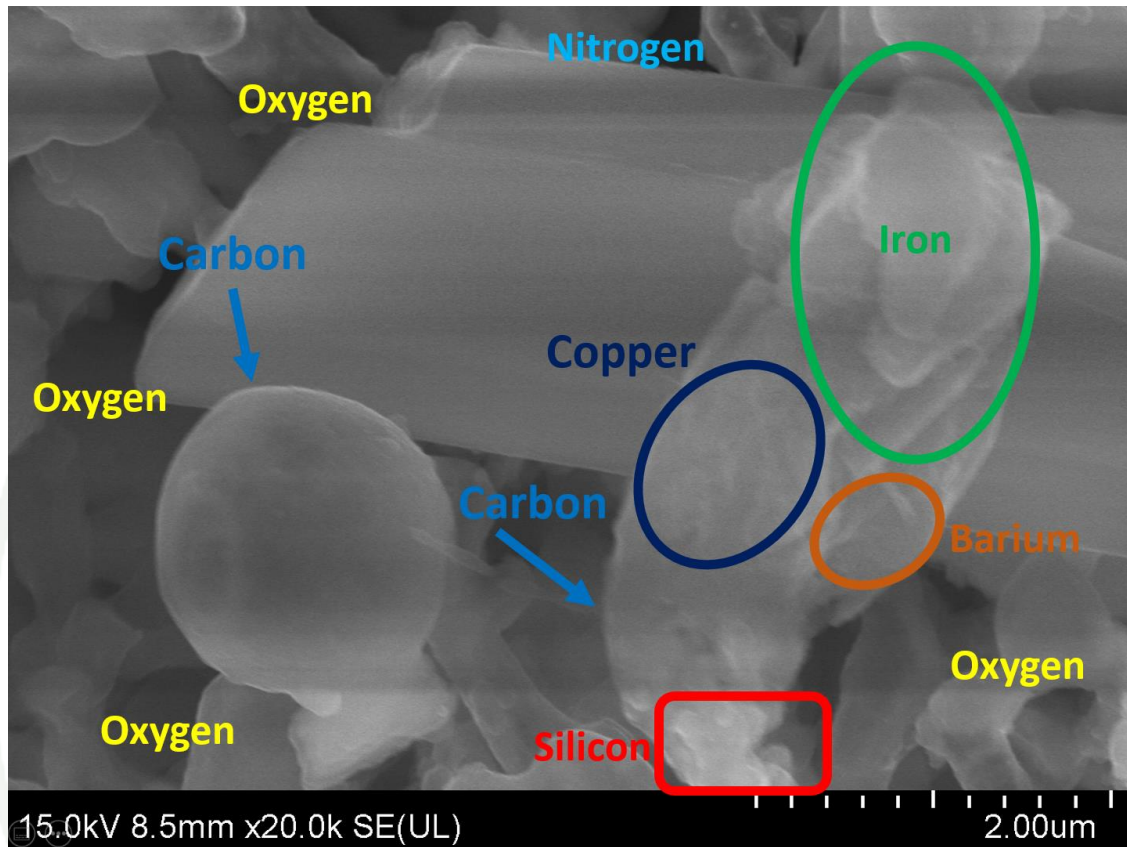
Figure 109 Mapping of hot test's filter from SUV

From this topic, it can be concluded that Oxygen, Carbon (mostly organic) and Nitrogen are found in the brake wear in both the cold and the hot tests. While in the hot test, the additional metal components are found. In term of shapes, PM from the cold test is spherical in shape (similar to shape of Oxygen and Carbon), while PM in the hot test is with rough surface due to metal covering.

Next part will describe about fundamental understanding of particulate matter characteristics from brake mechanisms.

Summarized data to identifying particulate matter characteristics from brake wear mechanisms

A braking system consists of a brake pad and a disc brake, the former being a soft polymer matrix impregnated with small, hard particles or fibers. During braking, the hard particles embedded in the pad wear the disc, generating additional particles which play adjunctive roles in friction and wear and which, because they are loosely held, escape into the environment.

All of results in this research (calculated from passenger car and SUV) can point out the PM concentration in each factor as shown in **Figure 110** this data range corresponds to what found in (Kukutschová & Filip, 2018). It can be seen that in the hot test with heavy payload have a more size distribution than the others test. The payload factor can increase PM_1, $PM_{2.5}$, PM_4, PM_{10} and total PM is 77.49%, 85.43%, 92.79%, 97.53% and 96.63%, respectively. While Temperature factor can increase PM_1, $PM_{2.5}$, PM_4, PM_{10} and total PM is 117.36%, 119.04%, 122.09%, 121.71% and 120.30%, respectively. The average PM concentration (0.12 – 0.5 mg/m^3 of PM_{10}, 0.1 - 0.38 mg/m^3 of $PM_{2.5}$, and 0.09 – 0.31 mg/m^3 of PM_1) and the mass PM concentration of brake wear per stop is ranging from 0.71 – 2.12 mg/m^3 are less than many researchers. Due to in the current study, conditions on PM measurement including driving cycle differs significantly from the literature. For example, in some literatures, the tests are done at longer distances and real traffic. The vehicle velocity is much higher than our study since the test is on a highway. The driving pattern in the current study is chosen only based on driving in city areas.
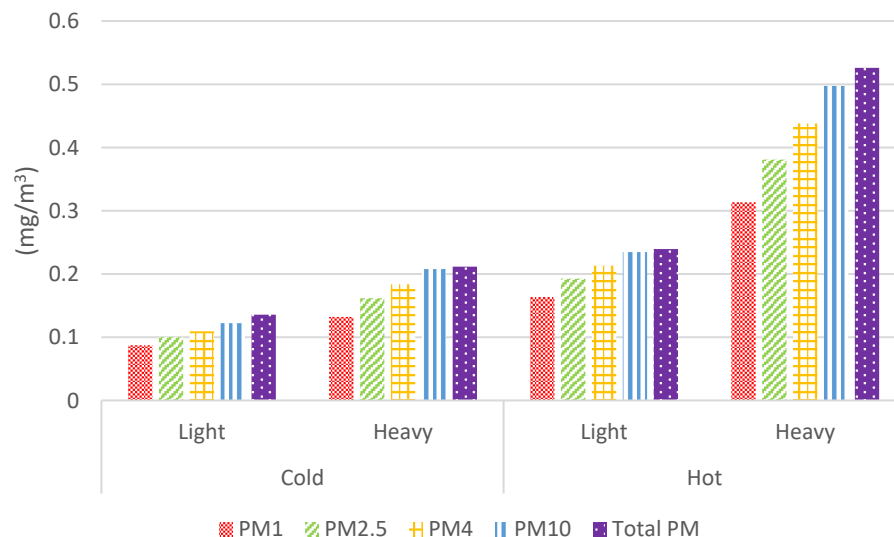
Figure 110 PM concentration in each factor

The schematic diagram of PM concentration and size distribution in payloads and brake temperature are shown in **Figure 111**. The increased payloads result in larger PM size as well as, higher brake temperature has significant effect to larger PM size.
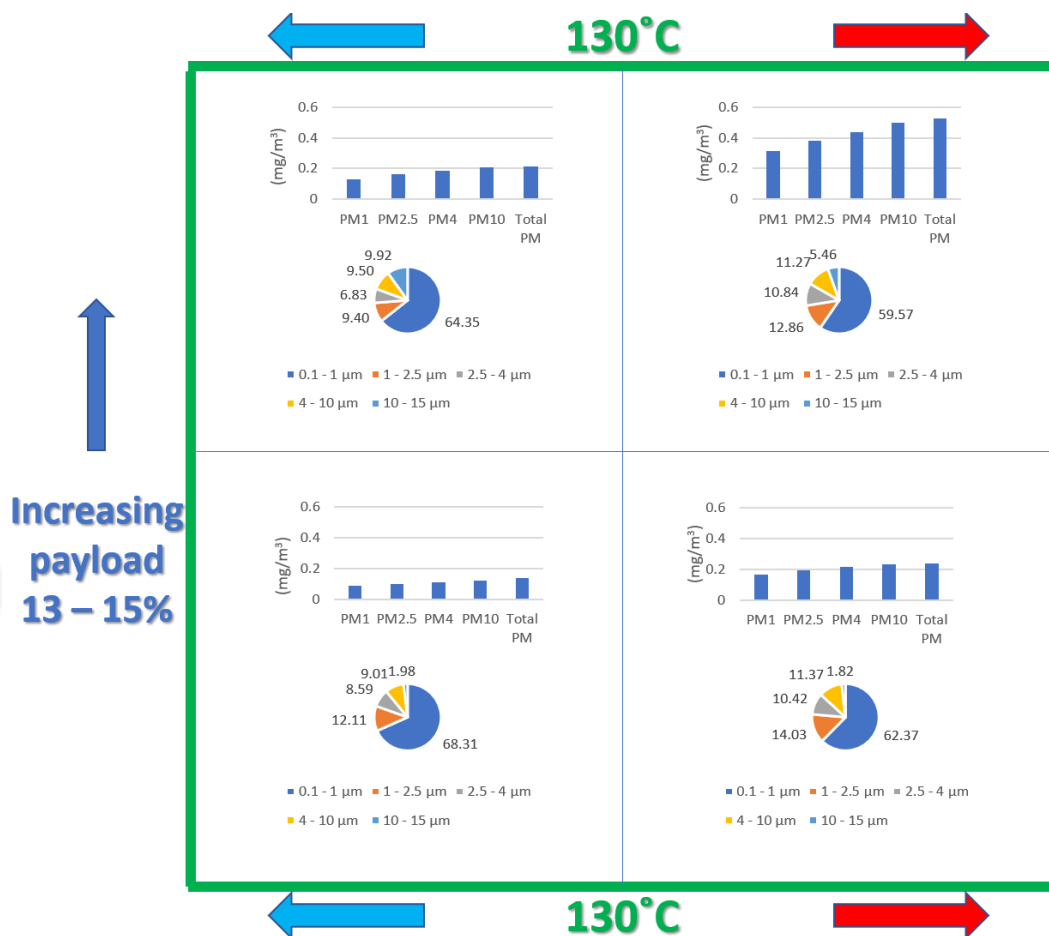
Figure 111 Schematic diagram of PM concentration and size distribution

Based on the current study, the fundamental understandings of PM formation from brake wear mechanism in on road measurement are as the follows:

The controlling factors in the PM formation of brake wear are, First, payloads of vehicle (i.e., heavier vehicles also have more friction to stop the vehicles). Second, Braking temperature (i.e., high friction can initiate high temperature of the brake pad). Third, vehicles type (i.e., the ventilation of braking system). All factors can be explained as follows:

Payloads is expected to play a role in emission factors. Current study provided evidence that there is indeed a correlation between weight and brake wear emissions. The impact of addition payload 200 kg has on brake wear emission factor. Heavy payloads are found to be 97.53% increasing brake wear PM_{10} concentration and 77.49% increasing brake wear PM_1 concentration. The increasing of payloads is effect to PM concentration as shown in **Figure 112**. Including in ISO 21994:2007 standard, various payloads affect to PM behavior that consistent with (Hagino et al., 2015) in passenger car.
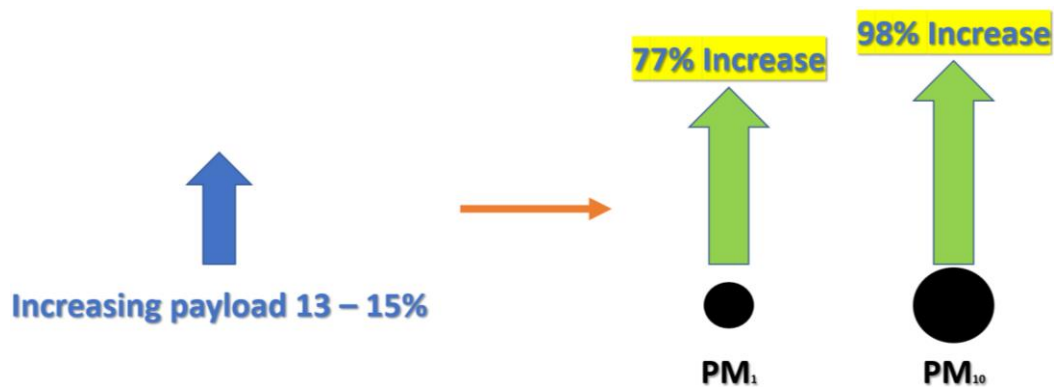
Figure 112 Schematic diagram of Increasing payload

Current PM emission of vehicle brake wear particles derive from constant driving and depend on the initial wheel speed and deceleration. In addition, brake wear particles are produced under transient driving cycles with acceleration and deceleration. The driving behavior has direct effect to brake temperature. For example, longer driving/braking time effects on accumulation of braking temperature.

Brake wear products can be generated by different wear mechanisms during friction processes. At temperatures under 130˚C, the PM concentration is lower and size distribution is smaller than when comparing with temperature above 130˚C. The chemical compositions of brake wear are only: 1.) Oxygen come from oxidation of raw materials, such as phenolic resin, in the pad during the braking depends on the temperature but also on the oxygen diffusion capability through the pad (Macías, Lorenzana, & Fernandez, 2020). 2.) Carbon (Organic Carbon due to the materials of semi-metallic brake is organic materials, as total organic carbon (Borawski, 2020)) come from not only epoxy resin (binder) their low resistance to heat (the results of some researchers show that even at a temperature of 100°C), a weight loss of about 7% can be noted (Agunsoye, Bello, Bamigabiye, Odunmosu, & Akinboye, 2018) this mass loss can be associated with the formation of volatiles during firing, but also reinforcement for supporting the structure is fallen out. And 3.) Nitrogen (it will investigate this observation more in future work). The physical of PM is spherical shape.

On the other hand, at temperature above 130˚C PM concentration is found to be 121.71% increasing brake wear PM_{10} concentration and 117.36% increasing brake wear PM_1 concentration (calculated from passenger car and SUV) as shown in **Figure 113**, the chemical compositions of brake wear are not only Oxygen, Carbon (Organic Carbon) and Nitrogen but also the metal components are found in brake wear, i.e., 1.) Iron come from not only fillers (fly ash) in (Sugözü, 2018), the value of the coefficient of friction in cooperation with cast iron is constant, or even rising with the temperature, it reaches little more than 0.3 at operating temperatures of 200°C (low resistant to high temperature) that cause to when the high temperature, it easy to crack, but also abrasive (steel) that unfortunately, due to friction in the contact areas, excessive temperatures are generated. This may lead to destruction of the pad's structure and lead to separation of its components. 2.) Silicon come from fillers (fly

ash). 3.) Aluminum come from fillers (fly ash) and abrasives (boron) it is also observed that when temperatures exceed 100°C, the coefficient of friction significantly drops. However, other studies have been found that it has thermal stability up to 200°C. 4.) Barium come from barite (fillers). 5.) Copper comes from abrasive. And 6.) Magnesium. Moreover, when the brake temperature reach to 230°C the compositions of disc brake are fallen out (Platinum and Zinc). The physical of PM is spherical covered with wavy shape cause to size distribution are bigger than PM from temperatures under 130°C although size of the most PM from brake wear is smaller than 1 µm.
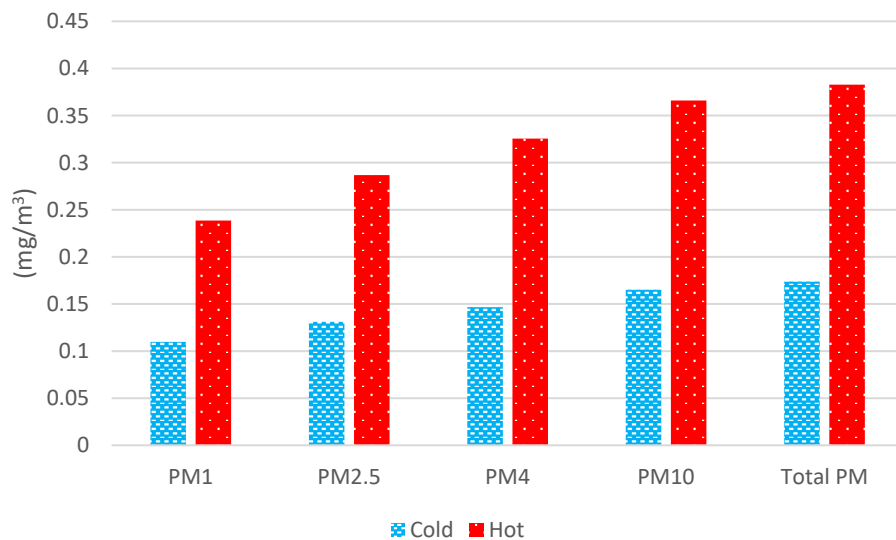
Figure 113 PM mass concentration of brake temperature

Considering, brake wear characteristics and morphology in each temperature range, it is found out that binder and reinforcement are fallen out when the braking temperature is low (under 130°C). This is why only C, O and N (which are found in binder and reinforcement from brake pad) are found in the PM from the cold test; while fillers and abrasive are fallen out (metal components) when the braking temperature is high (above 130°C). Furthermore, when the temperature rises above 230°C* (only in passenger car), Pt and Zn from disc brake are the additional fall-out. The PM characteristics and morphology in each temperature range as shown in **Figure 114**.

*(The brake temperature in SUV never reaches 230°C)
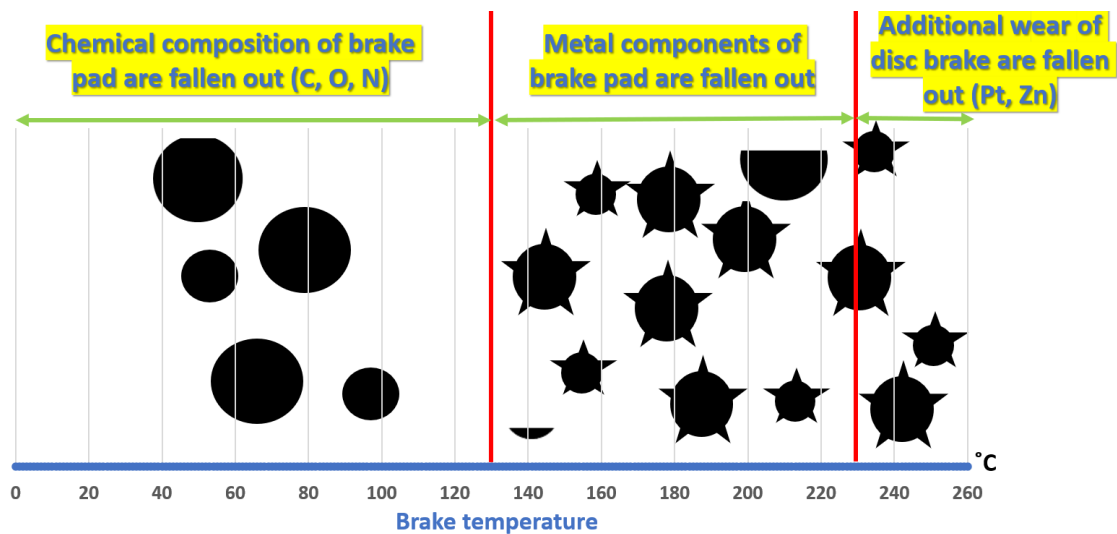
Figure 114 Schematic diagram of PM characteristics and morphology in each temperature range

In summary, high braking temperature adversely affect PM emissions from brake wear (at some point of braking in hot test, they can be as high as 15 mg/m^3). This study highly suggested that designing of vehicle braking system should take serious consideration on its ventilation to minimize the temperature of the brake pad (hot brake temperature, PM concentrations can be increased more than twice). In addition, minimizing the vehicle payload (with 200 kg of additional loads on the vehicle, PM concentrations can be increased almost twice) and the heavy braking behavior of the driver could also help reduce PM (from brake wear) emissions.

CONCLUSION AND RECOMMENDATION

Conclusion

This research study focuses on fundamental understandings of PM formation from brake wear mechanism. The following conclusions are made.

1.) PM sampling system for collecting direct brake wear particles are built and installed at the left front size wheel of the tested vehicle. The field test of real-world driving conditions can be done with repeatability. This system is applicable to all driving pattern and condition as it stabilize steering/wheel angle.

2.) The amount of PM concentration from brake wear emissions are influenced by not only driving cycle test, but also the brake temperature. The cut-point of brake temperature 130°C are introduced in the current study. Results shows different amounts of PM emissions between cold and hot tests. The amount of PM concentration from brake wear emissions are influenced by braking temperature with increasing around 120%. Payloads significantly effects brake wear PM emissions. With 200 kg of additional loads on the vehicle, PM concentrations can be increased more than twice. It is speculated that higher payloads not only increase brake wear PM emissions during deceleration, but also acceleration (resuspension effect).

3.) The size distribution of 0.1 – 1 µm, 1 – 2.5 µm, 2.5 – 4 µm, 4 – 10 µm and 10 – 15 µm from brake wear are 63.64%, 12.1%, 9.16%, 10.3% and 4.8%, respectively. In the cold tests only binder and reinforcement from brake pad are fallen out. while in the hot test binder, reinforcement, fillers, and abrasive from brake pad are fallen out. The components of disc brake are fallen out when the brake temperature higher than 230°C. PM in the cold test is in spherical shape (similar to shape of Oxygen and Carbon), while PM in the hot test is with rough surface due to metal covering.

Recommendations

The recommendations of this research are as the follows:

1.) Brake wear PM emission is investigated and mainly focuses on the factors that affect brake wear PM emissions by on-road vehicle measurement. The study is done on variable factors affecting brake temperature from real-world driving. From this study, further observations on: 1.) brake temperature distribution, which are related to real-time PM mass measurement (using thermal camera on rotor), 2.) brake wear formation (using laser diagnostics techniques) are open ends for further researches.

2.) In terms of PM size distribution from both passenger car and SUV, it is found that PM from brake wear of SUV is larger in size due to quicker rising of SUV's brake temperature (starting from 50°C). It is highly recommended that this finding shall be performed in future research works.

3.) From this research, payloads of vehicles and high brake temperature (metal components, come from fillers and abrasive are fallen out) contribute to PM mass concentration. It is recommended that further studies on ways and means to reduce vehicle weight and better ventilation of brake system shall be performed.

4.) All findings, data and information from this research should be verified in simulation for predicting formulas of brake wear PM emission factor and/or applied to further studies for saving the resources.

LITERATURE CITED

Adachi, K., & Tainosho, Y. (2004). Characterization of heavy metal particles embedded in tire dust. *Environ Int, 30*(8), 1009-1017. doi:10.1016/j.envint.2004.04.004

Agunsoye, J., Bello, S., Bamigabiye, A., Odunmosu, K., & Akinboye, I. (2018). Recycled ceramic composite for automobile brake pad application. *Journal of Research in Physics, 39*. doi:10.2478/jrp-2018-0004

Amato, F., Pandolfi, M., Moreno, T., Furger, M., Pey, J., Alastuey, A., . . . Querol, X. (2011). Sources and variability of inhalable road dust particles in three European cities. *Atmospheric Environment, 45*(37), 6777-6787. doi:https://doi.org/10.1016/j.atmosenv.2011.06.003

Antamba, J., Azanza, V., Reyes, G., Remache, Á., & Ruiz, S. (2020). Manufacture material characteristic analysis of original and alternative auto parts. Case Study: Brake Disc. *Enfoque UTE, 11*(3), 102-110. Retrieved from https://www.redalyc.org/articulo.oa?id=572263177010

Apeagyei, E., Bank, M. S., & Spengler, J. D. (2011). Distribution of heavy metals in road dust along an urban-rural gradient in Massachusetts. *Atmospheric Environment, 45*, 2310-2323. doi:10.1016/j.atmosenv.2010.11.015

Aranke, O., Algenaid, W., Awe, S., & Joshi, S. (2019). Coatings for Automotive Gray Cast Iron Brake Discs: A Review. *Coatings, 9*(9), 552. Retrieved from https://www.mdpi.com/2079-6412/9/9/552

Auto, F. (2019). The Different Types of Brake Pads. Retrieved from https://autorepairboulder.com/different-brake-pads/

Aza, C. A. (2014). Composites in Automotive Applications: Review on brake pads and discs. *Adv. Compos. Cent. Innov. Sci., Univ. Bristol*, 1-13.

AZUMA, T. (2020). Common Types Of Brake Pads You Need To Know. Retrieved from https://carfromjapan.com/article/car-maintenance/common-types-of-brake-pads-know/

Barlow, T. (2014). *Briefing paper on non-exhaust particulate emissions from road transport.*

Barreda, A., Sanz, J., & González, F. (2015). Using linear polarization for sensing and sizing dielectric nanoparticles. *Optics Express, 23*, 9157. doi:10.1364/OE.23.009157

Bergmann, M., Kirchner, U., Vogt, R., & Benter, T. (2009). On-road and laboratory investigation of low-level PM emissions of a modern diesel particulate filter equipped diesel passenger car. *Atmospheric Environment, 43*(11), 1908-1916. doi:https://doi.org/10.1016/j.atmosenv.2008.12.039

Bijwe, J. (1997). Composites as friction materials: Recent developments in non-asbestos fiber reinforced friction materials—a review. *Polymer composites, 18*(3), 378-396.

Borawski, A. (2020). Conventional and unconventional materials used in the production of brake pads – review. *Science and Engineering of Composite Materials, 27*(1), 374-396. doi:doi:10.1515/secm-2020-0041

Brewer, P. (1997). *Vehicles as a Source of Heavy Metal Contamination in the Environment.* (M.Sc.). University of Reading, Berkshire, UK.,

Brockmann, J., Lucero, D., Romero, T., & Pentecost, G. (1993). *Calibration of the On-Line Aerosol Monitor (OLAM) with ammonium chloride and sodium chloride*

aerosols. Retrieved from

Bukowiecki, N., Gehrig, R., Lienemann, P., Hill, M., Figi, R., & Buchmann, B. (2009). PM10 emission factors of abrasion particles from road traffic. *Swiss Fed. Dep. Environ. Transp. Energy Commun.*, 1-194.

Bukowiecki, N., Lienemann, P., Hill, M., Furger, M., Richard, A., Amato, F., . . . Gehrig, R. (2010). PM10 emission factors for non-exhaust particles generated by road traffic in an urban street canyon and along a freeway in Switzerland. *Atmospheric Environment, 44*(19), 2330-2340. doi:https://doi.org/10.1016/j.atmosenv.2010.03.039

Cadle, S. H., & Williams, R. L. (1978). Gas and Particle Emissions from Automobile Tires in Laboratory and Field Studies. *Journal of the Air Pollution Control Association, 28*(5), 502-507. doi:10.1080/00022470.1978.10470623

Cassee, F. R., Héroux, M.-E., Gerlofs-Nijland, M. E., & Kelly, F. J. (2013). Particulate matter beyond mass: recent health evidence on the role of fractions, chemical constituents and sources of emission. *Inhalation toxicology, 25*(14), 802-812. doi:10.3109/08958378.2013.850127

Chan, D., & Stachowiak, G. (2004). Review of automotive brake friction materials. *Proceedings of the Institution of Mechanical Engineers, Part D: Journal of Automobile Engineering, 218*(9), 953-966.

Chow, J. C., Watson, J. G., Houck, J. E., Pritchett, L. C., Fred Rogers, C., Frazier, C. A., . . . Ball, B. M. (1994). A laboratory resuspension chamber to measure fugitive dust size distributions and chemical compositions. *Atmospheric Environment, 28*(21), 3463-3481. doi:https://doi.org/10.1016/1352-2310(94)90005-1

Dahl, A., Gharibi, A., Swietlicki, E., Gudmundsson, A., Bohgard, M., Ljungman, A., . . . Gustafsson, M. (2006). Traffic-generated emissions of ultrafine particles from pavement–tire interface. *Atmospheric Environment, 40*(7), 1314-1323. doi:https://doi.org/10.1016/j.atmosenv.2005.10.029

Denier van der Gon, H., Hulskotte, J., Jozwicka, M., Kranenburg, R., Kuenen, J., & Visschedijk, A. (2018). Chapter 5 - European Emission Inventories and Projections for Road Transport Non-Exhaust Emissions: Analysis of Consistency and Gaps in Emission Inventories From EU Member States. In F. Amato (Ed.), *Non-Exhaust Emissions* (pp. 101-121): Academic Press.

Diez-Lazaro, A., Hitchman, M., & Littlejohn, D. (2005). Considerations for the Selection and Design of Sampling Systems for Heterogeneous Processes in a Stirred Tank Reactor. *Chemical Engineering Research & Design - CHEM ENG RES DES, 83*, 344-351. doi:10.1205/cherd.03414

Dmitriev, A. I., Öesterle, W., & Kloss, H. (2011). About the influence of automotive brakepad composition on frictional performance. Results of nano-scale modeling. *Наносистемы: физика, химия, математика, 2*(2), 58-64.

Duong, T. T., & Lee, B. K. (2011). Determining contamination level of heavy metals in road dust from busy traffic areas with different characteristics. *J Environ Manage, 92*(3), 554-562. doi:10.1016/j.jenvman.2010.09.010

Ekathai, W., Chalermpol, P.-A., & Worawat, S. (2021, 17 – 18 November 2021). *Effects of Payload on Non-exhaust PM Emissions from Hybrid Electric Vehicle during Braking Sequences.* Paper presented at the 1st International Conference of Air Quality & Climate Change 3rd Malaysia Air Quality Annual Symposium, The Clean Air Forum Society of Malaysia.

Eriksson, M., Lord, J., & Jacobson, S. (2001). Wear and contact conditions of brake pads: Dynamical in situ studies of pads on glass. *Wear, 249*, 272-278. doi:10.1016/S0043-1648(01)00573-7

Regulation (EC) No 715/2007 of the European Parliament and of the Council of 20 June 2007 on type approval of motor vehicles with respect to emissions from light passenger and commercial vehicles (Euro 5 and Euro 6) and on access to vehicle repair and maintenance information, (2007).

Europe-ICCT, I. C. o. C. T. (2018). EUROPEAN VEHICLE MARKET STATISTICS. *Pocketbook 2018/19.* Retrieved from https://theicct.org/sites/default/files/publications/ICCT_Pocketbook_2018_Final _20190408.pdf

Farwick zum Hagen, F. H., Mathissen, M., Grabiec, T., Hennicke, T., Rettig, M., Grochowicz, J., . . . Benter, T. (2019). On-road vehicle measurements of brake wear particle emissions. *Atmospheric Environment, 217*, 116943. doi:https://doi.org/10.1016/j.atmosenv.2019.116943

Fitz, D., & Bufalino, C. (2002). Measurement of PM10 emission factors from paved roads using on-board particle sensors. *Measurement of PM10 Emission Factors from Paved Roads Using On-board Particle Sensors*.

Ganguly, A., & George, R. (2008). Asbestos free friction composition for brake linings. *Bulletin of Materials Science, 31*(1), 19-22.

Garg, B. D., Cadle, S. H., Mulawa, P. A., Groblicki, P. J., Laroo, C., & Parr, G. A. (2000). Brake Wear Particulate Matter Emissions. *Environmental Science & Technology, 34*(21), 4463-4469. doi:10.1021/es001108h

Gietl, J. K., Lawrence, R., Thorpe, A. J., & Harrison, R. M. (2010). Identification of brake wear particles and derivation of a quantitative tracer for brake dust at a major road. *Atmospheric Environment, 44*, 141-146. doi:10.1016/j.atmosenv.2009.10.016

Gil, M., Ramos, I., Arauzo, I., & Román, J. (2009). Characterization of a biomass milling pilot plant.

Grigoratos, T., & Martini, G. (2014). Brake wear particle emissions: a review. *Environmental science and pollution research international, 22*. doi:10.1007/s11356-014-3696-8

Grigoratos, T., & Martini, G. (2015). Brake wear particle emissions: a review. *Environ Sci Pollut Res Int, 22*(4), 2491-2504. doi:10.1007/s11356-014-3696-8

Gudmand-Høyer, L., Bach, A., Nielsen, G. T., & Morgen, P. (1999). Tribological properties of automotive disc brakes with solid lubricants. *Wear, 232*(2), 168-175.

Gujrathi, T., & Damale, A. (2015). A review on friction materials of automobile disc brake pad. *International Journal Of Engineering, Education And Technology, 3*(2), 1-4.

Gustafsson, M., Blomqvist, G., Gudmundsson, A., Dahl, A., Jonsson, P., & Swietlicki, E. (2009). Factors influencing PM10 emissions from road pavement wear. *Atmospheric Environment, 43*(31), 4699-4702. doi:https://doi.org/10.1016/j.atmosenv.2008.04.028

Hagino, H., Oyama, M., & Sasaki, S. (2015). Airborne brake wear particle emission due to braking and accelerating. *Wear, 334*, 44-48.

Hagino, H., Oyama, M., & Sasaki, S. (2016). Laboratory testing of airborne brake wear

particle emissions using a dynamometer system under urban city driving cycles. *Atmospheric Environment, 131*, 269-278. doi:https://doi.org/10.1016/j.atmosenv.2016.02.014

Harrison, R. M., Jones, A. M., Gietl, J., Yin, J., & Green, D. C. (2012). Estimation of the Contributions of Brake Dust, Tire Wear, and Resuspension to Nonexhaust Traffic Particles Derived from Atmospheric Measurements. *Environmental Science & Technology, 46*(12), 6523-6529. doi:10.1021/es300894r

Hearl, F. J. (1998). Current Exposure Guidelines for Particulates Not Otherwise Classified or Regulated: History and Rationale. *Applied Occupational and Environmental Hygiene, 13*(8), 608-612. doi:10.1080/1047322X.1998.10390121

Hesse, D., Hamatschek, C., Augsburg, K., Weigelt, T., Prahst, A., & Gramstat, S. (2021). Testing of Alternative Disc Brakes and Friction Materials Regarding Brake Wear Particle Emissions and Temperature Behavior. *Atmosphere, 12*(4), 436. Retrieved from https://www.mdpi.com/2073-4433/12/4/436

Hutchings, I. M. (1992). Tribology: Friction and Wear of Engineering Materials. *Edward Arnold, London*.

Iijima, A., Sato, K., Yano, K., Kato, M., Kozawa, K., & Furuta, N. (2008). Emission Factor for Antimony in Brake Abrasion Dusts as One of the Major Atmospheric Antimony Sources. *Environmental Science & Technology, 42*(8), 2937-2942. doi:10.1021/es702137g

Iijima, A., Sato, K., Yano, K., Tago, H., Kato, M., Kimura, H., & Furuta, N. (2007). Particle size and composition distribution analysis of automotive brake abrasion dusts for the evaluation of antimony sources of airborne particulate matter. *Atmospheric Environment, 41*(23), 4908-4919. doi:https://doi.org/10.1016/j.atmosenv.2007.02.005

Ikpambese, K., Gundu, D., & Tuleun, L. (2016). Evaluation of palm kernel fibers (PKFs) for production of asbestos-free automotive brake pads. *Journal of King Saud University-Engineering Sciences, 28*(1), 110-118.

Ilea, L., & Iozsa, D. (2018). Wheels aerodynamics and impact on passenger vehicles drag coefficient. *IOP Conference Series: Materials Science and Engineering, 444*, 072005. doi:10.1088/1757-899x/444/7/072005

ISO. (2007). ISO 21994:2007. Passenger cars — Stopping distance at straight-line braking with ABS — Open-loop test method. Retrieved from https://www.iso.org/standard/40588.html

Kagawa, J. (2002). Health effects of diesel exhaust emissions—a mixture of air pollutants of worldwide concern. *Toxicology, 181-182*, 349-353. doi:https://doi.org/10.1016/S0300-483X(02)00461-4

Kelly, F. J., & Fussell, J. C. (2012). Size, source and chemical composition as determinants of toxicity attributable to ambient particulate matter. *Atmospheric Environment, 60*, 504-526. doi:https://doi.org/10.1016/j.atmosenv.2012.06.039

Keuken, M., Denier van der Gon, H., & van der Valk, K. (2010). Non-exhaust emissions of PM and the efficiency of emission reduction by road sweeping and washing in the Netherlands. *Sci Total Environ, 408*(20), 4591-4599. doi:10.1016/j.scitotenv.2010.06.052

Kim, S. J., Cho, M. H., Cho, K. H., & Jang, H. (2007). Complementary effects of solid lubricants in the automotive brake lining. *Tribology International, 40*(1), 15-20.

Kim, Y., Lee, D., Jung, E., Bae, J., Lee, S., Pyo, H.-B., & Kang, K. (2014). Preparation

and characterization of quercetin-loaded silica microspheres stabilized by combined multiple emulsion and sol-gel processes. *Chemical Industry and Chemical Engineering Quarterly, 21*, 10-10. doi:10.2298/CICEQ131002010K

Kim, Y. C., Cho, M. H., Kim, S. J., & Jang, H. (2008). The effect of phenolic resin, potassium titanate, and CNSL on the tribological properties of brake friction materials. *Wear, 264*(3-4), 204-210.

Kuenen, J. J. P., Visschedijk, A. J. H., Jozwicka, M., & Denier van der Gon, H. A. C. (2014). TNO-MACC_II emission inventory; a multi-year (2003–2009) consistent high-resolution European emission inventory for air quality modelling. *Atmos. Chem. Phys., 14*(20), 10963-10976. doi:10.5194/acp-14-10963-2014

Kukutschová, J., & Filip, P. (2018). Review of Brake Wear Emissions. In (pp. 123-146).

Kukutschová, J., Moravec, P., Tomášek, V., Matějka, V., Smolík, J., Schwarz, J., . . . Filip, P. (2011). On airborne nano/micro-sized wear particles released from low-metallic automotive brakes. *Environ Pollut, 159*(4), 998-1006. doi:10.1016/j.envpol.2010.11.036

Kukutschová, J., Roubíček, V., Malachová, K., Pavlíčková, Z., Holuša, R., Kubačková, J., . . . Filip, P. (2009). Wear mechanism in automotive brake materials, wear debris and its potential environmental impact. *Wear, 267*(5), 807-817. doi:https://doi.org/10.1016/j.wear.2009.01.034

Kukutschová, J., Roubíček, V., Mašláň, M., Jančík, D., Slovák, V., Malachová, K., . . . Filip, P. (2010). Wear performance and wear debris of semimetallic automotive brake materials. *Wear, 268*(1), 86-93. doi:https://doi.org/10.1016/j.wear.2009.06.039

Kumar, P., Pirjola, L., Ketzel, M., & Harrison, R. M. (2013). Nanoparticle emissions from 11 non-vehicle exhaust sources – A review. *Atmospheric Environment, 67*, 252-277. doi:https://doi.org/10.1016/j.atmosenv.2012.11.011

Kupiainen, K., Tervahattu, H., & Räisänen, M. (2003). Experimental studies about the impact of traction sand on urban road dust composition. *Science of The Total Environment, 308*(1), 175-184. doi:https://doi.org/10.1016/S0048-9697(02)00674-5

Kupiainen, K. J., Tervahattu, H., Räisänen, M., Mäkelä, T., Aurela, M., & Hillamo, R. (2005). Size and Composition of Airborne Particles from Pavement Wear, Tires, and Traction Sanding. *Environmental Science & Technology, 39*(3), 699-706. doi:10.1021/es035419e

Kwak, J.-h., Kim, H., Lee, J., & Lee, S. (2013). Characterization of non-exhaust coarse and fine particles from on-road driving and laboratory measurements. *Science of The Total Environment, 458-460*, 273-282. doi:https://doi.org/10.1016/j.scitotenv.2013.04.040

Lawrence, S., Sokhi, R., Ravindra, K., Mao, H., Prain, H. D., & Bull, I. D. (2013). Source apportionment of traffic emissions of particulate matter using tunnel measurements. *Atmospheric Environment, 77*, 548-557. doi:https://doi.org/10.1016/j.atmosenv.2013.03.040

Legret, M., & Pagotto, C. (1999). Evaluation of pollutant loadings in the runoff waters from a major rural highway. *Science of The Total Environment, 235*(1), 143-150. doi:https://doi.org/10.1016/S0048-9697(99)00207-7

Lemen, R. A. (2004). Asbestos in brakes: exposure and risk of disease. *American*

journal of industrial medicine, 45(3), 229-237.

Luekewille, A., Bertok, I., Amann, M., Cofala, J., Gyarfas, F., Heyes, C., . . . Schoepp, W. (2001). *A Framework to Estimate the Potential and Costs for the Control of Fine Particulate Emissions in Europe*.

Macías, G., Lorenzana, C., & Fernandez, J. (2020). *Determination of Diffusion Capability of Oxygen through Brake Pads from the Surface towards the Interior*. https://doi.org/10.4271/2020-01-1616

Mathissen, M., Grochowicz, J., Schmidt, C., Vogt, R., Farwick zum Hagen, F. H., Grabiec, T., . . . Grigoratos, T. (2018). A novel real-world braking cycle for studying brake wear particle emissions. *Wear, 414-415*, 219-226. doi:https://doi.org/10.1016/j.wear.2018.07.020

Mathissen, M., Scheer, V., Kirchner, U., Vogt, R., & Benter, T. (2012). Non-exhaust PM emission measurements of a light duty vehicle with a mobile trailer. *Atmospheric Environment, 59*, 232-242. doi:https://doi.org/10.1016/j.atmosenv.2012.05.020

Miler, M. (2021). Airborne particles in city bus: concentrations, sources and simulated pulmonary solubility. *Environmental Geochemistry and Health*. doi:10.1007/s10653-020-00770-5

Miller, R. W. (1996). *Flow measurement engineering handbook*. New York: McGraw-Hill.

Mitsumoto, M. (2017). Copper free brake pads with stable friction coefficient. *Tribol. Trans, 59*, 23-24.

Mosleh, M., Blau, P. J., & Dumitrescu, D. (2004). Characteristics and morphology of wear particles from laboratory testing of disk brake materials. *Wear, 256*(11), 1128-1134. doi:https://doi.org/10.1016/j.wear.2003.07.007

Mukhopadhyay, A. (2015). *MEASUREMENT OF MAGNETIC HYSTERESIS LOOPS IN CONTINUOUS AND PATTERNED FERROMAGNETIC NANOSTRUCTURES BY STATIC MAGNETO-OPTICAL KERR EFFECT MAGNETOMETER*.

Nertrium. (2015). Choked flow. Retrieved from https://neutrium.net/fluid-flow/choked-flow/

Nicolas, B., Robert, G., Peter, L., Matthias, H., Renato, F., & Brigitte, B. (2009). *PM10 emission factors of abrasion particles from road traffic.* . Retrieved from

Nosko, O., & Olofsson, U. (2017). Quantification of ultrafine airborne particulate matter generated by the wear of car brake materials. *Wear, 374-375*, 92-96. doi:10.1016/j.wear.2017.01.003

Nosko, O., Olofsson, U., Metinoz, I., & Alemani, M. (2015). A Study on Emission of Airborne Wear Particles from Car Brake Friction Pairs. *SAE International Journal of Materials and Manufacturing, 9*(1), 147-157. doi:https://doi.org/10.4271/2015-01-2665

Österle, W., Deutsch, C., Gradt, T., Orts-Gil, G., Schneider, T., & Dmitriev, A. (2014). Tribological screening tests for the selection of raw materials for automotive brake padformulations. *Tribology International, 73*, 148-155. doi:10.1016/j.triboint.2014.01.017

Österle, W., & Dmitriev, A. (2014). Some Considerations on the Role of Third Bodies During Automotive Braking. *SAE International Journal of Passenger Cars - Mechanical Systems, 7*, 1287-1294. doi:10.4271/2014-01-2490

Österle, W., Prietzel, C., Kloß, H., & Dmitriev, A. I. (2010). On the role of copper in brake friction materials. *Tribology International, 43*(12), 2317-2326. doi:https://doi.org/10.1016/j.triboint.2010.08.005

Österle, W., & Urban, I. (2006). Third body formation on brake pads and rotors. *Tribology International, 39*(5), 401-408. doi:https://doi.org/10.1016/j.triboint.2005.04.021

Ostermeyer, G. (2014). A comprehensive approach for the simulation of heat and heat-induced phenomena in friction materials. *Wear*. doi:10.1016/j.wear.2013.12.021

Ostermeyer, G. P. (2007). The mesoscopic particle approach. *Tribology International, 40*(6), 953-959. doi:https://doi.org/10.1016/j.triboint.2006.02.046

Ostermeyer, G. P., & Müller, M. (2008). New insights into the tribology of brake systems. *Proceedings of The Institution of Mechanical Engineers Part D-journal of Automobile Engineering - PROC INST MECH ENG D-J AUTO, 222*, 1167-1200. doi:10.1243/09544070JAUTO595

Ostro, B., Broadwin, R., Green, S., Feng, W. Y., & Lipsett, M. (2006). Fine particulate air pollution and mortality in nine California counties: results from CALFINE. *Environ Health Perspect, 114*(1), 29-33. doi:10.1289/ehp.8335

Paul Baron, A., Pramod, K., & Klaus, W. (2011). *Aerosol Measurement: Principles, Techniques, and Applications, 3rd Edition*.

Perricone, G., Alemani, M., Metinöz, I., Matějka, V., Wahlström, J., & Olofsson, U. (2017). Towards the ranking of airborne particle emissions from car brakes – a system approach. *Proceedings of the Institution of Mechanical Engineers, Part D: Journal of Automobile Engineering, 231*(6), 781-797. doi:10.1177/0954407016662800

Perricone, G., Matějka, V., Alemani, M., Valota, G., Bonfanti, A., Ciotti, A., . . . Ibrahim, M. (2018). A concept for reducing PM10 emissions for car brakes by 50%. *Wear, 396-397*, 135-145. doi:https://doi.org/10.1016/j.wear.2017.06.018

RAC. (2019). Euro 1 to Euro 6 guide – find out your vehicle's emissions standard. Retrieved from https://www.rac.co.uk/drive/advice/emissions/euro-emissions-standards/

Sakai, E. H. (1995). Measurement and Visualization of the Contact Pressure Distribution of Rubber Disks and Tires. *23*(4), 238-255. doi:10.2346/1.2137506

Sanders, P. G., Dalka, T. M., Xu, N., Maricq, M. M., & Basch, R. H. (2002). *Brake Dynamometer Measurement of Airborne Brake Wear Debris*. https://doi.org/10.4271/2002-01-1280

Sanders, P. G., Xu, N., Dalka, T. M., & Maricq, M. M. (2003). Airborne brake wear debris: size distributions, composition, and a comparison of dynamometer and vehicle tests. *Environ Sci Technol, 37*(18), 4060-4069. doi:10.1021/es034145s

Shimadzu. (2021). TOC-L Laboratory Total Organic Carbon Analyzers. Retrieved from https://www.ssi.shimadzu.com/products/toc-analyzers/toc-l-features.html

Simons, A. J. T. I. J. o. L. C. A. V. (2013). Road transport: new life cycle inventories for fossil-fuelled passenger cars and non-exhaust emissions in ecoinvent v3. (9), 1299-1313.

Sjöberg, K., & Ferm, M. (2005). Measurements of PM10 and PM2. 5 in Malmö.

Sloley, A. (2012). Don't Be Fazed By Multiphase Sampling An isokinetic system can provide accurate samples. Retrieved from https://www.chemicalprocessing.com/articles/2012/don-t-be-fazed-by-

multiphase-sampling/

Söderberg, A., Sellgren, U., & Andersson, S. (2008). *Using Finite Element Analysis to Predict the Brake Pressure Needed for Effective Rotor Cleaning in Disc Brakes*. https://doi.org/10.4271/2008-01-2565

Song, F., & Gao, Y. (2011). Size distributions of trace elements associated with ambient particular matter in the affinity of a major highway in the New Jersey–New York metropolitan area. *Atmospheric Environment - ATMOS ENVIRON, 45*, 6714-6723. doi:10.1016/j.atmosenv.2011.08.031

Soret, A., Guevara, M., & Baldasano, J. M. (2014). The potential impacts of electric vehicles on air quality in the urban areas of Barcelona and Madrid (Spain). *Atmospheric Environment, 99*, 51-63. doi:https://doi.org/10.1016/j.atmosenv.2014.09.048

Sternbeck, J., Sjödin, Å., & Andréasson, K. (2002). Metal Emissions from Road Traffic and the Influence of Resuspension – Results from Two Tunnel Studies. *Atmospheric Environment, 36*, 4735-4744. doi:10.1016/S1352-2310(02)00561-7

Sugözü, B. (2018). Tribological properties of brake friction materials containing fly ash. *Industrial Lubrication and Tribology, 70*(5), 902-906. doi:10.1108/ILT-04-2017-0100

Szpica, D. (2019). New Leiderman–Khlystov coefficients for estimating engine full load characteristics and performance. *Chinese Journal of Mechanical Engineering, 32*(1), 1-14.

Thorpe, A., & Harrison, R. M. (2008). Sources and properties of non-exhaust particulate matter from road traffic: A review. *Science of The Total Environment, 400*(1), 270-282. doi:https://doi.org/10.1016/j.scitotenv.2008.06.007

Thorpe, A. J., Harrison, R. M., Boulter, P. G., & McCrae, I. S. (2007). Estimation of particle resuspension source strength on a major London Road. *Atmospheric Environment, 41*(37), 8007-8020. doi:https://doi.org/10.1016/j.atmosenv.2007.07.006

Timmers, V. R. J. H., & Achten, P. A. J. (2016). Non-exhaust PM emissions from electric vehicles. *Atmospheric Environment, 134*, 10-17. doi:https://doi.org/10.1016/j.atmosenv.2016.03.017

U.S. Environmental Protection Agency. (2014). *Brake and Tire Wear Emissions from On-road Vehicles in MOVES2014*: U.S. Environmental Protection Agency, Office of Transportation and Air Quality, Assessment and Standards Division.

Uexküll, O., Skerfving, S., Doyle, R., & Braungart, M. (2005). Antimony in Brake Pads–A Carcinogenic Component? *Journal of Cleaner Production - J CLEAN PROD, 13*, 19-31. doi:10.1016/j.jclepro.2003.10.008

Vainio, O. (2021, 30th March 2021). *Brake wear particulate matter emission measurements in wide particle size range*, Webinar.

Varrica, D., Bardelli, F., Dongarrà, G., & Tamburo, E. (2013). Speciation of Sb in airborne particulate matter, vehicle brake linings, and brake pad wear residues. *Atmospheric Environment, 64*, 18-24. doi:10.1016/j.atmosenv.2012.08.067

Verma, P. C., Ciudin, R., Bonfanti, A., Aswath, P., Straffelini, G., & Gialanella, S. (2016). Role of the friction layer in the high-temperature pin-on-disc study of a brake material. *Wear, 346-347*, 56-65. doi:https://doi.org/10.1016/j.wear.2015.11.004

VROM. (1997). Emissies van Metalen en PAK door Wegverkeer., from Veiligheid

Wahlström, J. (2009). *Towards a simulation methodology for prediction of airborne wear particles from disc brakes.*

Wahlström, J. (2011). *A study of airborne wear particles from automotive disc brakes.* (Doctoral thesis, comprehensive summary). KTH Royal Institute of Technology, Stockholm. Retrieved from http://urn.kb.se/resolve?urn=urn:nbn:se:kth:diva-31152 DiVA database. (2011:04)

Wahlström, J., Olander, L., & Olofsson, U. (2010). Size, Shape, and Elemental Composition of Airborne Wear Particles from Disc Brake Materials. *Tribology Letters, 38*(1), 15-24. doi:10.1007/s11249-009-9564-x

Wahlström, J., Söderberg, A., Olander, L., Olofsson, U., & Jansson, A. (2010). Airborne wear particles from passenger car disc brakes: A comparison of measurements from field tests, a disc brake assembly test stand, and a pin-on-disc machine. *Proceedings of the Institution of Mechanical Engineers, Part J: Journal of Engineering Tribology, 224*(2), 179-188. doi:10.1243/13506501jet633

Westerlund, K.-G. (2001). *METAL EMISSIONS FROM STOCKHOLM TRAFFIC - WEAR OF BRAKE LININGS*.

Xiao, X., Yin, Y., Bao, J., Lu, L., & Feng, X. (2016). Review on the friction and wear of brake materials. *Advances in Mechanical Engineering, 8*(5), 1687814016647300. doi:10.1177/1687814016647300

APPENDIX

Patent of sampling system
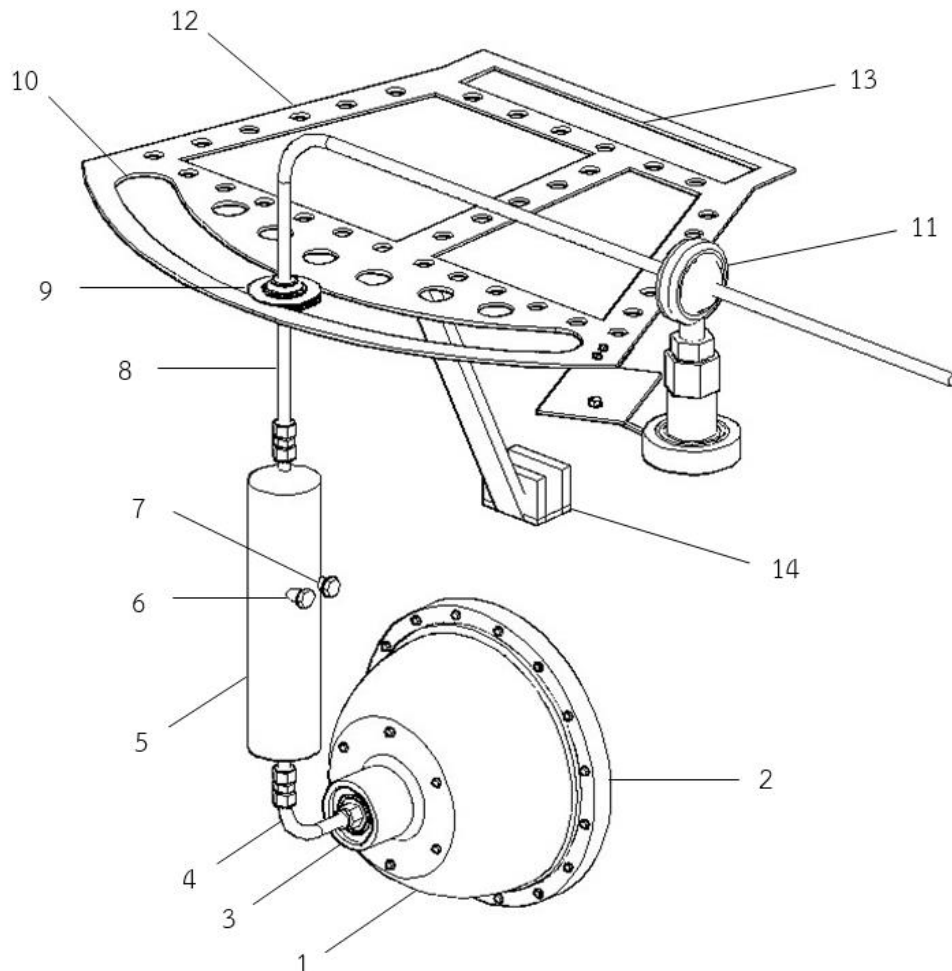
Appendix Figure 1 Sampling system

The real-time brake wear measurement consists of two parts: the first part is the dust collector, the dust chamber (1) is attached to the wheels by the wheel mounting kit (2). There is a bearing assembly (3) at the end of the chamber. It is connected to the lower part air duct (4), which is connected to the lower part of the sampling chamber (5), there are a temperature sensor (6) and the dust sampling chamber (7). The top part of the sample chamber (5) is connected to the top part of air duct (8) by the other end of the pipe is connected to the vacuum pump in vehicle. which has 2 tube support points, namely turning support (9) and leveling platform (11). The second part of the turning support set (12) is a steel plate (10) according to the turning angle of the vehicle, which has a support point (9) installed in the hood (13). The bottom of the steel plate holds the lower body (14), and a leveler (11) is attached to the side corner near the side mirrors of the vehicle.

Mid-size passenger car

Appendix Table 1 The absolute value result of passenger car

		Light#1			Light#2			Heavy#1			Heavy#2		
		Overall	Cold	Hot	Overall	Cold	Hot	Overall	Cold	Hot	Overall	Cold	Hot
Distance (km)		28.74	8.74	20.01	24.81	7.17	17.64	26.38	9.84	16.55	28.74	8.51	20.23
Time (s)		3880	1430	2450	3762	1318	2444	3864	1712	2152	3749	1361	2388
Velocity (km/h)	Max.	71.57	54.49	71.57	68.98	56.45	68.98	80	54.13	80	75.17	53.68	75.17
	Average	34.04	29.4	36.19	32.85	28.8	34.68	33.22	28.88	36.04	37.07	30.84	39.91
Temperature (°c)	Max.	218.9	104.6	218.9	211.6	104.6	211.6	N/A	N/A	N/A	250.5	125.3	250.4
	Min.	33.3	33.3	79.3	32.9	32.9	77.9	N/A	N/A	N/A	33.9	33.9	90.2
	Average	104.71	67.34	126.75	97.43	60.23	115.21	N/A	N/A	N/A	130.71	75.34	162.13
PM Average (mg/m³)	PM_1	0.14615	0.04154	0.20925	0.07814	0.03115	0.10184	0.19558	0.0529	0.29654	0.44912	0.07924	0.64701
	$PM_{2.5}$	0.15074	0.04233	0.21608	0.08014	0.0316	0.10389	0.20172	0.05369	0.30645	0.46944	0.08148	0.677
	PM_4	0.16163	0.04475	0.23196	0.08417	0.03285	0.10926	0.21518	0.0557	0.32799	0.5163	0.087	0.74598
	PM_{10}	0.17419	0.04796	0.25004	0.0893	0.03496	0.11588	0.22815	0.0578	0.34865	0.56677	0.09289	0.82031
	Total PM	0.17678	0.04846	0.25383	0.0912	0.03577	0.11832	0.23037	0.05822	0.35215	0.57576	0.0941	0.83345
Weight of Filter		0.1	0	0.1	0.1	0	0.1	N/A	0	0.2	0.4	0.1	0.4
Concentration form filter (mg/m³)		0.68729	0	0.54422	0.70884	0	0.54555	N/A	0	1.23916	2.84520	0.97967	2.23339

Light#1
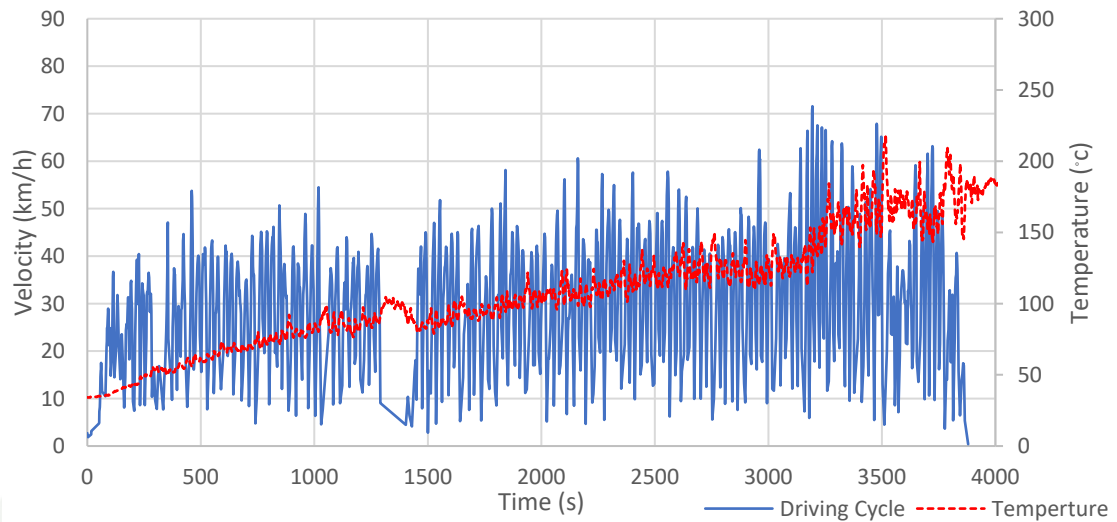
Appendix Figure 2 Driving cycle vs brake temperature of passenger car (Light#1)
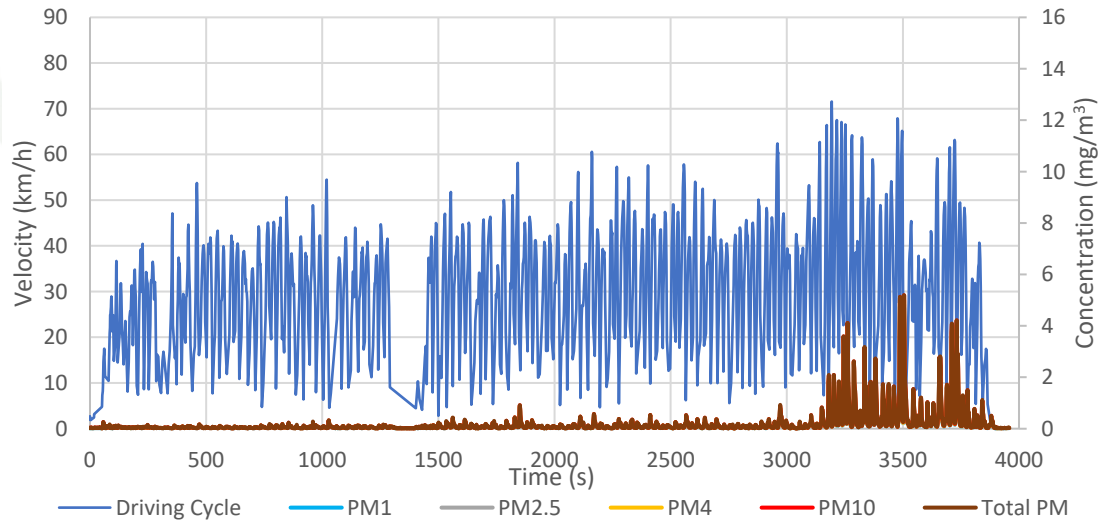
Appendix Figure 3 Driving cycle vs PM of passenger car (Light#1)
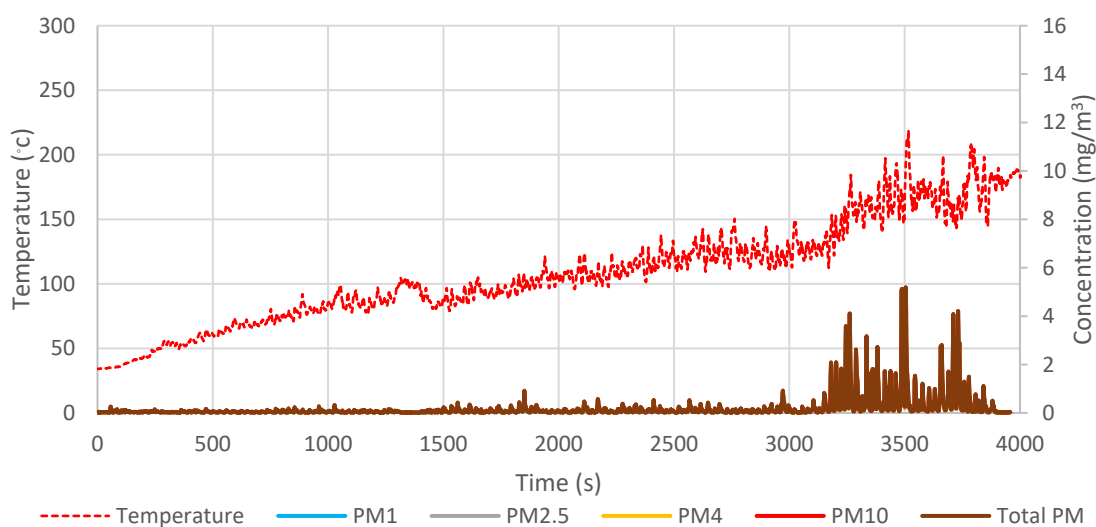
Appendix Figure 4 Brake temperature vs PM of passenger car (Light#1)
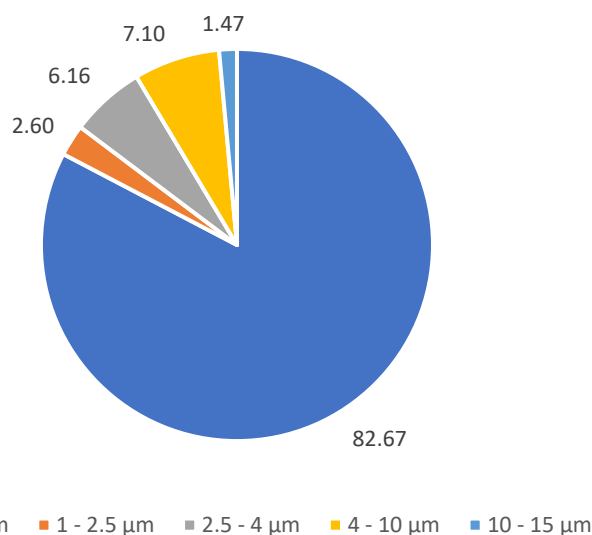
Appendix Figure 5 PM size distributions of passenger car (Light#1)

Filter from TSI, cold and hot test (addition weight of filter = 0.1, 0 and 0.1 mg)

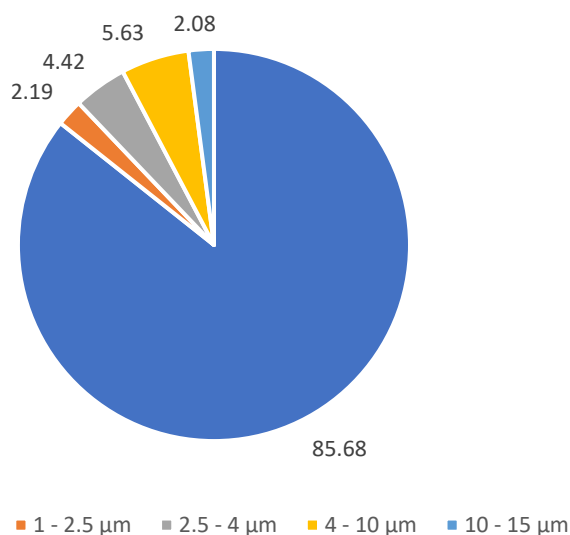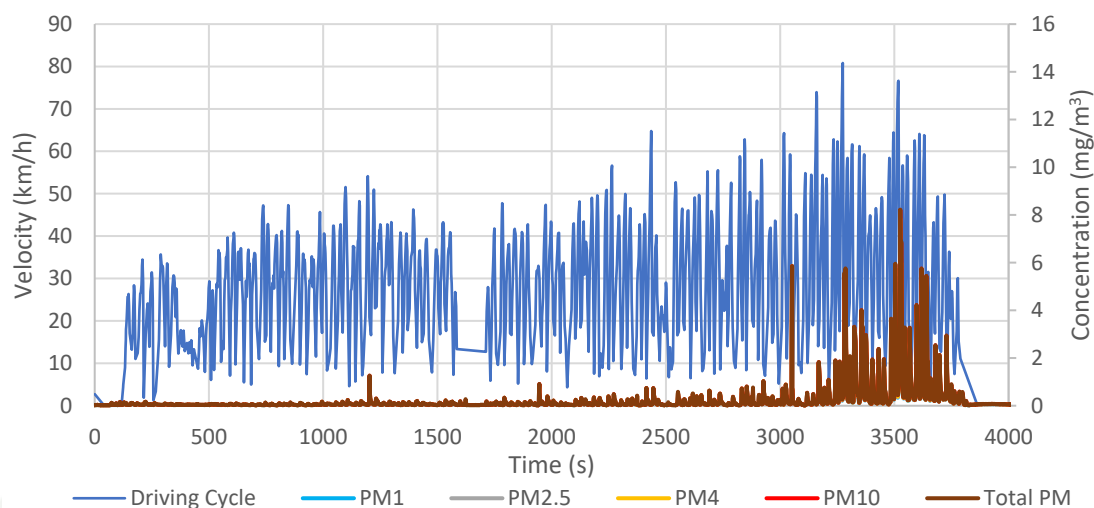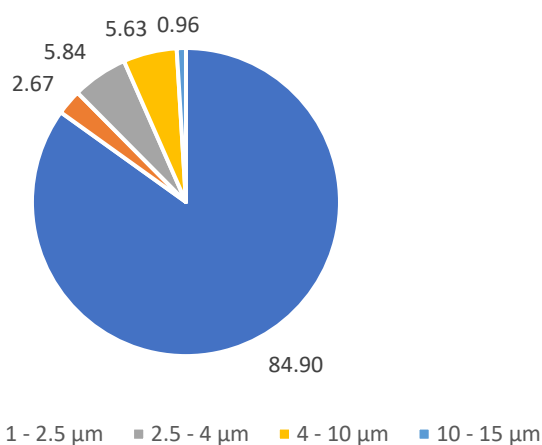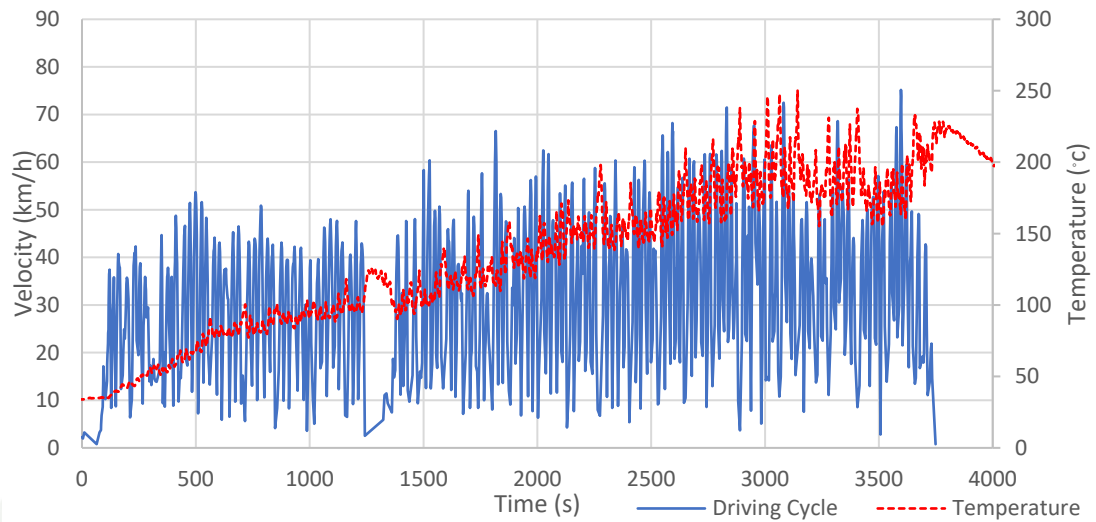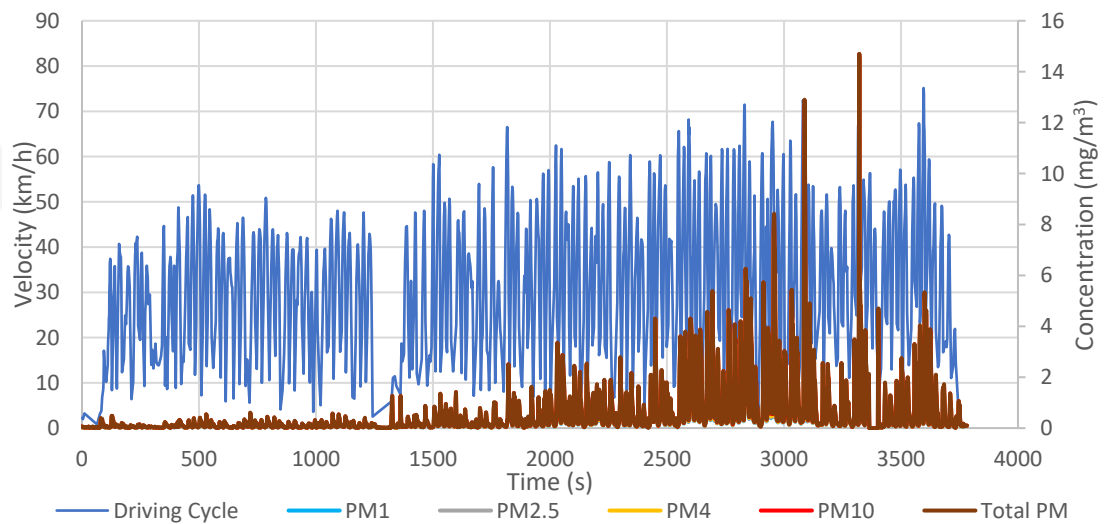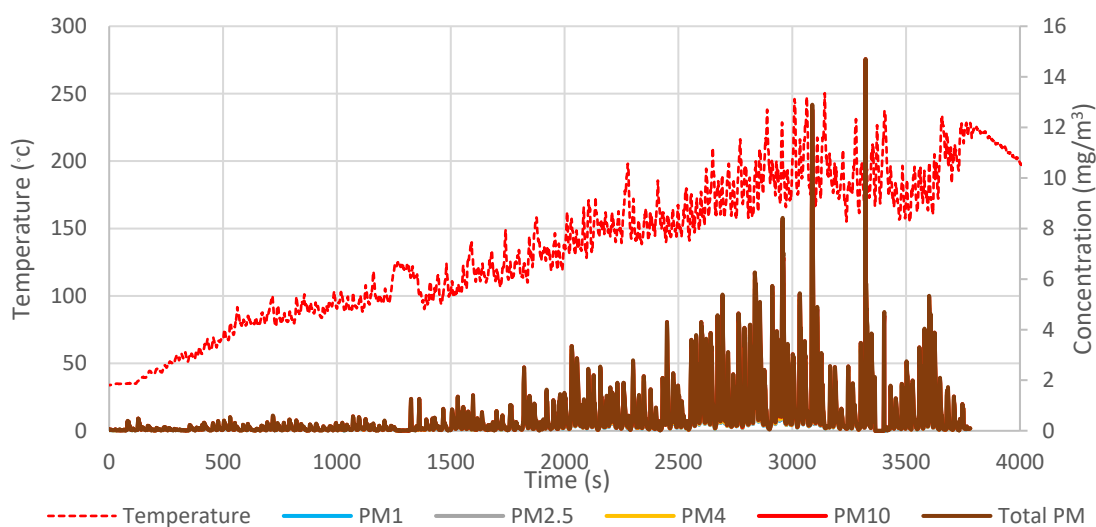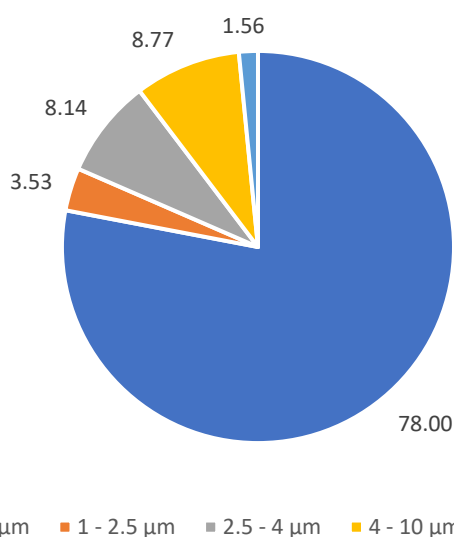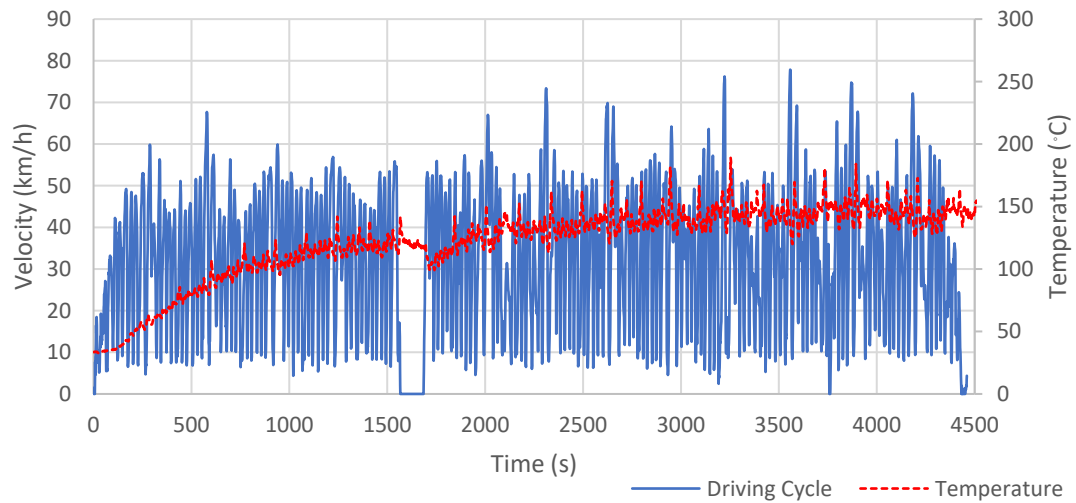**Appendix Figure 6** Filter from passenger car test (Light#1)

Light#2
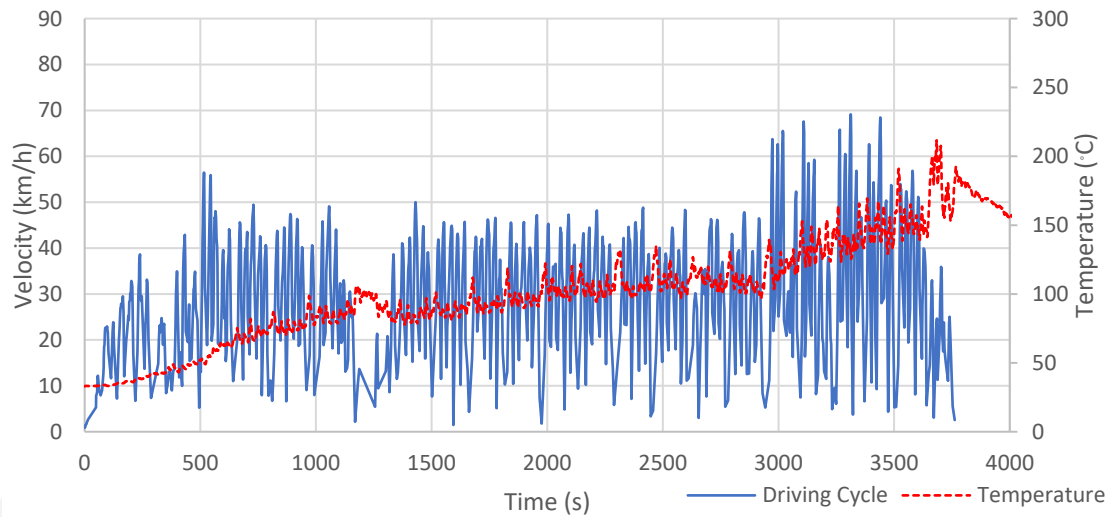
Appendix Figure 7 Driving cycle vs brake temperature of passenger car (Light#2)
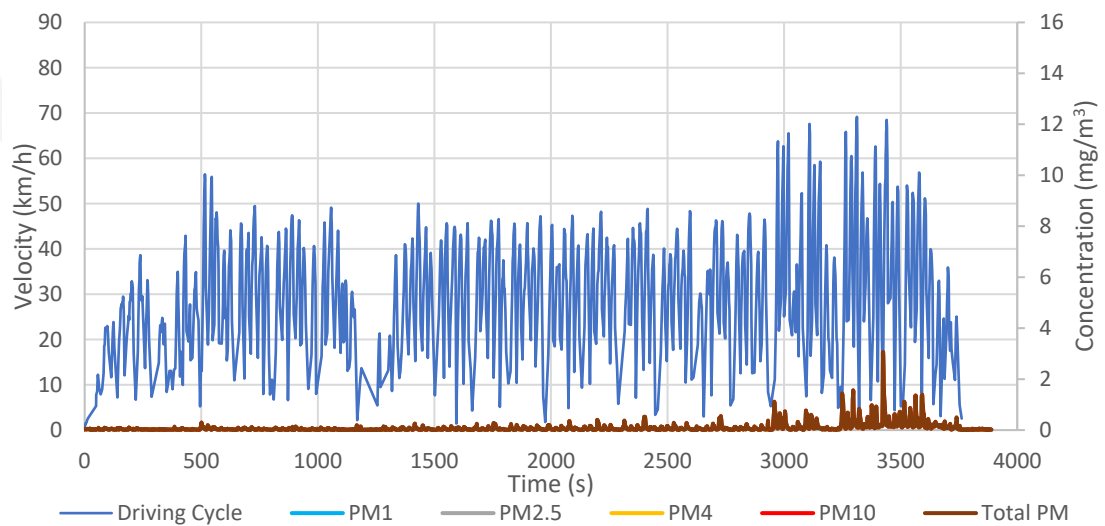
Appendix Figure 8 Driving cycle vs PM of passenger car (Light#2)
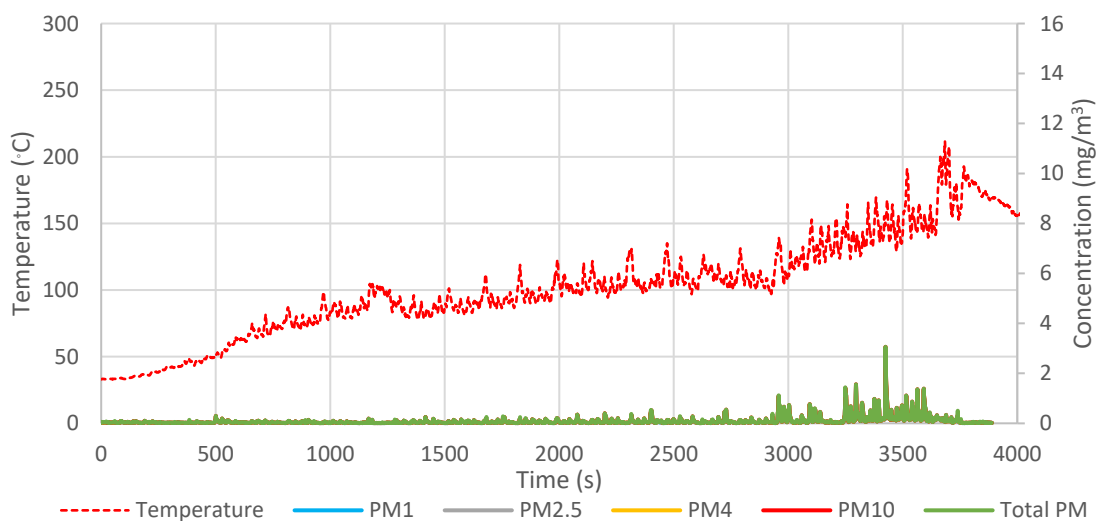
Appendix Figure 9 Brake temperature vs PM of passenger car (Light#2)

Appendix Figure 10 PM size distributions of passenger car (Light#2)

Filter from TSI, cold and hot test (addition weight of filter = 0.1, 0 and 0.1 mg)

Appendix Figure 11 Filter from passenger car test (Light#2)

Heavy#1

Appendix Figure 12 Driving cycle vs PM of passenger car (Heavy#1)

Appendix Figure 13 PM size distributions of passenger car (Heavy#1)

Filter from cold and hot test(Addition weight of filter = 0 and 0.2 mg)

Appendix Figure 14 Filter from passenger car test (Heavy#1)

Heavy#2

Appendix Figure 15 Driving cycle vs brake temperature of passenger car (Heavy#2)

Appendix Figure 16 Driving cycle vs PM of passenger car (Heavy#2)

Appendix Figure 17 Brake temperature vs PM of passenger car (Heavy#2)

Appendix Figure 18 PM size distributions of passenger car (Heavy#2)

Filter from TSI, cold and hot test (addition weight of filter = 0.4, 0.1 and 0.4 mg)

Appendix Figure 19 Filter from passenger car test (Heavy#2)

Subcompact crossover SUV

Appendix Table 2 The absolute value result of SUV (light)

|		Light#1			Light#2			Light#3		
		Overview	Cold	Hot	Overview	Cold	Hot	Overview	Cold	Hot
Distance (km)		39.67	13.90	25.77	33.07	12.83	20.24	34.81	10.10	24.71
Time (s)		4460	1567	2893	3727	1621	2106	3864	1059	2805
Velocity (km/h)	Max.	77.87	67.72	77.87	75.96	65.124	75.96	78.95	69.77	78.95
	Average	32.02	31.93	32.07	31.95	28.5	34.6	32.43	34.34	31.71
Temperature (°c)	Max.	189	141.9	189	185.6	143.1	185.6	204.06	147.34	204.06
	Min.	32.7	32.7	99.1	32.9	33.6	101.9	29.1	29.1	91
	Average	121.74	90.68	138.81	117.14	86.65	139.93	127.29	91.29	144.74
PM Average (mg/m³)	PM_1	0.13403	0.14040	0.13132	0.12567	0.08866	0.15564	0.18846	0.13516	0.21975
	$PM_{2.5}$	0.15437	0.15008	0.15758	0.15628	0.11163	0.19256	0.24624	0.16510	0.29271
	PM_4	0.16563	0.15749	0.17101	0.17533	0.12640	0.21514	0.28288	0.18561	0.33828
	PM_{10}	0.18051	0.17691	0.18355	0.19738	0.14387	0.24103	0.31958	0.20791	0.38303
	Total PM	0.20017	0.22913	0.18570	0.20510	0.15313	0.24769	0.32674	0.21246	0.39167
Weight of Filter (mg)		0.038	0.02	0.045	0.034	0.025	0.042	0.055	0.021	0.091
Concentration form filter (mg/m³)		0.22720	0.17018	0.20740	0.24327	0.20563	0.26591	0.18979	0.26440	0.43256

Appendix Table 3 The absolute value result of SUV (heavy)

		Heavy#1			Heavy#2			Heavy#3		
		Overview	Cold	Hot	Overview	Cold	Hot	Overview	Cold	Hot
Distance (km)		36.90	11.03	25.86	35.79	9.35	26.44	36.82	8.89	27.93
Time (s)		3904	1213	2691	3782	1043	2739	3749	937	2812
Velocity (km/h)	Max.	77.44	71.35	77.44	77.9	77.9	72.4	78.52	72.47	78.52
	Average	34.02	32.74	34.6	34.07	32.29	34.75	35.36	34.15	35.76
Temperature (°c)	Max.	199.8	156.7	199.8	215.5	156	215.5	205.6	152.64	205.6
	Min.	37.4	37.4	114.6	36.4	36.4	117.8	33.4	33.4	105.3
	Average	134.29	94.81	152.75	140.93	91.51	159.84	132.94	89.6	147.88
PM Average (mg/m³)	PM_1	0.26153	0.20369	0.29112	0.21819	0.16609	0.24126	0.17644	0.15826	0.18454
	$PM_{2.5}$	0.36391	0.26001	0.41583	0.30030	0.21514	0.33743	0.24006	0.19836	0.25690
	PM_4	0.43079	0.29808	0.49645	0.36209	0.25101	0.41018	0.28627	0.22718	0.30952
	PM_{10}	0.50045	0.34036	0.57865	0.42773	0.29003	0.48705	0.33625	0.25825	0.36643
	Total PM	0.51179	0.34635	0.59249	0.43995	0.29642	0.50173	0.42549	0.26346	0.48508
Weight of Filter (mg)		0.089	0.036	0.126	0.059	0.027	0.117	0.066	0.022	0.112
Concentration form filter (mg/m³)		0.60792	0.39571	0.62430	0.41601	0.34516	0.56955	0.46946	0.31306	0.53106

Light#1

Appendix Figure 20 Driving cycle vs brake temperature of SUV (Light#1)
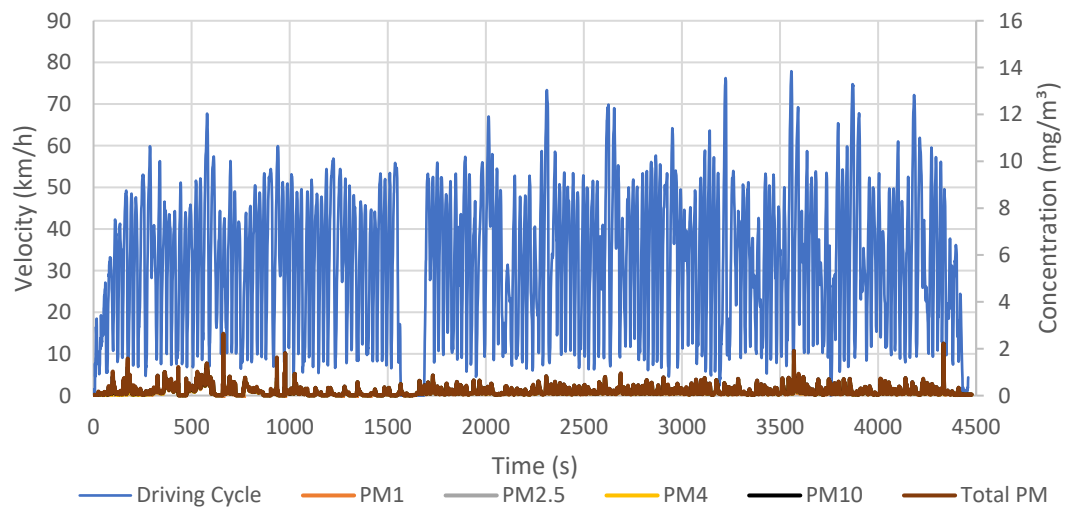
Appendix Figure 21 Driving cycle vs PM of SUV (Light#1)
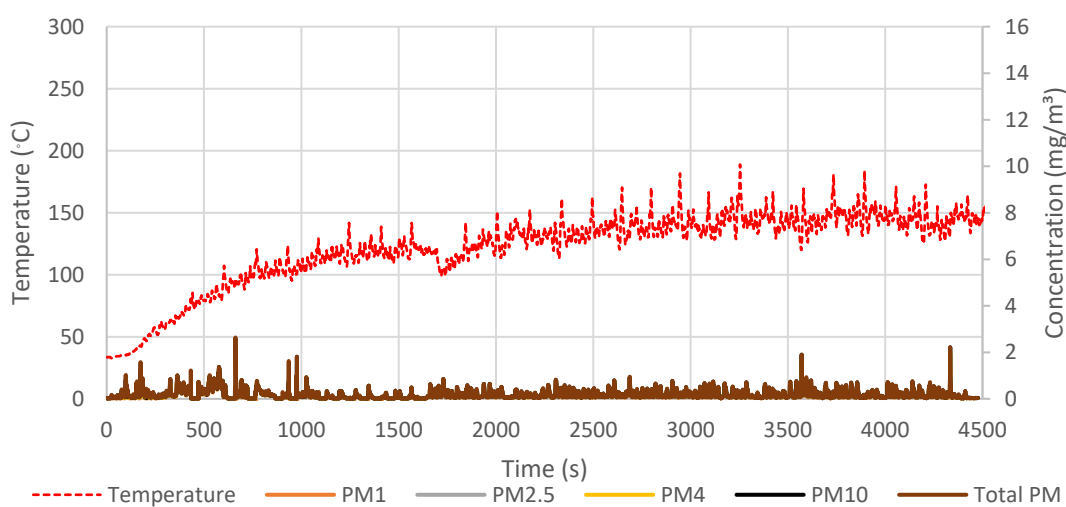
Appendix Figure 22 Brake temperature vs PM of SUV (Light#1)
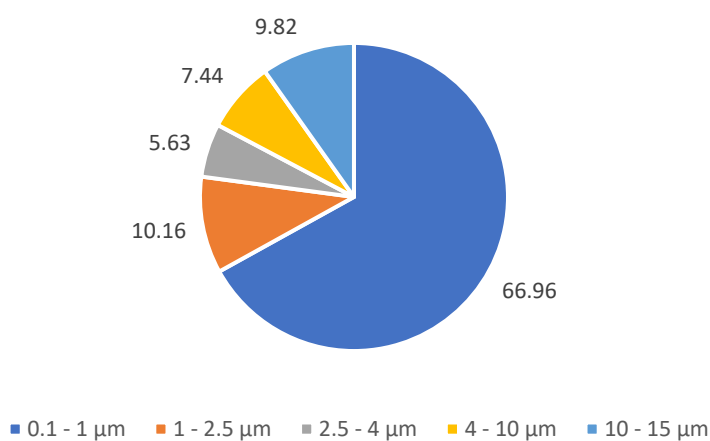
Appendix Figure 23 Size distributions of SUV (Light#1)

Filter from TSI, cold and hot test (addition weight of filter = 0.038, 0.02 and 0.045 mg)

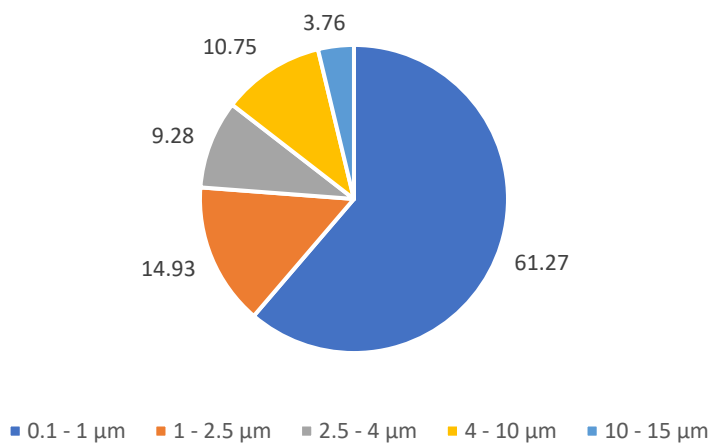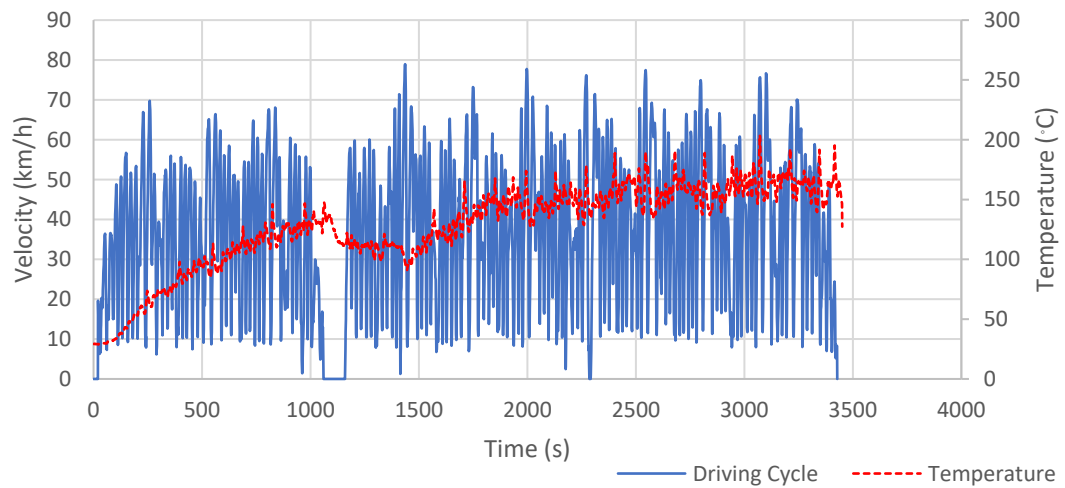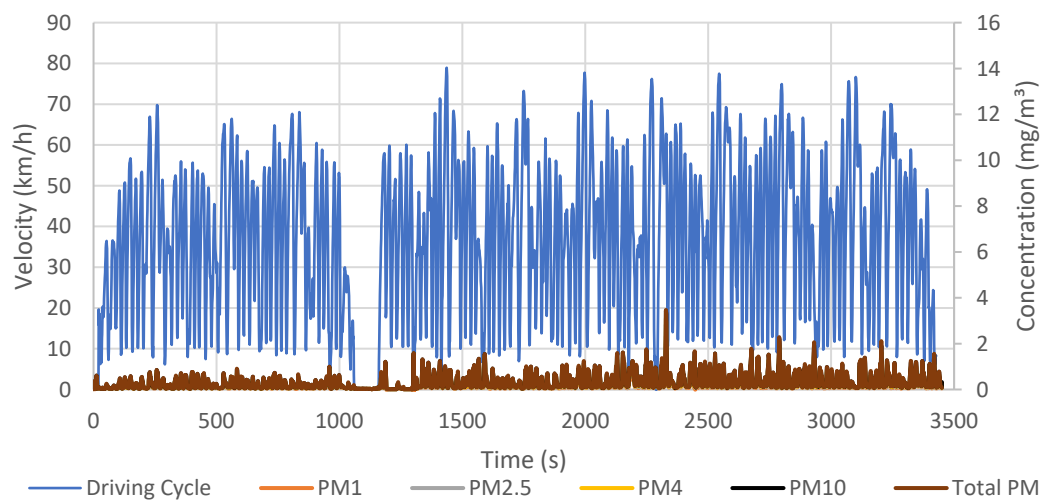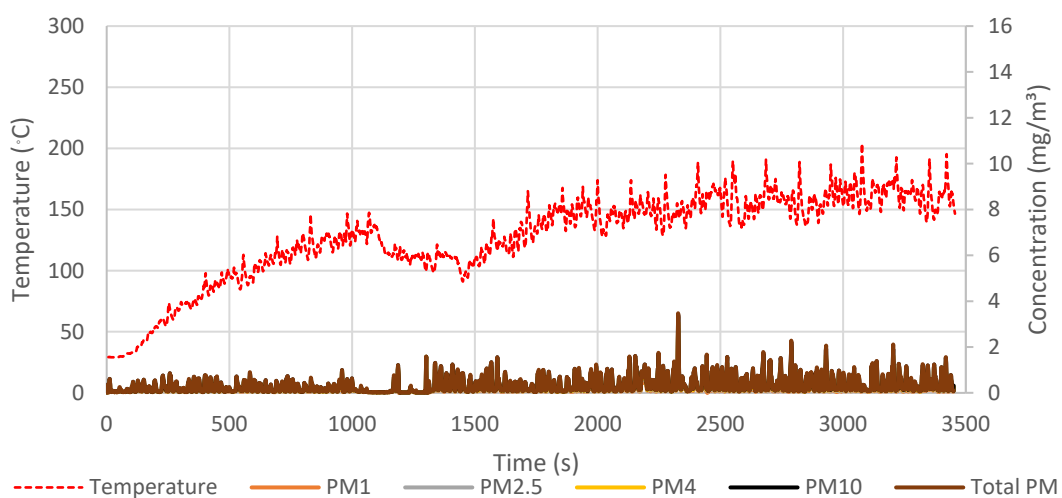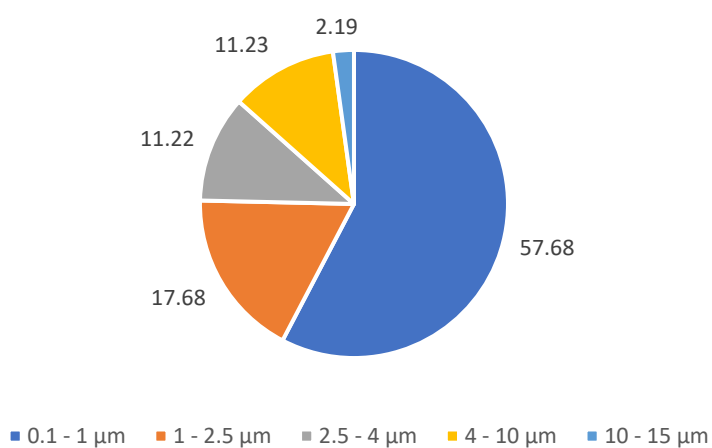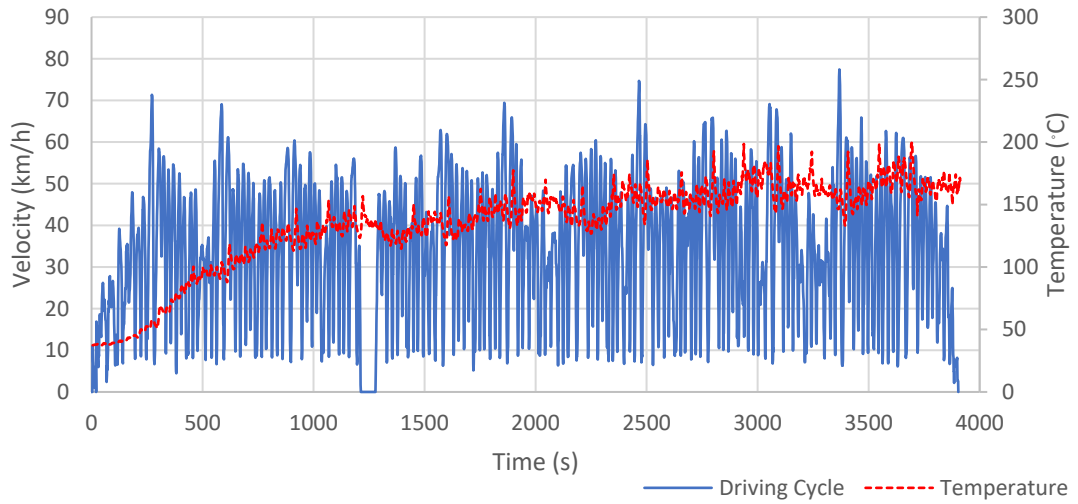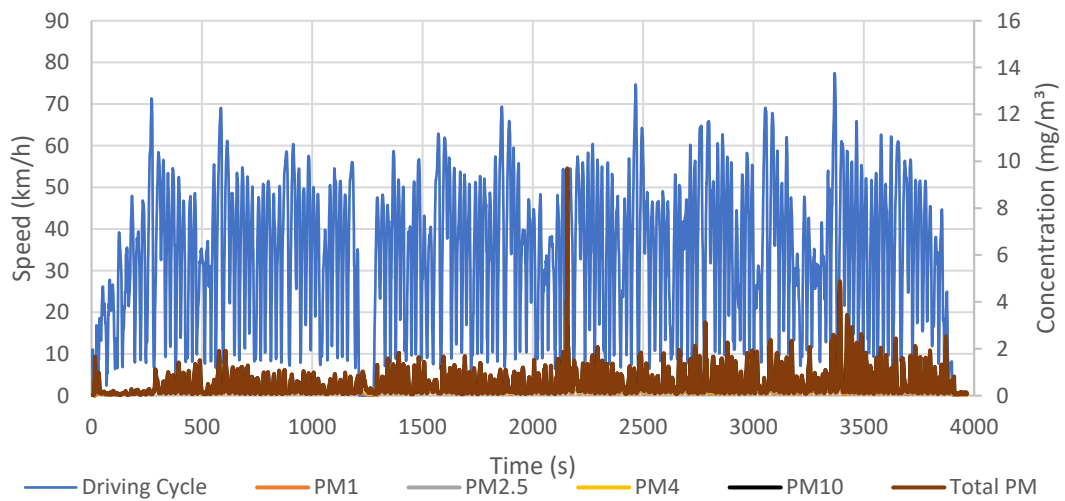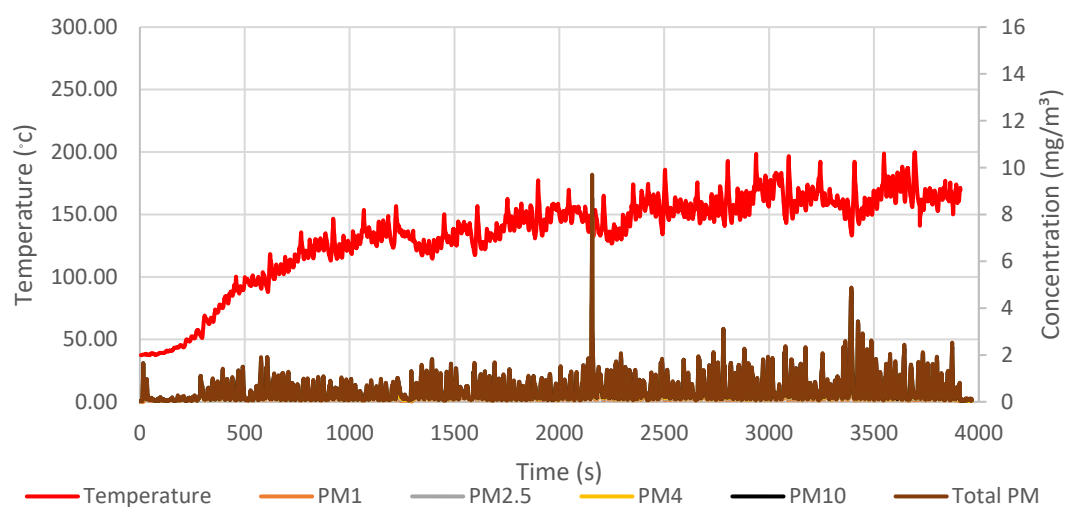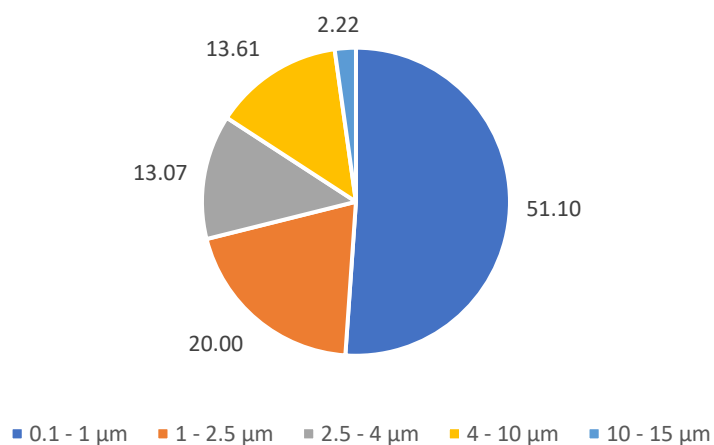**Appendix Figure 24** Filter from SUV test (Light#1)

Light#2
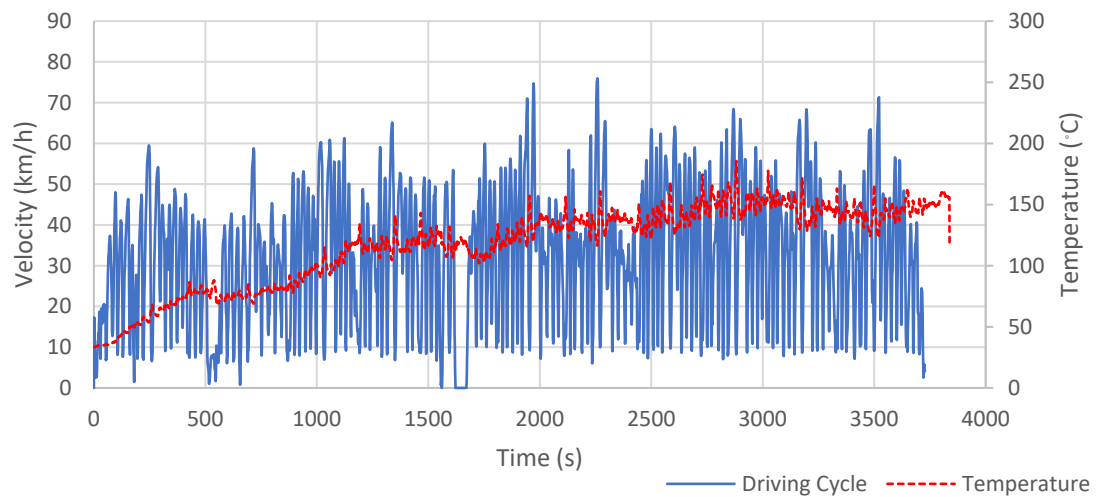
Appendix Figure 25 Driving cycle vs brake temperature of SUV (Light#2)
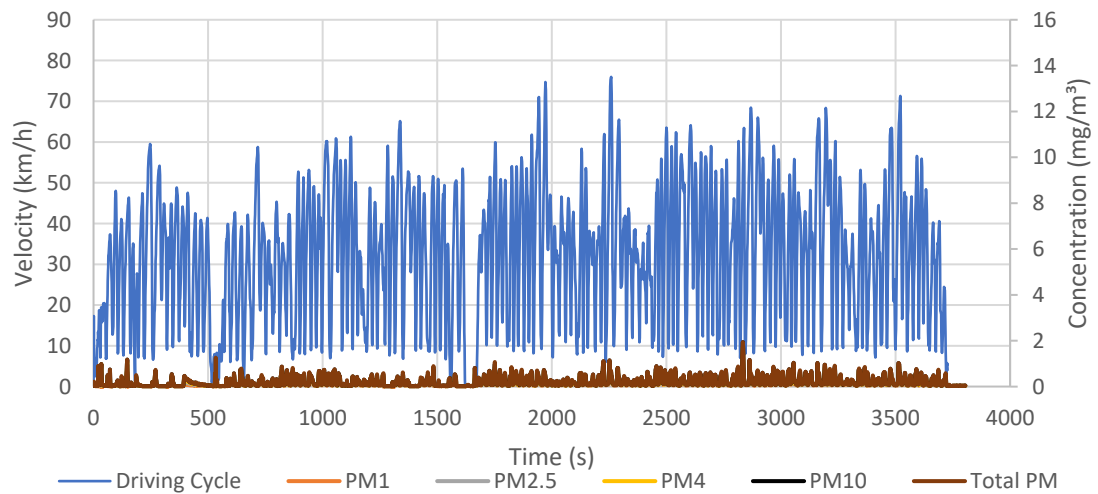
Appendix Figure 26 Driving cycle vs PM of SUV (Light#2)
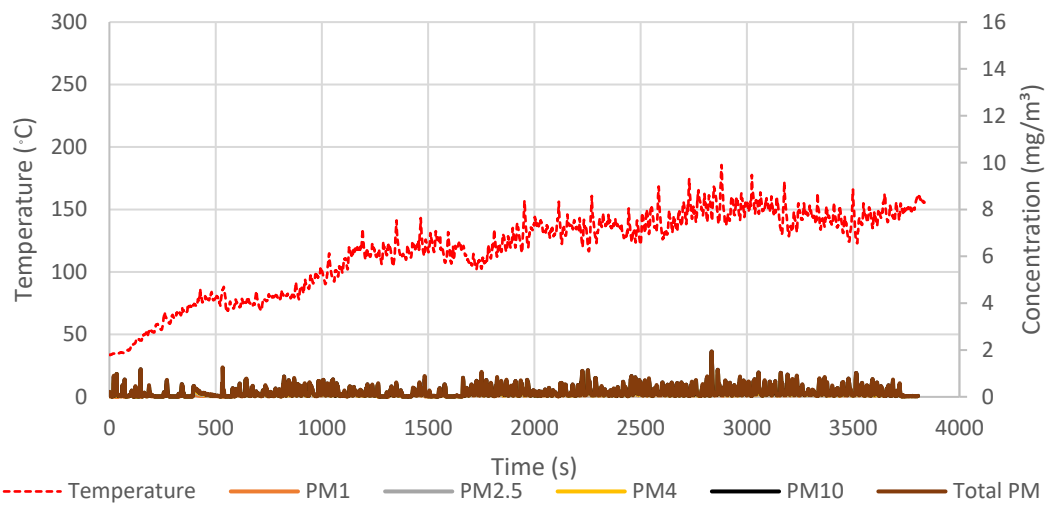
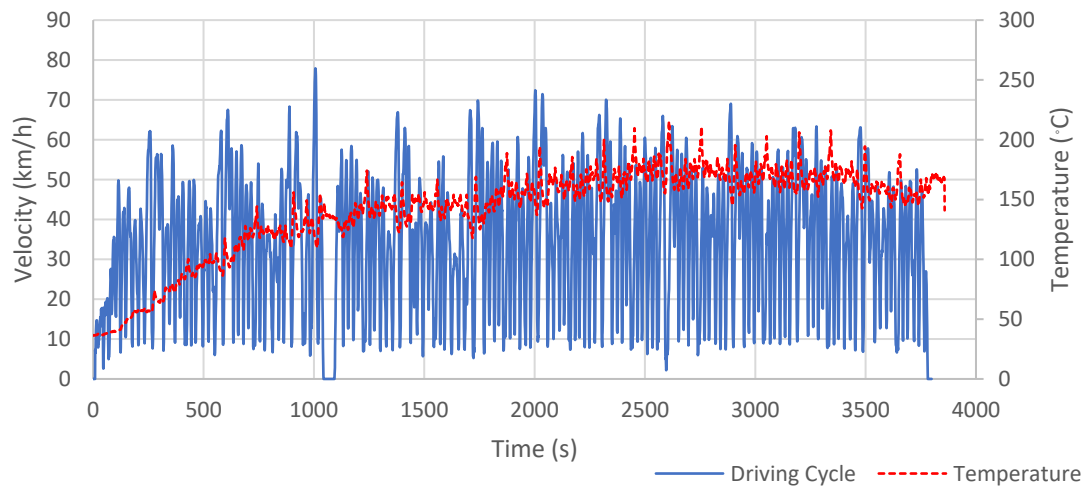**Appendix Figure 27** Brake temperature vs PM of SUV (Light#2)

Appendix Figure 28 Size distributions of SUV (Light#2)

Filter from TSI, cold and hot test (addition weight of filter = 0.034, 0.025 and 0.042 mg)

Appendix Figure 29 Filter from SUV test (Light#2)

Light#3

Appendix Figure 30 Driving cycle vs brake temperature of SUV (Light#3)

Appendix Figure 31 Driving cycle vs PM of SUV (Light#3)

Appendix Figure 32 Brake temperature vs PM of SUV (Light#3)

Appendix Figure 33 Size distributions of SUV (Light#3)

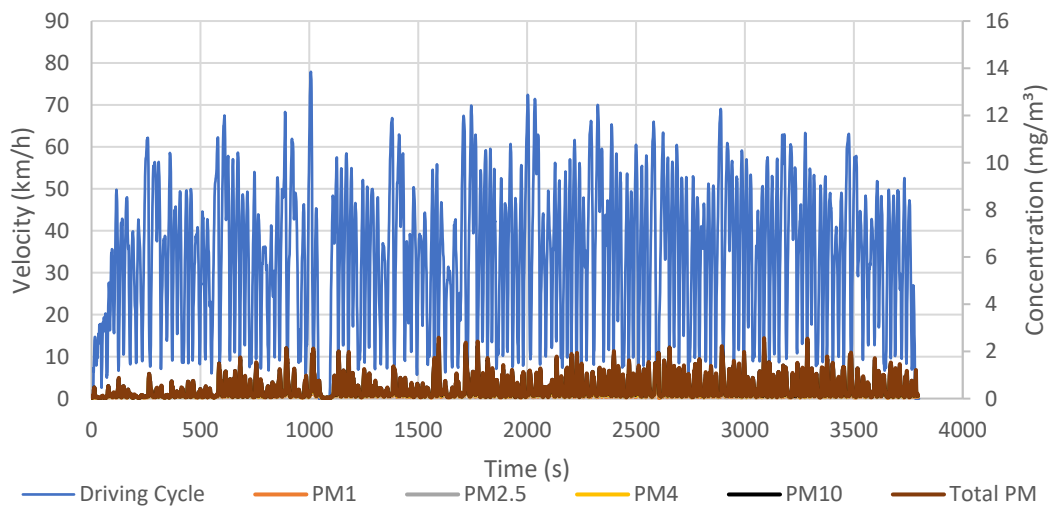Filter from TSI, cold and hot test (addition weight of filter = 0.055, 0.021 and 0.091 mg)

Appendix Figure 34 Filter from SUV test (Light#3)

Heavy#1

Appendix Figure 35 Driving cycle vs brake temperature of SUV (Heavy#1)

Appendix Figure 36 Driving cycle vs PM of SUV (Heavy#1)

Appendix Figure 37 Brake temperature vs PM of SUV (Heavy#1)

Appendix Figure 38 Size distributions of SUV (Heavy#1)

Filter from TSI, cold and hot test (addition weight of filter = 0.089, 0.036 and 0.126 mg)

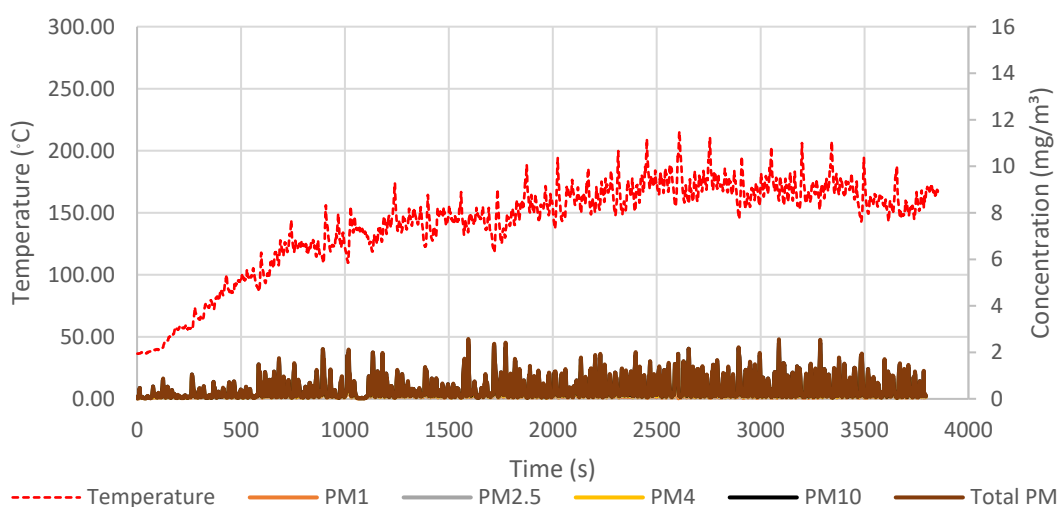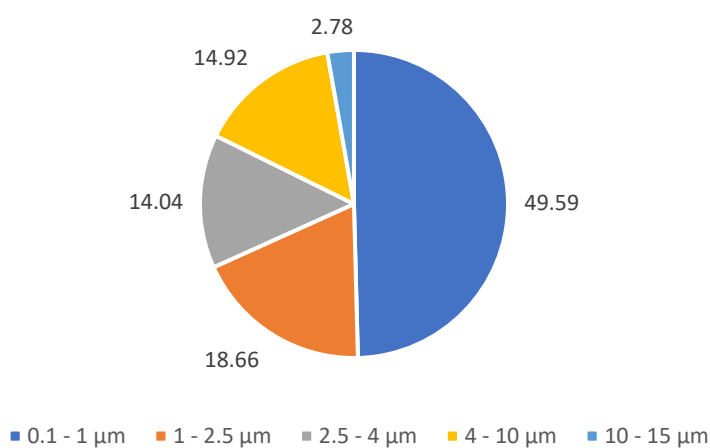**Appendix Figure 39** Filter from SUV test (Heavy#1)

Heavy#2

Appendix Figure 40 Driving cycle vs brake temperature of SUV (Heavy#2)

Appendix Figure 41 Driving cycle vs PM of SUV (Heavy#2)

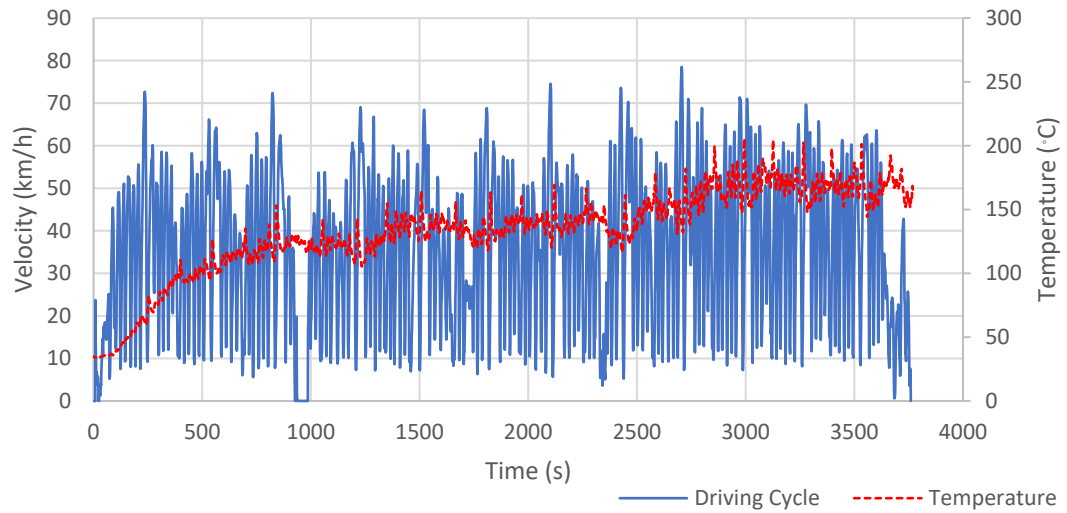**Appendix Figure 42** Brake temperature vs PM of SUV (Heavy#2)

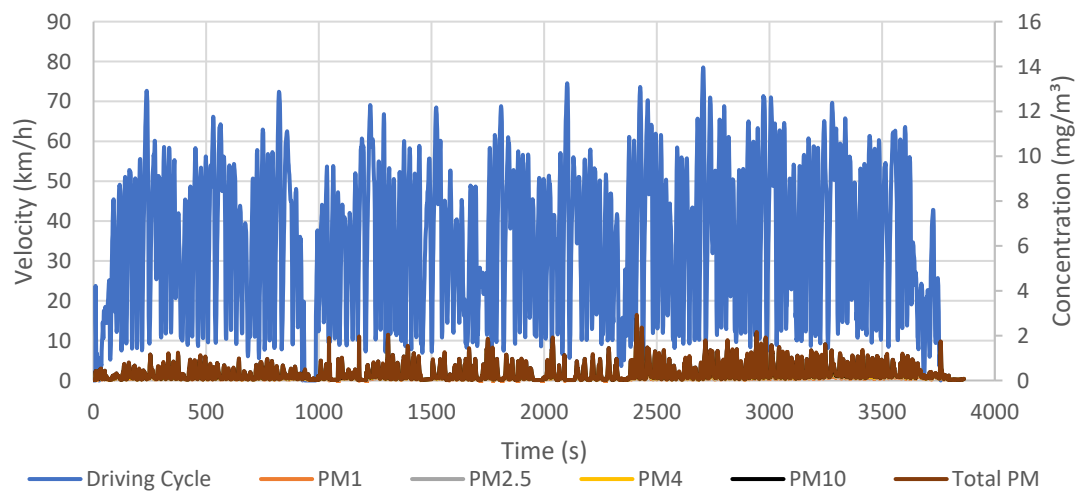**Appendix Figure 43** PM size distributions of SUV (Heavy#2)

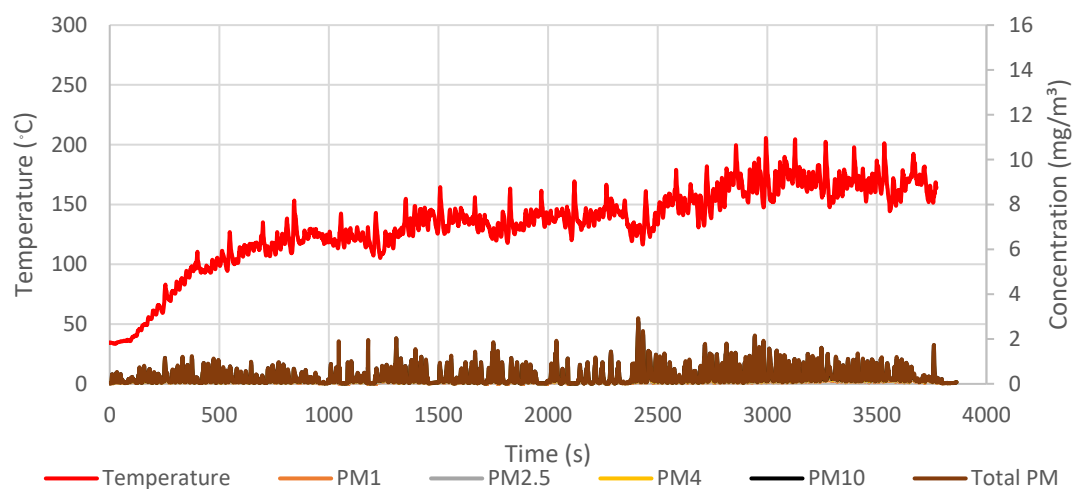Filter from TSI, cold and hot test (addition weight of filter = 0.059, 0.027 and 0.117mg)

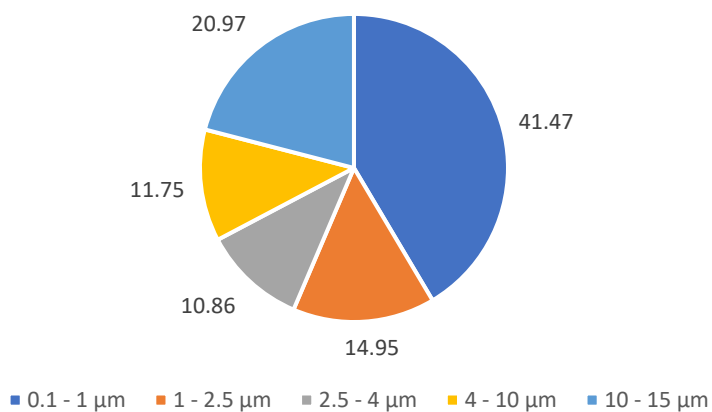**Appendix Figure 44** Filter from SUV test (Heavy#2)

Heavy#3

Appendix Figure 45 Driving cycle vs brake temperature of SUV (Heavy#3)

Appendix Figure 46 Driving cycle vs PM of SUV (Heavy#3)

Appendix Figure 47 Brake temperature vs PM of SUV (Heavy#3)

Appendix Figure 48 PM size distributions of SUV (Heavy#3)

Filter from TSI, cold and hot test (addition weight of filter = 0.066, 0.022 and 0.112 mg)

Appendix Figure 49 Filter from SUV test (Heavy#3)

CURRICULUM VITAE

NAME	Worawat Songkitti
DATE OF BIRTH	9 August 1993
BIRTH PLACE	Bangkok
ADDRESS	Bangkok, Thailand
EDUCATION	B.Eng. (Mechanical Engineering) Kasetsart University
	M.Eng. (Mechanical Engineering) Kasetsart University